HEATS OF MIXING AND PHASE SEPARATION

OF POLYMER MIXTURES

A Thesis submitted for the Degree of
Doctor of Philosophy of the University of London
and the Diploma of Membership of the
Imperial College of Science and Technology

by

Chong Chiew Let B.Sc.(Hons.) (Hull)

Department of Chemical Engineering and Chemical Technology

Imperial College of Science and Technology, London SW 7

March 1981

ABSTRACT

The aim of the project was to make accurate experimental measurements of the heats of mixing of oligomers, and hence to explore the shapes of the mixing curves as a function of composition. For this purpose, a modified NBS batch-type calorimeter was constructed. Operated at temperatures up to 110^{0}C, it has a machine accuracy of 1%, as characterised by the acid-base neutralisation reaction. The enthalpies of mixing of the oligomers were carried out with an accuracy of 4% for the less viscous systems and 8% for the more viscous systems, in the temperature range 30^{0}C to 70^{0}C. The following oligomer pairs were investigated:

(a) polypropylene glycol ($\bar{M}_n$=400)-polypropylene glycol ($\bar{M}_n$=1025,1500 and 2000),

(b) methoxylated polypropylene oxide ($\bar{M}_n$=400)-methoxylated polypropylene oxide ($\bar{M}_n$=1500),

(c) methoxylated polyethylene oxide ($\bar{M}_n$=600)-methoxylated polypropylene oxide ($\bar{M}_n$=400,1000,1500,2000),

(d) polystyrene ($\bar{M}_n$=1010)-polybutadiene ($\bar{M}_n$=960 and 2350).

Phase boundaries were also measured using a specially constructed light scattering turbidimeter equipped with an automatic data acquisition system capable of scanning four samples in rapid succession. For blends containing at least one fluid component, the cloud point can be determined with an accuracy of 2^{0}C. The turbidimeter is also capable of

measuring the cloud points of high molecular weight blends in the form of thin films.

From the enthalpy measurements and calculations of the entropies of mixing, free energy of mixing curves were constructed. These curves predicted partial miscibility in composition ranges where total miscibility was observed by present and past cloud point measurements. This indicates that theoretical estimates of the entropies of mixing require modification.

CONTENTS

		Page
	Abstract	2
	Acknowledgements	4
	List of Tables	9
	List of Figures	11
1.	Introduction	14
2.	Thermodynamics of Polymer Mixtures	20
	2:1. Derivation of the Flory-Huggins Equation for a Binary Polymer Blend	21
	2:2. Phase Separation	27
	2:3. Flory's Equation of State	34
	2:3.1. Extension of the Equation of State to Binary Mixtures	37
3.	Description of Calorimeter and Light Scattering Turbidimeter	47
	3:1. Description of Calorimeter	47
	3:1.1. The Outer Heat Jacket	50
	3:1.2. The Inner Heat Jacket	51
	3:1.3. The Central Heat Sink Unit	52
	3:1.4. The Heat Flow Detecting Units	55
	3:1.5. Calorimeter Cell	57
	3:1.6. Preheating Oven	59
	3:1.7. Temperature and Temperature Control of Calorimeter	59
	3:1.8. Signal Detection	62
	3:2. Light Scattering Turbidimeter	62
	3:2.1. Sample Holder	63

Page

3:2.2. Constant Light Source 69

3:2.3. Lens and Photodiode Assemblies 69

3:2.4. Sample Cells 72

3:2.5. Stirring of Liquid Samples 73

3:2.6. Temperature Control and Measurement 73

3:2.7. Data Logger and Controller 74

3:2.8. Software Control 75

4. Experiments and Results 77

4:1. Calorimeter Characteristics 77

4:1.1. The Quality of Baseline 78

4:1.2. Sensitivity, Heat Flow and Time Constant of The Calorimeter 78

4:1.3. Electrical Calibrations and Calculation of Areas 81

4:2. Materials 91

4:2.1. Hydrochloric Acid and Sodium Hydroxide Solutions 91

4:2.2. Oligomeric Polystyrene 91

4:2.3. Oligomeric Polybutadiene 92

4:2.4. Oligomeric Polyethylene Oxide(PEGM) and Polypropylene Oxide(PPGM) 93

4:3. Methods of Loading Reaction Cell 93

4:3.1. Loading of Samples 94

4:3.2. Cell Assembly After Sample Loading 96

4:4. Experimental Run 97

4:4.1. Actual Run 97

4:4.2. Run Time and Calculation of Area Under The Curve 99

4:4.3. Blank Heat Effects 100

Page

4:5. Results 100

4:5.1. HCl-NaOH Chemical Test 100

4:5.2. Chain Length Compatibility 102

4:5.3. PEGM-PPGM System 110

4:5.4. PS-PBD System at 70.1°C 129

4:6. Light Scattering Turbidimeter Characteristics 134

4:6.1. Stability of the Tungsten Light Source and Photodiodes 135

4:6.2. Temperature Lag 136

4:7. Materials 136

4:8. Sample Preparation 137

4:8.1. PS 1010-PBD 2350 System 137

4:8.2. PS 1520-PBD 2350 System 138

4:8.3. Degassing and Sealing of Samples 138

4:9. Cloud Point Measurements 138

4:10. Results 139

5. Discussion 149

5:1. Experimental 149

5:1.1. Calorimeter 149

5:1.2. Light Scattering Turbidimeter 153

5:2. Results 154

5:2.1. Chain Length Compatibility at 30.1°C 154

5:2.2. PEGM-PPGM System in the Temperature Range 30°C to 70°C. 155

5:2.3. Polystyrene-Polybutadiene System 161

6. Conclusions 165

Appendix A,B and C (see List of Tables) 170/1

References 172

ACKNOWLEDGEMENTS

The development of this project would not have been possible without the assistance and support of a number of people to whom I am greatly indebted to.

I would like to express my gratitude to Professor Sir Geoffrey Allen for initiating the project and to Professor Sir Geoffrey Allen and Dr. J.S. Higgins for their untiring supervision of the project and their continual moral support.

I am indebted to the following people for the help rendered, which is so necessary for the completion of the project:-

Dr. H.J. Michels for the helpful discussions on the designing aspects of the calorimeter,

Mr. M. Dix for designing and constructing the electronic parts of the calorimeter and the light scattering turbidimeter,

Messrs. T. Stephenson, B. Lucas, R. King and R. Wallington for constructing the calorimeter and light scattering turbidimeter,

Dr. D.A. Young for his helpful discussions regarding some operating aspects of the calorimeter,

Thanks are also due to Dr. A. Maconnachie for carrying out the GPC runs, Dr. K. Weeraperooma for carrying out the PICS measurements at Essex University, Drs. D.J. Walsh and R.H. Hall for the use of laboratory apparatus and advice during the initial part of the project and general, technical and glassblowing services for their services , especially Mr. P. Amrit.

Financial support from the Science Research Council for the whole of the project is gratefully acknowledged.

Finally, I would like to thank my colleagues Drs. M. R. Letherby and J. Davies, Mrs. K. Ma, Miss A. Hill, A. Carter, Z.K. Chai, P. Nwammo, K. Sardelis and L.H. Shi for their friendships and good cheer. I would also like to thank my parents for their abounding love and encouragements. This thesis is dedicated to both of them with all my love.

LIST OF TABLES

Tables:-		Page
4:1.	Results of electrical calibration of distilled water at 30 °C.	83
4:2a.	Results of electrical calibration of PEGM-PPGM system at 30.1 °C for energy above 1J.	85
4:2b.	Results of electrical calibration of PEGM-PPGM system at 30.1 °C for energy below 1J	87
4:3.	Results of electrical calibration of PS-PBD system at 70.1 °C.	89
4:4.	Microstructures of PBD samples.	92
4:5.	Molecular weights and designations of PPGM and PEGM samples.	93
4:6.	Results of heat of neutralization measurements at 30 °C.	101
4:7.	Results of PPG 400-PPG 1025 system at 30.1 °C.	103
4:8.	Results of PPG 400-PPG 1500 system at 30.1 °C.	104
4:9.	Results of PPG 400-PPG 2000 system at 30.1 °C.	105
4:10.	Results of PPGM 400-PPGM 1500 system at 30.1 °C.	106
4:11.	Results of reproducibility runs at 30.1 °C.	110
4:12.	Results of PEGM 600-PPGM 400 system at 30.1 °C.	112
4:13.	Results of PEGM 600-PPGM 1000 system at 30.1 °C.	113
4:14.	Results of PEGM 600-PPGM 1500 system at 30.1 °C.	114
4:15.	Results of PEGM 600-PPGM 2000 system at 30.1 °C.	115
4:16.	Results of PEGM 600-PPGM 1000 system at 50.1 °C.	116
4:17.	Results of PEGM 600-PPGM 1500 system at 50.1 °C.	117
4:18.	Results of PEGM 600-PPGM 2000 system at 50.1 °C.	118

Tables:- Page

4:19. Results of PEGM 600-PPGM 1000 system at 70.1°C. 119

4:20. Results of PEGM 600-PPGM 1500 system at 70.1°C. 120

4:21. Results of PEGM 600-PPGM 2000 system at 70.1°C. 121

4:22. Results of PEGM 600*-PPGM 2000 system at 70.1°C. 122

4:23. Results of PS 1010-PBD 2350 system at 70.1°C. 130

4:24. Results of PS 1010-PBD 960 system at 70.1°C. 131

4:25. Cloud points of PS 1010-PBD 2350 system. 140

4:26. Cloud points and 'spinodal' temperatures of PS 1520-PBD 2350 system. 142

4:27. Values of χ_{12} and χ_{21} calculated from equations 4:16 and 4:17 for the concentrations of the components indicated. 148

5:1. Heats of mixing of equivolume mixtures. 156

Appendix A Table of chart recorder full scale deflection for amplifier gain control setting 170

Appendix B Table of temperature control setting and temperature of calorimeter obtained. 170

Appendix C Listing format of turbidimeter results. 171

LIST OF FIGURES

		Page
Fig. 2:1.	Free enthalpy(Gibbs free energy) of mixing as a function of concentration showing (a) complete and (b) partial miscibility.	29
Fig. 2:2.	Graphs of ΔG_m versus ϕ_2 at different temperatures giving rise to (a) UCST and (b) LCST phase boundary if a plot of temperature versus ϕ_2 is made.	31
Fig. 3:1.	Side view cross-section of modified NBS microcalorimeter.	48
Fig. 3:2.	End view cross-section of microcalorimeter.	49
Fig. 3:3.	Heat sink cross-section.(side view).	53
Fig. 3:4.	Heat sink-heat detection(flow) unit.	56
Fig. 3:5.	Sample cell components and assembly.	56
Fig. 3:6.	Block diagram of microcalorimeter electronics.	61
Fig. 3:7.	Schematic block diagram of light scattering turbidimeter electronics.	64
Fig. 3:8.	Side view cross-section of light scattering turbidimeter sample holder.	65
Fig. 3:9	Light scattering turbidimeter plan.	66
Fig. 3:10.	Light scattering turbidimeter front view cross-section.	67
Fig. 3:11.	Lamp holder assembly.	70
Fig. 3:12.	Lens holder and photodiode assembly.	71
Fig. 3:13.	Solid sample cell.	71
Fig. 4:1.	Integrator reading and area versus energy plots for the electrical calibration of distilled water at 30^0C.	84

Page

Fig. 4:2a. Integrator reading and area versus energy plots for the electrical calibration of PEGM-PPGM system at 30.1°C for energy above 1J. 86

Fig. 4:2b. Integrator reading and area versus energy plots for the electrical calibration of PEGM-PPGM system at 30.1°C for energy below 1J. 88

Fig. 4:3. Integrator reading and area versus energy plots for the electrical calibration of PS(1010)-PBD(960) system at 70.1°C. 90

Fig. 4:4. Heat and entropy of mixing versus PPG 400 volume fraction plots for PPG-PPG system at 30.1°C. 107

Fig. 4:5. Interaction parameter and free energy of mixing versus PPG 400 volume fraction plots for PPG-PPG system at 30.1°C. 108

Fig. 4:6. Heat, entropy and free energy of mixing and interaction parameter versus PPGM 400 volume fraction plots for PPGM-PPGM system at 30.1°C. 109

Fig. 4:7. Heat of mixing and entropy of mixing versus PEGM 600 volume fraction plots for PEGM-PPGM system at 30.1°C. 123

Fig. 4:8. Interaction parameter and free energy of mixing versus PEGM 600 volume fraction plots for PEGM-PPGM system at 30.1°C. 124

Fig. 4:9. Heat and entropy of mixing versus PEGM 600 volume fraction plots for PEGM-PPGM system at 50.1°C. 125

Fig. 4:10. Interaction parameter and free energy of mixing versus PEGM 600 volume fraction plots for PEGM-PPGM system at 50.1°C. 126

Page

Fig. 4:11. Heat and entropy of mixing versus PEGM 600 volume fraction plots for PEGM-PPGM system at 70.1°C. 127

Fig. 4:12. Interaction parameter and free energy of mixing versus PEGM 600 volume fraction plots for PEGM-PPGM system at 70.1°C. 128

Fig. 4:13. Heat and entropy of mixing versus PS 1010 volume fraction plots for PS-PBD system at 70.1°C. 132

Fig. 4:14. Interaction parameter and free energy of mixing versus PS 1010 volume fraction plots for PS-PBD system at 70.1°C. 133

Fig. 4:15. Phase boundary of PS 1010-PBD 2350 system. 141

Fig. 4:16. Scattered intensity versus temperature plot for PS 1520-PBD 2350 sample (typical plot). 143

Fig. 4:17. Reciprocal intensity versus temperature plot for PS 1520-PBD 2350 sample (best case). 144

Fig. 4:18. Reciprocal intensity versus temperature plot for PS 1520-PBD 2350 sample (worst case). 145

Fig. 4:19. Phase boundary of PS 1520-PBD 2350 system 147

CHAPTER 1

INTRODUCTION

The compatibility (or incompatibility) of polymers has been studied by various workers using different physical parameters as an assessment of the degree of compatibility. For example, processability in practical production has been used by technologists as a criterion for compatibility (miscibility) on a macroscopic scale. On a smaller scale, but more often cited, is the glass transition temperature of the polymer blend compared to the glass transition temperature of the pure components. A single blend glass transition temperature , in between those of the pure components signifies compatibility. The glass transition temperature can be measured mechanically using various equipment or dielectrically. A review of the various instruments used as well as numerous other methods of investigation employed in the study of polymer-polymer compatibility have been comprehensively dealt with by Olabisi et al[1].

In terms of equilibrium thermodynamics, compatibility implies miscibility on a molecular scale. Hence the free energy of mixing should provide an unambiguous criterion for determining the equilibrium states in a mixture, and a consideration of the thermodynamic free energy should give a true picture of the compatibility of the polymer-polymer mixture, both qualitatively and quantitatively. This can be done empirically by an extension of the thermodynamic treatment of simple liquid mixtures to binary or multicomponent polymer mixtures via the lattice

models. Certain modifications are required due to the special characteristics of the polymer molecule, as compared to simple molecules. This criterion has been used by Konningsveld[2] et al in most of their work on polymer solutions and polymer mixtures, as well as by numerous other workers, and it is also the criterion adopted in the present work.

One of the earliest methods used in the study of polymer compatibility was the mutual solvent method, in which two high polymers were dissolved in a common solvent and the solution allowed to stand for a few days. If phase separation occurs in which one phase is rich in one component while the other phase is rich in the other polymeric component, then the two polymers are termed incompatible (even if the solvent is absent) and compatible if no phase separation occurs. The most thorough and systematic investigation of polymer compatibility using this method was the work carried out by Dobry and Boyer-Kawenoki[3] on 78 mixtures of 14 high polymers in 13 solvents. Amongst their numerous observations and conclusions, which were supported by the later work of Kern and Slocombe[4], the most important was that miscibility is the exception, immiscibility is the rule. This observation holds true even today, although recent work[5] [6] has shown that this method can give spurious results, depending on the concentration and nature of the solvent used, as well as being non-representative of binary polymer mixtures in the absence of the solvent.

As was noted by Yu[7], due to the high viscosity of polymer-polymer mixtures, their homogeneity will depend on their methods of preparation and the length of time and thermal histories to which they are subjected. For example, in

freezing samples for electron microscopy, the final picture obtained could be due to the effect of the quenching process and not a true picture of the situation prior to quenching. In the case of glass transition measurements, the measurements are valid only for the temperature range in which the measurements were carried out, and are not representative of the mixture at higher temperatures. This observation was supported by the earlier work of Allen, Gee and Nicholson[8]. Using oligomers to circumvent the viscosity problem and yet retaining some of the characteristic properties of long chain molecules, their work on the mutual solvent method showed that the mixing of two polymers in a mutual solvent is incomplete or non-random. This is in direct contrast to their work on the heats of mixing of the oligomers in bulk, which showed complete or random mixing, a concentration dependence of the Flory-Huggins polymer-polymer interaction parameter and an irregular entropy of mixing. The polyisobutene-polydimethysiloxane phase-diagram obtained by these workers was the first phase diagram which showed as-ymmetric, odd-shaped curves with shoulders which were sensitive to chain length variation. They also observed a shift in the maximum of the phase diagram towards regions richer in the component with the larger chain length on increasing the average chain length of one of the component, and no apparent temperature dependence of the heats of mixing. Such peculiar-shaped miscibility curves, together with bimodal curves, have since then been observed to occur quite often in polymer-polymer mixtures[9].

Konningsveld[2] et al have shown that, if a concentration independent interaction parameter is used in the Flory-Huggins

theory for oligomeric systems, the entropies of mixing tend to shift the miscibility gap towards the composition region which is richer in the constituent with the smaller average chain length, a direct contrast to the experimental results obtained by Allen[8] et al. They also showed that a distribution of the average chain length(i.e.polydispersity) in at least one of the components will alter the shape of the miscibility gap significantly, by widening it. McIntyre[10 11] et al have also observed that the shape of the miscibility gap can be affected by polydispersity in their work on oligomeric polystyrene-polyisoprene and polystyrene-cyclohexane.

Noting the conclusions and observations drawn by Allen[8] et al, Konningsveld[2] et al managed to reproduce and extend their cloud point curve(to lower temperatures) qualitatively by considering a quadratic dependence of the interaction parameter on concentration, with a restriction on the temperature dependence in the expression, and neglecting polydispersity. Their work showed that a concentration dependent interaction parameter can outweigh the effect of the entropy of mixing, and the results of Allen[8]et al could be explained on this basis. The correction term(s) so applied could be either of an entropic(non-combinatorial) or enthalpic nature or both. Although polydispersity can and does affect the shape of the miscibility gap, it does not account for the bimodality observed in some systems. In fact, the bimodality becomes more pronounced as the polydispersity decreases. Konningsveld[2] et al have also shown that the bimodality observed in the polystyrene-polyisoprene system can be similarly explained by a concentration dependent interaction parameter, although the agreement is more qualitative than quantitative,

and that the location of the critical point, with respect to the maximum of the spinodal, is more sensitive to the differences in the average chain length in the concentration dependent case than in the concentration independent case. End group effects, though significant, were shown to be unlikely to cause the bimodality observed, due to the unacceptably large interaction free enthalpies involved. Yip[12] found that for the polystyrene-polybutadiene system, the miscibility gap exhibits normal, smooth upper critical solution behavior if the components have sharp molecular weights. Tripathi[13] has shown that for the methoxylated(polyethylene oxide-polypropylene oxide) system with sharp molecular weights, normal, smooth upper critical solution behavior is observed. He also showed that the effect of increasing the pressure on this, as well as the polystyrene-polybutadiene, system was to elevate the miscibility curves to higher temperature regions.

Although the Flory-Huggins theory is a powerful tool in the description of liquid-liquid phase relationships in polymer-polymer mixtures, however, it lacks predictive powers, since the concentration dependent interaction parameter cannot be derived directly from theory. It is in this aspect that the equation-of-state, developed by Flory[14], is superior over the Flory-Huggins theory. McMaster's[15] generalisation of Flory's equation-of-state showed that the equation-of-state approach predicts a lower critical solution behavior for polymer mixtures, a fact which is observed often experimentally, and showed also the observed sensitivity of the curves to the average chain length, thermal expansion and thermal pressure coefficients. The concentration dependence of the interaction parameter is well established from the theoretical derivation. On the other

hand, powerful though it may be in its predictive capabilities, the equation-of-state lacks the ability to describe the odd-shaped curves observed by Allen[8] et al as well as the bimodality in the polystyrene-polyisoprene system.

Hence, although the numerous extensive work on binary polymer mixtures has shown good qualitative agreement between the various theories and experimental data, quantitative agreement between the theories and experiments, on the other hand, is far from complete. In the words of Konningsveld et al, "polymer compatibility has proved to be a very subtle phenomenon indeed".

CHAPTER 2

THERMODYNAMICS OF POLYMER MIXTURES

A polymer blend can be envisaged as a solution of a polymeric solute(the component with the larger chain length) dissolved in a polymeric solvent(the component with the smaller chain length). Hence, it is not surprising that the theory developed for the thermodynamics of polymer blends is an extension of the polymer solution theory, which in turn, is an extension of the liquid lattice model that was developed for mixtures of molecules with weak interactions and approximately similar sizes.

It was Van der Waals who first gave a qualitative description of the partial miscibility of polymer solutions in terms of his equation of state, and ascribed the asymmetric shapes of their co-existence curves to the large differences in the molecular size of the components. The first attempt to quantify the situation was made by Fowler and Rushbrooke[16] who proposed to calculate the combinatorial entropy of two dissimilar species by considering dimeric molecules constrained to occupy pairs of adjacent sites and monomers in single sites in a lattice, even though the resulting mixture was shown to be non-ideal. Chang[17 18] later managed to obtain the combinatory free energy in closed form. This, and later attempts by other workers such as Miller[19], were to culminate in the derivation of the Flory-Huggins equation, an equation derived simultaneously and independently by Flory[20 21] and Huggins[22 23]. Their equation was divided into two parts, namely a contribution due to the combinatorial entropy change(relative to the pure state) on distributing the X-mer chains successively into a lattice

structure, with each cell capable of accommodating a monomer unit and the solvent molecules occupying the remaining vacant cells singly, and a correction enthalpic contribution due to the energetic exchange between like and unlike species. Although most derivations of the Flory-Huggins equation for binary polymeric blends tend to start from ternary systems, i.e.two different polymers dissolved in a mutual solvent, and then allow the solvent term to approach zero concentration to yield the required equation, the following modified derivation avoids the use of a mutual solvent.

2:1. Derivation of the Flory-Huggins equation for a binary polymer blend.

A: Entropy change of mixing (combinatory).

The combinatorial entropic contribution due to the mixing can be obtained by considering the mixing of N_1 molecules of a monodisperse polymer 1 each of x_1 segments and N_2 molecules of another monodisperse polymer 2 each of x_2 segments, both with an arbitrary common segmental volume V^0. Assuming a regular three dimensional lattice with a total of $N_1x_1+N_2x_2$ cells(sites), the total volume of the mixture is $(N_1x_1+N_2x_2)V^0$. If n_1 and n_2 are the number of moles of polymer 1 and polymer 2 respectively, and N_A is Avogadro's number, then

$$n_1 N_A = N_1 \qquad \text{and} \qquad n_2 N_A = N_2 \qquad 2:1$$

therefore

$$\phi_1 = \frac{n_1x_1}{n_1x_1+n_2x_2} \qquad \text{and} \qquad \phi_2 = \frac{n_2x_2}{n_1x_1+n_2x_2} \qquad 2:2$$

where ϕ_i is the volume fraction of polymer i respectively. Firstly, considering the placing of N_2X_2 segments of polymer 2 into the lattice, assuming that there are already i_2 molecules

of component 2 in the lattice,

$$\text{the fraction of occupied sites} = \frac{i_2 x_2}{N_1 x_1 + N_2 x_2} = f_{i_2} \qquad 2:3$$

$$\text{and the fraction of unoccupied sites} = 1 - f_{i_2} \qquad 2:4$$

For the (i_2+1)th molecule,

the first segment can be introduced in $(1-f_{i_2})(N_1x_1+N_2x_2)$ ways

the second segment in $(1-f_{i_2})z$ ways where z is the number of immediate neighbouring sites,

the third and subsequent segments are assumed to be introduced in $(1-f_{i_2})^{x_2-2}(z-1)^{x_2-2}$ ways.

Hence, all the segments of the (i_2+1)th molecule can be introduced into the lattice as a concatenated molecule in

$$\nu_{i_2+1} = \tfrac{1}{2}(1-f_{i_2})^{x_2} z (z-1)^{x_2-2} (N_1x_1+N_2x_2) \text{ ways} \qquad 2:5$$

the factor of half being introduced since the two chain ends are indistinguishable.

The N_2 molecules of polymer 2 can therefore be introduced in a total of W_2 ways where

$$W_2 = \frac{1}{N_2!} \prod_{i_2=0}^{N_2-1} \nu_{i_2+1} \text{ ways}$$

$$= \frac{1}{N_2!} \prod_{i_2=0}^{N_2-1} \tfrac{1}{2}(1-f_{i_2})^{x_2} z (z-1)^{x_2-2} (N_1x_1+N_2x_2) \text{ ways.} \qquad 2:6$$

By an analogous argument for the segments of polymer 1 introduced into the remaining vacant sites, one obtains,

$$W_1 = \frac{1}{N_1!} \prod_{i_1=0}^{N_1-1} \tfrac{1}{2}(1-j_{i_1})^{x_1} z (z-1)^{x_1-2} (N_1x_1+N_2x_2) \text{ ways.} \qquad 2:7$$

where $$j_{i_1} = (N_2x_2+i_1x_1)/(N_1x_1+N_2x_2) \qquad 2:8$$

is the fraction of sites already occupied by (N_2+i_1) molecules

of polymer 2 and polymer 1 respectively. Hence, the total number of ways of introducing $(N_1x_1+N_2x_2)$ segments into the lattice in concatenated forms is

$$W = W_1W_2 \qquad 2:9$$

The entropy of the mixture is

$$S_{mix} = k\ln W_1W_2 \qquad 2:10$$

where k is Boltzmann's constant. Therefore,

$$\begin{aligned}\frac{S_{mix}}{k} &= -\ln N_1! - N_1\ln 2 + N_1\ln(N_1x_1+N_2x_2) + N_1\ln z(z-1)^{x_1-2} \\ &\quad + x_1\int_0^{N_1}\ln\{1-(i_1x_1+N_2x_2)/(N_1x_1+N_2x_2)\}di_1 - \ln N_2! \\ &\quad - N_2\ln 2 + N_2\ln(N_1x_1+N_2x_2) + N_2\ln z(z-1)^{x_2-2} \\ &\quad + x_2\int_0^{N_2}\ln\{1-(i_2x_2)/(N_1x_1+N_2x_2)\}di_2 \qquad 2:11\end{aligned}$$

Applying Stirling's approximation for a logarithmic factorial and simplifying,

$$\begin{aligned}\frac{S_{mix}}{k} &= -N_1\ln N_1 - N_2\ln N_2 + N_1 + N_2 - N_1\ln 2 - N_2\ln 2 + N_1\ln z(z-1)^{x_1-2} \\ &\quad + N_2\ln z(z-1)^{x_2-2} + N_1\ln(N_1x_1+N_2x_2) + N_2\ln(N_1x_1+N_2x_2) \\ &\quad - N_1x_1 - N_2x_2 \qquad 2:12\end{aligned}$$

From equation 2:12, the entropy S_1 of polymer 1 in a lattice of N_1x_1 sites and the entropy S_2 of polymer 2 in a lattice of N_2x_2 sites can be obtained separately since $N_2$is zero in the former and N_1 is zero in the latter case.

Since $$\frac{\Delta S_{mix}}{k} = \frac{1}{k}(S_{mix} - S_1 - S_2) \qquad 2:13$$

therefore,

$$\begin{aligned}\frac{\Delta S_{mix}}{k} &= N_1\ln(N_1x_1+N_2x_2) + N_2\ln(N_1x_1+N_2x_2) - N_1\ln N_1x_1 \\ &\quad - N_2\ln N_2x_2 \qquad 2:14\end{aligned}$$

Hence,

$$-\frac{\Delta S_{mix}}{k} = N_1 \ln\{(N_1x_1)/(N_1x_1+N_2x_2)\}+N_2 \ln\{(N_2x_2)/(N_1x_1+N_2x_2)\}$$

$$=n_1N_A \ln\{(n_1x_1)/(n_1x_1+n_2x_2)\}+$$

$$n_2N_A \ln\{(n_2x_2)/(n_1x_1+n_2x_2)\} \qquad 2:15$$

Therefore,

$$-\Delta S_{mix} = R(n_1 \ln\phi_1+n_2 \ln\phi_2) \qquad 2:16$$

where R is the gas constant. In general, for a polymer blend of any number of monodisperse components,

$$-\Delta S_{mix} = R\Sigma n_i \ln\phi_i \qquad 2:17$$

B: The enthalpy of mixing.

The enthalpic contribution was obtained in a form similar to that of Van Laar and Scatchard[24] by considering the energy change involved in replacing neighbouring sites occupied by like segments by unlike segments. Let the energy of attraction between like segments of polymer 1 and of polymer 2 be ε_{11} and ε_{22} respectively, and that between unlike segments be ε_{12}. On average, surrounding each segment of polymer 1 in the mixture are $(zN_1x_1)/(N_1x_1+N_2x_2)$ segments of polymer 1 and $(zN_2x_2)/(N_1x_1+N_2x_2)$ segments of polymer 2. The total energy of the pure components before mixing are

$$H_{pure} = -\{(N_1x_1\varepsilon_{11})/2\}-\{(N_2x_2\varepsilon_{22})/2\} \qquad 2:18$$

and the total energy of the mixture is

$$H_{mix} = -\{(zN_1^2x_1^2\varepsilon_{11})/2(N_1x_1+N_2x_2)\}-\{(zN_1x_1N_2x_2\varepsilon_{12})/(N_1x_1+N_2x_2)\}$$

$$-\{(zN_2^2x_2^2\varepsilon_{22})/2(N_1x_1+N_2x_2)\} \qquad 2:19$$

Hence, the enthalpy of mixing is

$$\Delta H_{mix} = H_{mix} - H_{pure} \qquad 2:20$$

Substituting 2:1, 2:18 and 2:19 into 2:20 and simplifying yields,

$$\Delta H_{mix} = n_1 x_1 \phi_2 \Delta\varepsilon \qquad 2:21$$

where,

$$\Delta\varepsilon = zN_A\{(\varepsilon_{11})/2 + (\varepsilon_{22})/2 - (\varepsilon_{12})\} \qquad 2:22$$

Defining,

$$\frac{\Delta\varepsilon}{RT} = \chi_{12} \qquad 2:23$$

and substituting 2:23 into 2:21 gives,

$$\Delta H_{mix} = n_1 x_1 \phi_2 \chi_{12} RT \qquad 2:24$$

From thermodynamic considerations, the Gibbs free energy change of mixing,

$$\Delta G_{mix} = \Delta H_{mix} - T\Delta S_{mix} \qquad 2:25$$

becomes, on substituting with 2:16 and 2:24,

$$\Delta G_{mix} = RT(n_1 \ln\phi_1 + n_2 \ln\phi_2 + n_1 x_1 \phi_2 \chi_{12}) \qquad 2:26$$

This is the equation for the Gibbs free enthalpy change for a blend of two monodisperse polymers. In general, for a multi-component mixture of monodisperse polymers,

$$\frac{\Delta G_{mix}}{RT} = \{(\Sigma(\phi_i/x_i)\ln\phi_i) + \phi_i\phi_j\chi_{ij}\} \qquad 2:27$$

where $i \neq j$ and ΔG_{mix} is the Gibbs free enthalpy change per mole segment. Equation 2:27 can be generalised to take into account polydispersity[21 25 26 27] in the two components viz.,

$$\frac{\Delta G_{mix}}{RT} = \{\Sigma(\phi_{1i}/x_{1i})\ln\phi_{1i} + \Sigma(\phi_{2j}/x_{2j})\ln\phi_{2j} + \Sigma\phi_{1i}\Sigma\phi_{2j}\chi_{1i2j}\} \times \{\Sigma n_{1i}x_{1i} + \Sigma n_{2j}x_{2j}\} \qquad 2:28$$

where ϕ_{1i} and ϕ_{2j} are the volume fractions of species i in polymer 1 and species j in polymer 2 respectively.

Differentiation of 2:26 with respect to n_1 and simplifying gives the chemical potential of component 1, viz.,

$$\frac{\Delta\mu_1}{RT} = (\partial\Delta G_{mix}/RT\partial n_1)_{T,p,n_2} = \ln\phi_1 + (1 - x_1/x_2)\phi_2 + \chi_{12}x_1\phi_2^2 \qquad 2:29$$

The chemical potential of component 2 is

$$\frac{\Delta\mu_2}{RT} = (\partial\Delta G_{mix}/RT\partial n_2)_{T,p,n} = \ln\phi_2+(1-x_2/x_1)\phi_1+\chi_{21}x_2\phi_1^2 \quad 2:30$$

The foregoing derivations have all the inherent assumptions used in the original Flory-Huggins derivations. The most important of these inherent assumptions and properties are:-

1)The lattice structure is used for the individual pure components as well as for the intermediate mixtures, except for the number of sites considered. This is not true for the mixture due to the stereochemistry of the individual polymer type, but mathematical refinement to avoid this has resulted in little significance.

2)All polymer segments of the various components have the same segmental volume. This implies that an interchange of site by unlike segments should lead to no volume change. Excluded volume effects are neglected.

3)Only immediate neighbour interactions are considered, of which each site has z. This is especially true for non-polar polymer mixtures, as the interactions are inversely proportional to their separations.

4)The segments of the molecules are introduced into each lattice site with a better than average probability that one of the adjacent neighbouring site is vacant and vice-versa, and double occupancy is avoided.

5)Only combinatorial(configurational) entropy is considered. The internal situation of the polymer is ignored and the entropy component due to specific interactions between neighbouring species is neglected.

6)The reference states are the pure, perfectly ordered polymer.

7)Refinements to use accurate values of f_i instead of an

average value in the derivation of ν_{i+1} by Huggins[23], Miller[28], Orr[29] and Guggenheim[30] has resulted in complicated expressions that do not have improved agreement with practical results, as demonstrated by Flory[31] et al. Other refinements considered the influence of preferential interactions on the entropy of mixing. If such preferential interactions occur between unlike segments, then the distribution of unlike segments would be non-random, due to modifications by these interactions. Orr[29] and Guggenheim[30] considered such cases and found that for interactions which usually occur in polymers, the calculations of the entropy of mixing due to non-randomness causes no significant modification of the expression, as compared to other effects or approximations.

9) A consequence of assumption 2 is that, since the mixture will actually have a smaller free volume as compared to the pure states, the configurational entropy calculated will be larger than the actual one observed due to the reduced spatial freedom.

2:2. Phase Separation.

In general, endothermic (positive) free enthalpy change of mixing implies non-compatibility, while an exothermic (negative) free enthalpy change implies miscibility, with a boundary between the two given by $\Delta G_{mix}=0$, which is a balance between the entropy and enthalpy components. The enthalpy of mixing does not differ much for a binary monomeric mixture per mole, but the entropy of mixing decreases rapidly on going from a binary monomeric to a binary polymeric mixture, since the number of arrangements is severely restricted for the latter. For this reason, polymer-polymer mixtures are very susceptible to phase separation. A small positive heat of mixing suffices

to overcome the small entropy change, leading to phase separation, although at present, non-combinatory entropy of mixing is thought to play a large part in preventing phase separation in some systems.

For a polymer pair to be completely miscible, the free energy curve must be concave upwards over the whole composition range, as shown in figure 2:1a, where the intercepts of the tangents at any points will give the chemical potentials of the pure states. Since

$$\Delta G_{mix} = \phi_1 \Delta\mu_1 + \phi_2 \Delta\mu_2 \qquad 2:31$$

therefore,

$$\frac{\partial \Delta G_{mix}}{\partial \phi_2} = \Delta\mu_2 - \Delta\mu_1 \qquad (\text{since } 1-\phi_2=\phi_1) \qquad 2:32$$

is the chemical potential change of the mixture. If a convexity occurs in the free energy curve, as in figure 2:1b, a mixture of composition ϕ_2'' will phase separate out into two phases, of compositions ϕ_2' and ϕ_2'', in order to attain a minimum free energy for the system, provided that these two concentrations are attainable. The common tangent gives the compositions in which the chemical potentials of any component is the same in both phases, i.e. $\Delta\mu_1'=\Delta\mu_1''$,etc. All compositions between ϕ_2' and ϕ_2'' will phase separate out into the two phases given by the compositions at points P and Q. M and N are inflexion points. Compositions between PM and NQ are stable to phase separation into neighbouring phases, but not into phases of compositions ϕ_2' and ϕ_2''. These are termed the meta-stable phases. Points between M and N are absolutely unstable and cannot exist in practice. The limits of the unstable region M to N is given by the condition,

$$\frac{\partial^2 \Delta G_{mix}}{\partial \phi_2^2} = \frac{\partial \Delta\mu_2}{\partial \phi_2} = \frac{\partial \Delta\mu_1}{\partial \phi_2} = 0 \qquad 2:33$$

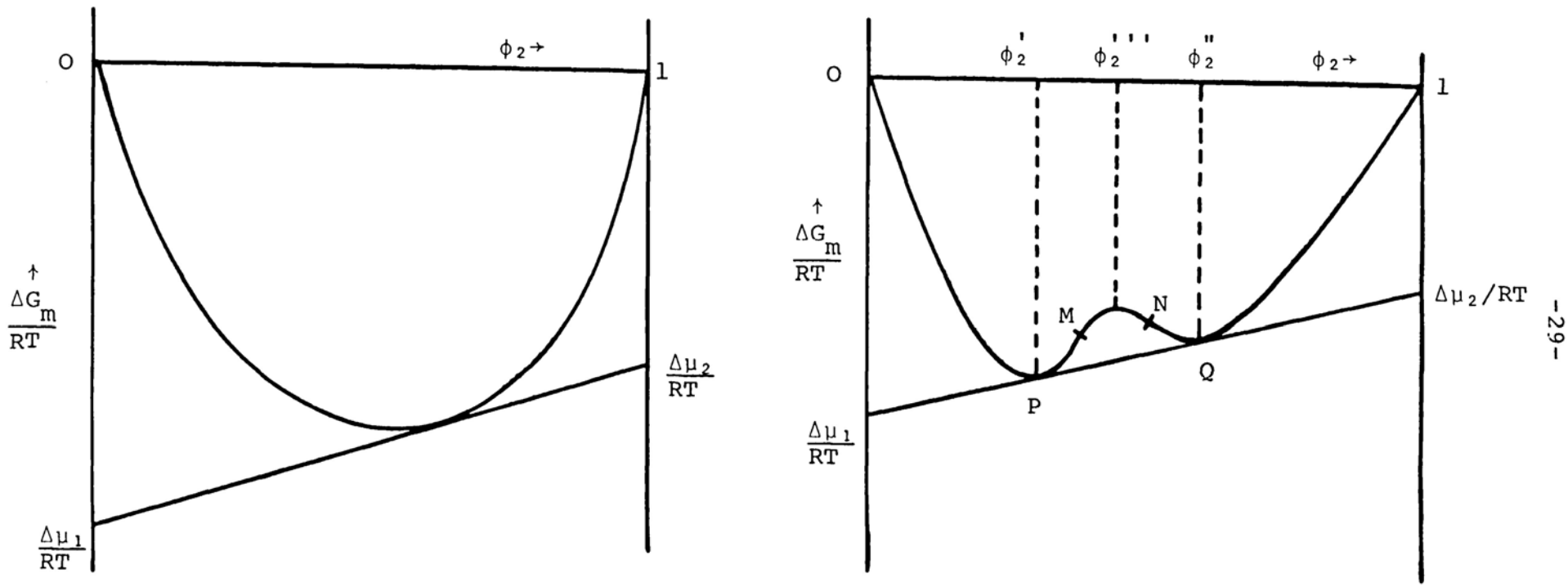


Fig. 2:1. Free enthalpy (Gibbs free energy) of mixing as a function of concentration showing (a) complete and (b) partial miscibility.

If the temperature of mixing is increased, then the curves of type figure 2:1b can go over to curves of type 2:1a. Here the two points of contact of the double tangent and the points of inflexion approach each other until they coincide. The condition for coincidence is given by

$$\frac{\partial^3 \Delta G_{mix}}{\partial \phi_2^3} = 0 \text{ i.e. } \frac{\partial^2 \Delta \mu_1}{\partial \phi_2^2} = \frac{\partial^2 \Delta \mu_2}{\partial \phi_2^2} \qquad 2:34$$

This is a critical condition and the coincident point is called the critical or plait point , and condition 2:34 gives

$$\chi_{12c} = (1-x_1/x_2)/2x_1(1-2\phi_{2c}) \qquad 2:35$$

Applying 2:35 to the equation obtained after applying 2:33 to 2:29 gives, after simplification,

$$\phi_{2c} = (x_1^{\frac{1}{2}})/(x_1^{\frac{1}{2}} + x_2^{\frac{1}{2}}) \quad \text{and} \quad \phi_{1c} = (x_2^{\frac{1}{2}})/(x_1^{\frac{1}{2}} + x_2^{\frac{1}{2}}) \qquad 2:36$$

Substitution of 2:36 into 2:35 gives

$$\chi_{12c} = \frac{1}{2}\{(1/x_1^{\frac{1}{2}}) + (1/x_2^{\frac{1}{2}})\}^2 \qquad 2:37$$

If a graph of T versus ϕ_2 is plotted, a phase diagram is obtained as shown in figures2:2a and 2:2b which show an upper critical solution temperature(UCST) and a lower critical solution temperature(LCST) respectively. The locus of the double tangent points forms the binodal (cloud point curve) ($\partial \Delta G_{mix}/\partial \phi_2 = 0$) which separates the completely miscible region from the meta-stable region, while the locus of the inflexion points forms the spinodal ($\partial^2 \Delta G_{mix}/\partial^2 \phi_2^2 = 0$) separating the meta-stable from the unstable regions. The critical state is denoted by T_c and ϕ_{2c} and is the point where the spinodal meets the binodal. Examples of UCST behavior are the polystyrene-polybutadiene[12 13] and polystyrene-polyisoprene[2 10] systems while examples of LCST behavior are the polystyrene-polyvinyl methyl ether[32] and polyvinylidene fluoride[33] with various

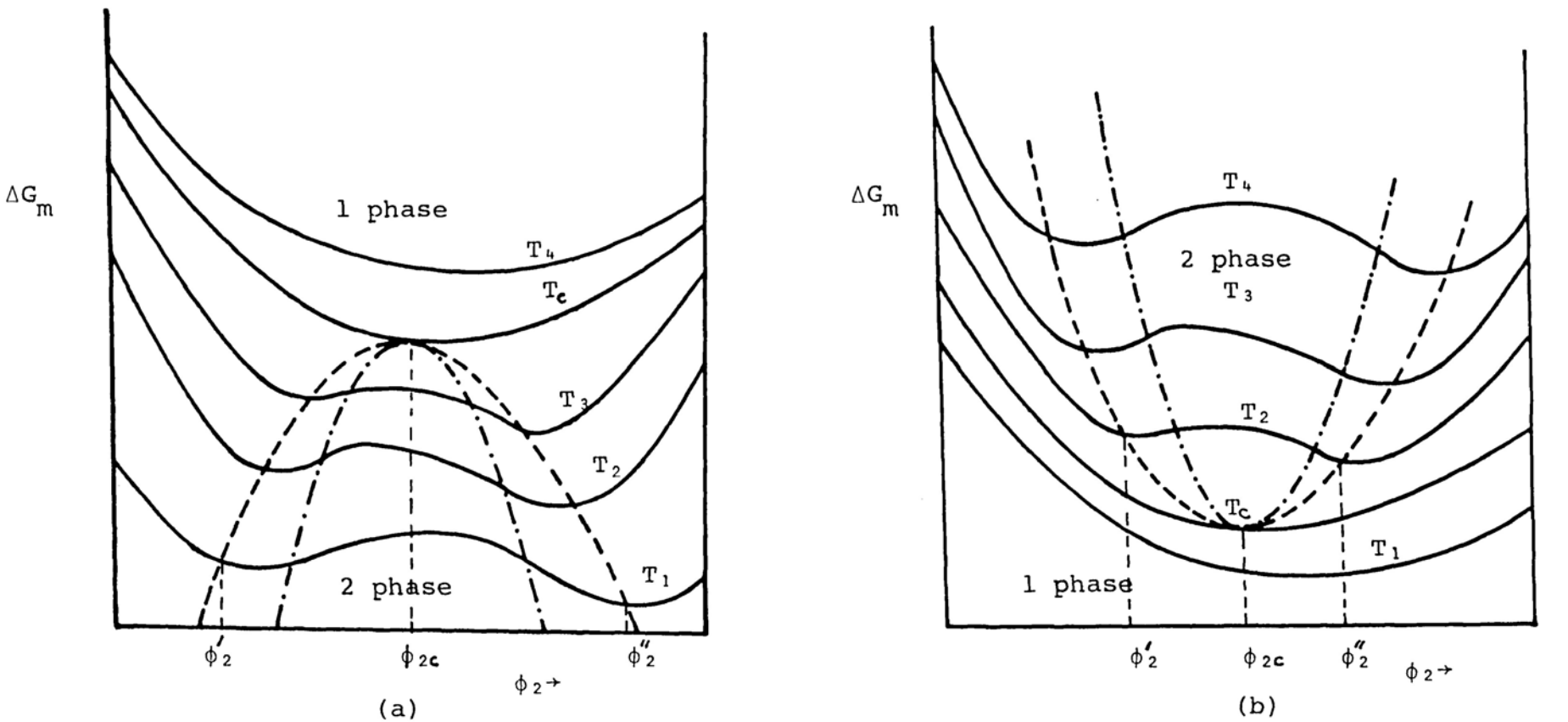


Fig. 2:2. Graphs of ΔG_m versus ϕ_2 at different temperatures giving rise to a (a) UCST and (b) LCST phase boundary if a plot of T(temperature) versus ϕ_2 is made. $T_4 > T_1$, T_c is the critical temperature. (---- cloud point curve, -·-·- spinodal curve).

polyacrylates. McMaster[34] has shown that phase separation occurs in the metastable region by nucleation and growth, which is stable to continuous composition change but not to large composition fluctuations, hence resulting in the formation of nuclei rich in one of the component X. These nuclei have lower energies than the surrounding matrix molecules due to the work done in aggregating the contents of the nuclei and in forming the nuclei surfaces. Thus nucleation is a thermally induced process. The nuclei grow by means of the downhill molecular diffusion of X from the matrix to the X concentration poor region in the immediate vicinity of the nuclei surfaces as a result of the chemical potential gradient set up. The concentrations of X inside the nuclei remain constant, but the boundaries of the nuclei expand with time. The opposing nature of diffusion rate and the rate of nuclei formation results in a maximum growth rate a few degrees below the binodal. In the latter stages, nuclei coarsening occurs via coalescence and Ostwald ripening whereby larger nuclei grow at the expense of the smaller nuclei.

Within the spinodal, the system is unstable to small amplitude concentration fluctuations forming statistical permanent clusters of low energies rich in one of the component X, with regions of lower concentration surrounding these clusters. Molecules of X will spontaneously and continuously diffuse from the regions of lower concentrations into the permanent clusters, resulting in the decomposition of the system into two phases via an oscillating concentration field whose wavelength is determined by minimum free energy considerations, which also determines the scale of the phase structure. Once composition equilibrium is reached, particle coarsening occurs due to viscous flow driven by interfacial tension as the system

minimises its interfacial energies by minimising the amount of interfacial area, giving rise to a spherically dispersed structure and eventually two layers, one on top of the other, if the viscosities of the two phases are low enough. Hence spinodal decomposition is an unstable process which requires no activation energies and is characterised by a high level of phase interconnectivities in both the major and minor phases. However, the level of interconnectivity in the phases is no conclusive indication of the type of process, since shearing during nucleation and growth could also result in interconnecting phases, while on the other hand, coarsening of an originally interconnected structure could lead to a dispersed structure. Spinodal decomposition is usually confirmed by the observation of an isothermal continuous growth of small amplitude composition modulation. At the critical temperature, the phase separation mechanism is solely that of spinodal decomposition due to the absence of the metastable state. These two decomposition mechanisms were observed by Nishi[32] et al in their respective regions in their study of the thermally induced phase separation of polystyrene-polyvinyl methyl ether.

From the above considerations, it can be seen that a negative value of ΔG_{mix} is a necessary, but not absolute, condition for miscibility of a polymer mixture. For complete miscibility over the whole composition range, the second and third derivatives of ΔG_{mix} must be considered in terms of the conditions listed. In general, polymer-polymer mixtures were observed to exhibit lower critical solution behavior with upper critical solution behavior being the exception rather than the rule. This is to be expected, when it is remembered that only very small amounts of energy are required to overcome the interfacial forces which lead to phase separation.

The definition of the interaction parameter, χ_{12}, implies that it is inversely proportional to the absolute temperature, but is independent of the concentration of the mixture. Studies by Gee and Treloar[35] on natural rubber-benzene solutions seem to indicate good agreement between theory and experiments. However, cases in which χ_{12} is concentration dependent have been found[2 8 36 37 38]. Flory and Schultz[39] have shown that the temperature dependence of χ_{12} was not as simple as theory predicted. Although the definition of χ_{12} could cope with both positive and negative heats of mixing by a change in sign, the equation of the spinodal and the critical value of the interaction parameter χ_{12} do not, however, permit negative χ_{12} values. Hence the Flory-Huggins equation can only predict upper critical solution behavior and fails to predict the lower critical solution behavior which is more frequently observed experimentally. All this experimental evidence points towards a reappraisal of the theoretical concepts involved which leads to Flory's formulation of the equation of state. Although the equation of state is an improvement over the Flory-Huggins approach in terms of agreement between theory and experiments in several aspects, the Flory-Huggins approach is still used by numerous experimentalists due to its simplicity compared to the equation of state approach.

2:3. Flory's Equation of State.

Flory's equation of state, initially developed for pure components[40 41] and later extended to binary simple as well as polymeric mixtures[42] is an improvement over the Flory-Huggins theory in that it takes into account the excluded volume effects which are related to the volume change on mixing, as

well as expressing the equivalence of χ_{12} in terms of equation of state parameters which can, and do, predict lower critical solution behavior for polymer blends. Though similar in many ways to the corresponding state theory proposed by Prigogine[43 44] and co-workers, it differs from it in that the relation between a molecule(or segment) and its neighbours is not restricted to their mean positions, thus giving a more realistic representation of the intermolecular energy, beside retaining the randomness of the liquid state. Using three characteristic parameters v*, T* and p*, which can be obtained from density, thermal expansion coefficient and thermal pressure coefficient for the respective pure components, the reduced partition functions for the pure components and the mixture are obtained, from which their respective Helmholtz free energy can be specified, and hence, the free energy of mixing. Since the theoretical aspects of the theory are well outlined[42], only the essential parts will be presented here.

Tonks[45] has shown that the partition function Ω for a one dimensional system of N hard, non-attractive particles arranged on a line of length L could be expressed as

$$\Omega = \{(\ell-\ell^*)e\}^N \qquad 2:38$$

where $\ell=L/N$ and ℓ^* is the hard-core length of a particle. Extending this to three dimensions, the approximate partition function for non-attractive spherical molecules is given by

$$\Omega = \{\gamma_g e^3 v^* (\tilde{v}^{\frac{1}{3}}-1)^3\}^{Nrc} \qquad 2:39$$

where each of the N molecules are divided into r segments (each segment not necessarily equal to a monomeric unit) and

defining $\ell = (\gamma_g v)^{\frac{1}{3}}$ and $\ell^* = (\gamma_g v^*)^{\frac{1}{3}}$, where v^* is the hard core segmental volume and v the volume per molecule(=V/N where V is the total volume of the system). γ_g is a numerical factor which is the same for the pure components and the mixture. The factor 3c(with c<1) represents the number of intermolecular degrees of freedom per segment and $\tilde{v}=v/v^*$ is the reduced volume.

Introducing the mean molecular (attractive) energy E_0 as being additive over the area of surface contacts between segments, the partition function of the pure component takes the form,

$$Z = Z_{comb}\Omega exp^{(-E_0/kT)} = Z_{comb}\Omega exp^{(-Nrs\eta/2v)} \qquad 2:40$$

where s is the number of contact sites per segment (proportional to the surface area per segment) and $-\eta/v$ is the intermolecular energy per contact. Z_{comb} is a combinatorial factor for the number of ways in which rN segments can be arranged over rN sites in space. Defining a reduced temperature $\tilde{T}$ as

$$\tilde{T} = T/T^* = 2v^*ckT/s\eta \qquad 2:41$$

substitution of 2:39 and 2:41 into 2:40 gives

$$Z = Z_{comb}\{[\gamma v^*(\tilde{v}^{\frac{1}{3}}-1)]^{3Nrc} exp^{(Nrc/\tilde{v}\tilde{T})}\} \qquad 2:42$$

where the communal entropy e^{3Nrc} has been absorbed into the constant γ. From thermodynamic considerations, the pressure p of the system is given by

$$p = \frac{kT}{Nr}\left(\frac{\partial \ln Z}{\partial v}\right)_T \qquad 2:43$$

which, following from 2:42 and expressed in reduced form, is

$$\tilde{p}\tilde{v}/\tilde{T} = \{\tilde{v}^{\frac{1}{3}}/(\tilde{v}^{\frac{1}{3}}-1)\} - 1/\tilde{v}\tilde{T} \qquad 2:44$$

where $\tilde{p}=p/p^*=2pv^{*2}/s\eta$ and $\tilde{v}=v/v^*$ as before, with the characteristic parameters obeying the equation

$$p^*v^* = ckT^* \qquad 2:45$$

For matter in the condensed phase where the pressure p is small or equal to zero,

$$\tilde{T} = (\tilde{v}^{\frac{1}{3}}-1)/\tilde{v}^{\frac{3}{4}} \qquad 2:46$$

Defining the thermal expansion coefficient as

$$\alpha = (\partial \ln v/\partial T)_{p=0} \qquad 2:47$$

it follows from 2:45 that

$$\tilde{v}^{\frac{1}{3}}-1 = (\alpha T/3)/(1+\alpha T) \qquad 2:48$$

Defining the thermal pressure coefficient (not to be confused with the numerical factor γg), in the limit of zero pressure as

$$\gamma = (\partial p/\partial T)_v \qquad 2:49$$

From conditions 2:44, 2:45 and the definition of reduced pressure, one obtains

$$p^* = \gamma T \tilde{v}^2 \qquad 2:50$$

2:3.1. Extension of the equation of state to binary mixtures.

To extend the theory developed for the pure components outlined above to mixtures, the following assumptions have to be made:

1) the mixing is assumed to be random and the perturbation due to the differences in the interaction between neighbouring species are negligible.

2) segments of both molecules in the mixture have equal core volume, v^*.

3) for condensed matter, no distinction is made between the Helmholtz and Gibbs free energies since the pressure is low or approximately zero.

Since the form of the partition function is independent of the geometry and disposition of the molecules, the partition function of the mixture will assume a similar

form to that of the pure components, viz.,

$$Z_{mix} = Z_{comb}\{[\gamma v^*(\tilde{v}^{\frac{1}{3}}-1)]^{3N\bar{r}\bar{c}}\exp(N\bar{r}\bar{c}/\tilde{v}\tilde{T})\} \qquad 2:51$$

where Z_{comb} is the combinatory factor for intermixing the two components and

$$N = N_1+N_2 \qquad 2:52$$

$$\bar{r} = (r_1N_1+r_2N_2)/N \qquad 2:53$$

$$\bar{c} = (r_1N_1c_1+r_2N_2c_2)/\bar{r}N \qquad 2:54$$

Due to the introduction of these mixture parameters, it will be more convenient, later on, to redefine ϕ_i as the segment instead of the volume fraction. Then

$$\phi_i = r_iN_i/\bar{r}N \qquad 2:55$$

Using the thermodynamic relationship for the Helmholtz free energy,

$$F = -kT\ln Z \qquad 2:56$$

gives,

$$F_{mix} = -kT\{\ln Z_{comb}+3N\bar{r}\bar{c}\ln(\gamma v^*)+3N\bar{r}\bar{c}\ln(\tilde{v}^{\frac{1}{3}}-1)+N\bar{r}\bar{c}/\tilde{v}\tilde{T}\} \qquad 2:57$$

$$F_1 = -kT\{\ln Z_{1_{comb}}+3N_1r_1c_1\ln(\gamma v^*)+3N_1r_1c_1\ln(\tilde{v}_1^{\frac{1}{3}}-1)+N_1r_1c_1/\tilde{v}_1\tilde{T}_1\} \qquad 2:58$$

$$F_2 = -kT\{\ln Z_{2_{comb}}+3N_2r_2c_2\ln(\gamma v^*)+3N_2r_2c_2\ln(\tilde{v}_2^{\frac{1}{3}}-1)+N_2r_2c_2/\tilde{v}_2\tilde{T}_2\} \qquad 2:59$$

$$\Delta F_{mix} = Fmix - F_1 - F_2$$

$$= -kT\ln(Z_{comb}/Z_{1_{comb}}Z_{2_{comb}})+3kTN_1r_1c_1\ln\{(\tilde{v}_1^{\frac{1}{3}}-1)/(\tilde{v}^{\frac{1}{3}}-1)\}$$

$$+3kTN_2r_2c_2\ln\{(\tilde{v}_2^{\frac{1}{3}}-1)/(\tilde{v}^{\frac{1}{3}}-1)\}+kTN_1r_1c_1\{(1/\tilde{v}_1\tilde{T}_1)-(1/\tilde{v}\tilde{T})\}$$

$$+kTN_2r_2c_2\{(1/\tilde{v}_2\tilde{T}_2)-(1/\tilde{v}\tilde{T})\} \qquad 2:60$$

Substituting the first term of equation 2:60 by the combinatorial entropy term from the Flory-Huggins considerations and applying 2:45 of the pure components to the other terms yields

$$\Delta F_{mix} = -kT\bar{r}N\{(\phi_1/r_1)\ln\phi_1+(\phi_2/r_2)\ln\phi_2\}$$
$$+3N_1p_1^*V_1^*\tilde{T}_1\ln\{(\tilde{v}_1^{\frac{1}{3}}-1)/(\tilde{v}^{\frac{1}{3}}-1)\}$$
$$+3N_2p_2^*V_2^*\tilde{T}_2\ln\{(\tilde{v}_2^{\frac{1}{3}}-1)/(\tilde{v}^{\frac{1}{3}}-1)\}$$
$$+N\bar{r}v^*\{(\phi_1p_1^*/\tilde{v}_1)+(\phi_2p_2^*/\tilde{v}_2)-(\phi_1p_1^*\tilde{T}_1/\tilde{v}\tilde{T})-(\phi_2p_2^*\tilde{T}_2/\tilde{v}\tilde{T})\} \quad 2:61$$

where $V_i^* = r_iv^*$ = core molecular volume. For a mixture, equation 2:45 assumes the form

$$p^*v^* = \bar{c}kT \quad 2:62$$

From 2:54,

$$p^*v^*/T^* = k(c_1\phi_1+c_2\phi_2) = (\phi_1p_1^*v^*/T_1^*)+(\phi_2p_2^*v^*/T_2^*)$$

therefore,

$$p^* = (\phi_1p_1^*\tilde{T}_1/\tilde{T}) + (\phi_2p_2^*\tilde{T}_2/\tilde{T}) \quad 2:63$$

Substituting 2:63 into 2:61 gives

$$\Delta F_{mix} = -kT\bar{r}N\{(\phi_1/r_1)\ln\phi_1+(\phi_2/r_2)\ln\phi_2\}$$
$$+3N_1p_1^*V_1^*\tilde{T}_1\ln\{(\tilde{v}_1^{\frac{1}{3}}-1)/(\tilde{v}^{\frac{1}{3}}-1)\}$$
$$+3N_2p_2^*V_2^*\tilde{T}_2\ln\{(\tilde{v}_2^{\frac{1}{3}}-1)/(\tilde{v}^{\frac{1}{3}}-1)\}$$
$$+N\bar{r}v^*\ (\phi_1p_1^*/\tilde{v}_1)+(\phi_2p_2^*/\tilde{v}_2)-(p^*/\tilde{v}) \quad 2:64$$

The energy of the mixture E_{0_m} assumes a similar form to that of the pure components, i.e.,

$$-E_{0_m} = (A_{11}\eta_{11}+A_{22}\eta_{22}+A_{12}\eta_{12})/v \quad 2:65$$

where A_{ij} is the number of i,j contacts, each contact characterised by an energy $-\eta_{ij}/v$. For random mixing,

$$A_{12} = s_1r_1N_1\theta_2 = s_2r_2N_2\theta_1 \quad 2:66$$

and

$$2A_{11}+A_{12} = s_1r_1N_1 \quad \text{and} \quad 2A_{22}+A_{12} = s_2r_2N_2 \quad 2:67$$

where

$$\theta_2 = 1-\theta_1 = s_2r_2N_2/(s_1r_1N_1+s_2r_2N_2)$$

$$= \phi_2(s_2/s_1)/\{\phi_1+\phi_2(s_2/s_1)\} \qquad 2:68$$

Applying 2:66 and 2:67 to 2:65 gives,

$$\frac{-E_{0_m}}{\bar{r}n} = \{\theta_1\eta_{11}+\theta_2\eta_{22}-\theta_1\theta_2\Delta\eta\}\{s/2v\} \qquad 2:69$$

where

$$\Delta\eta = \eta_{11}+\eta_{22}-2\eta_{12} \qquad 2:70$$

and

$$s = (s_1r_1N_1+s_2r_2N_2)/\bar{r}N = \phi_1s_1+\phi_2s_2 \qquad 2:71$$

By an analogous definition to the energy of a pure component, the energy of the mixture can be defined as

$$\frac{-E_{0_m}}{\bar{r}n} = \frac{p^*v^*}{\tilde{v}} \qquad 2:72$$

Comparision of equation 2:72 with 2:69 yields,

$$\frac{p^*v^*}{\tilde{v}} = \frac{1}{2v}(\phi_1s_1\eta_{11}+\phi_2s_2\eta_{22}+\phi_1\theta_2s_1\Delta\eta)$$

therefore,

$$p^* = \{(\phi_1s_1\eta_{11}/2v^{*2})+(\phi_2s_2\eta_{22}/2v^{*2})+(\phi_1\theta_2s_1\Delta\eta/2v^{*2})\} \qquad 2:73$$

Substituting the pure component equivalent of the reduced pressure into 2:73 gives,

$$p^* = \phi_1p_1^* + \phi_2p_2^* + \phi_1\theta_2X_{12} \qquad 2:74$$

where

$$X_{12} = \frac{s_1\Delta\eta}{2v^{*2}} \qquad 2:75$$

Hence, equation 2:64 takes the form

$$\Delta F_{mix} = \Delta G_{mix} = -kT\bar{r}N[(\phi_1/r_1)\ln\phi_1+(\phi_2/r_2)\ln\phi_2]$$
$$+3N_1p_1^*V_1^*\tilde{T}_1\ln[(\tilde{v}_1^{\frac{1}{3}}-1)/(\tilde{v}^{\frac{1}{3}}-1)]$$
$$+3N_2p_2^*V_2^*\tilde{T}_2\ln[(\tilde{v}_2^{\frac{1}{3}}-1)/(\tilde{v}^{\frac{1}{3}}-1)]$$
$$+\bar{r}Nv^*[\phi_1p_1^*(1/\tilde{v}_1-1/\tilde{v})+\phi_2p_2^*(1/\tilde{v}_2-1/\tilde{v})+(\phi_1\theta_2X_{12}/\tilde{v})] \qquad 2:76$$

The first square bracketed term contains the combinatorial entropy contribution while the last square bracketed terms are the usual heats of mixing correction expressed in equation of state parameters. The middle two terms are the residual entropy of mixing contribution which arises from the differences between the equation of state parameters for the pure components. From equation 2:76, the chemical potential of component 1 is

$$\Delta\mu_1 = \frac{\partial \Delta F_{mix}}{\partial N_1}\bigg|_{T,\tilde{v},N_2} + \frac{\partial \Delta F_{mix}}{\partial \tilde{v}}\bigg|_{T,N_1,N_2}\left|\frac{\partial \tilde{v}}{\partial N_1}\right|_{T,V,N_2}$$

$$= RT\{\ln\phi_1 + (1-r_1/r_2)\phi_2\} + \theta_2^2(V_1^* X_{12}/\tilde{v})$$

$$+ p_1^* V_1^* \{3\tilde{T}_1 \ln\{(\tilde{v}_1^{\frac{1}{3}}-1)/(\tilde{v}^{\frac{1}{3}}-1)\} + (1/\tilde{v}_1 - 1/\tilde{v}) + \tilde{p}_1(\tilde{v}-\tilde{v}_1)\} \qquad 2:77$$

Flory and Eichinger[42] neglected the $\tilde{p}_1(\tilde{v}-\tilde{v}_1)$ term at atmospheric pressure, as was pointed out by McMaster[15] who, in turn, was found to have evaluated the $\frac{\partial \tilde{v}}{\partial N_1}\Big|_{T,V,N_2}$ derivative at constant pressure and not at constant volume by Sanchez[46]

Hence

$$\frac{\Delta\mu_1}{RT} = \ln\phi_1 + \phi_2(1-r_1/r_2) + \{(\mu_1-\mu_1^0)^R/RT\phi_2^2\}\phi_2^2 \qquad 2:78$$

where $(\mu_1-\mu_1^0)^R$ is called the residual chemical potential. Comparision between 2:29 and 2:77 establishes that

$$r_1\chi_{12} = (\mu_1-\mu_1^0)^R/RT\phi_2^2 \qquad 2:79$$

where x and r denote the same quantity in the two notations used, while for polymer solution

$$\chi_{12} = (\mu_1-\mu_1^0)^R/RT\phi_2^2 \qquad 2:80$$

since $r_1 = 1$. From the definitions of the interaction parameter (cf. equations 2:23 and 2:80), it is obvious that whereas the Flory-Huggins theory can only predict an inverse dependence

of the interaction parameter on the absolute temperature, the equation of state can predict both the inverse temperature dependence and the concentration dependence. Neglecting the $\tilde{p}_1(\tilde{v}-\tilde{v}_1)$ term at atmospheric pressure,

$$\chi_{12} = \frac{\Delta\mu_1^R}{RT\phi_2^2} = \frac{p_1^* V_1^*}{RT\phi_2^2}[3\tilde{T}_1 \ln\{(\tilde{v}_1^{\frac{1}{3}}-1)/(\tilde{v}^{\frac{1}{3}}-1)\}+(1/\tilde{v}_1-1/\tilde{v})]+\frac{V_1^* X_{12}\theta_2^2}{RT\tilde{v}\phi_2^2} \qquad 2:81$$

while from the chemical potential of component 2,

$$\chi_{12}' = \frac{\Delta\mu_2^R}{RT\phi_1^2}\frac{V_1^*}{V_2^*} = \frac{1}{RT\phi_1^2}\frac{V_1^*}{V_2^*}\{p_2^* V_2^*[3\tilde{T}_2 \ln\{(\tilde{v}_2^{\frac{1}{3}}-1)/(\tilde{v}^{\frac{1}{3}}-1)\}+(1/\tilde{v}_2-1/\tilde{v})]$$

$$+ V_2^* X_{12}(s_2/s_1)\theta_1^2/\tilde{v}\} \qquad 2:82$$

In the limit of $\phi_2 \to 0$, the square bracketed terms in equations 2:81 and 2:82 are either zero or negligibly small. Hence at the limit of infinite dilutions,

$$\chi_{12}^0 = \lim_{\phi_2 \to 0} \chi_{12} \simeq \frac{V_1^* X_{12}}{RT\tilde{v}_1}(s_2/s_1)^2 \qquad 2:83$$

and

$$\chi_{12}^{0\prime} = \lim_{\phi_2 \to 0} \chi_{12} \simeq \frac{V_1^* X_{12}}{RT\tilde{v}_1}(s_2/s_1) \qquad 2:84$$

Hence,

$$\frac{\chi_{12}^0}{\chi_{12}^{0\prime}} = \frac{s_2}{s_1} \qquad 2:85$$

This discrepancy was pointed out by Chai[47] and equations 2:81 and 2:82 when plotted against ϕ_2 will result in two different concentration dependent curves. The introduction of the surface contact areas, though convenient in explaining the concentration dependence of X_{12}, has an inherent difficulty when s_2 is not equal to s_1. This could possibly account for Flory[42] et al's introduction of a correction

factor (Q_{ij}) introduced empirically to give better agreement between experiment and theory. They also observed that the agreement improves as the ratio of s_2/s_1 approaches unity. The importance of the part played by surface contact areas in the thermodynamics of polymer mixtures should not be underestimated. As was pointed out by Konningsveld[48] et al, Huggins[49 50 51] new theory, which also considers interacting contact surfaces, can qualitatively describe some of the peculiar features of phase boundaries of some oligomer/polymer mixtures, although quantitative agreement is still lacking. Using Sanchez's[46] approach, the equation of the spinodal(from the free energy equation) is given by

$$(\partial\Delta\mu_1/RT\partial\phi_2)_{T,p} = 0 \qquad 2:86$$

Hence from equation 2:76,

$$-(1/\phi_1) - (p_1^*V_1^*/RT_1^*)\{1/\tilde{v}^{\frac{2}{3}}(\tilde{v}^{\frac{1}{3}}-1)\}(\partial\tilde{v}/\partial\phi_2) + (1-r_1/r_2)$$

$$+ (p_1^*V_1^*/RT)\{(1/\tilde{v}^2)+\tilde{p}_1\}(\partial\tilde{v}/\partial\phi_2)$$

$$+ (V_1^*X_{12}/RT)\{(2\theta_2\theta_1\theta_2/\tilde{v}\phi_1\phi_2)-(\theta_2^2/\tilde{v}^2)(\partial\tilde{v}/\partial\phi_2)\} = 0 \qquad 2:87$$

where

$$\frac{\partial\tilde{v}}{\partial\phi_2} = \frac{\{(\partial\tilde{p}/\partial\phi_2)-(1/\tilde{T})\{\tilde{p}+(1/\tilde{v}^2)\}(\partial\tilde{T}/\partial\phi_2)\}}{\{\tilde{v}^{\frac{2}{3}}-\tilde{T}(\tilde{v}^{\frac{1}{3}}-2/3)/\tilde{v}^{\frac{5}{3}}(\tilde{v}^{\frac{1}{3}}-1)^2\}} \qquad 2:88$$

and

$$(\partial\tilde{p}/\partial\phi_2) = (p/p^{*2})\{p_1^*-p_2^*+X_{12}\theta_2(\frac{\theta_1}{\phi_2}-1)\} \qquad 2:89$$

and

$$(\partial\tilde{T}/\partial\phi_2) = (T/p^*)\{(p_2^*/T_2^*)-(p_1^*/T_1^*)\}$$

$$+ (\tilde{T}/p^*)\{p_1^*-p_2^*+X_{12}\theta_2(\frac{\theta_1}{\phi_2}-1)\} \qquad 2:90$$

while the critical condition is given by,

$$(\partial^2\Delta\mu_1/RT\partial\phi_2^2) = 0 \qquad 2:91$$

Therefore,

$$-(1/\phi_1^2)+(p_1^*V_1^*/RT_1^*)\left[\{(1-2/3\tilde{v}^{\frac{1}{3}})(\partial\tilde{v}/\partial\phi_2)^2/\tilde{v}^{\frac{4}{3}}(\tilde{v}^{\frac{1}{3}}-1)^2\}\right.$$

$$\left.-(\partial^2\tilde{v}/\partial\phi_2^2)\{\tilde{v}^{\frac{2}{3}}(\tilde{v}^{\frac{1}{3}}-1)\}^{-1}\right]+(p_1^*V_1^*/RT)\left[(-2/\tilde{v}^3)(\partial\tilde{v}/\partial\phi_2)^2\right.$$

$$\left.+\{(1/\tilde{v}^2)+\tilde{p}_1\}(\partial^2\tilde{v}/\partial\phi_2^2)\right]+(V_1^*X_{12}/RT)\left[(1/\tilde{v})\left[2(\partial\theta_2/\partial\phi_2)^2\right.\right.$$

$$\left.+2\theta_2(\partial^2\theta_2/\partial\phi_2^2)\right]-(1/\tilde{v}^2)\left[4\theta_2(\partial\theta_2/\partial\phi_2)(\partial\tilde{v}/\partial\phi_2)+\theta_2^2(\partial^2\tilde{v}/\partial\phi_2^2)\right]$$

$$\left.+(\theta_2^2/\tilde{v}^3)(\partial\tilde{v}/\partial\phi_2)^2\right] = 0 \qquad 2:92$$

These two equations could also be used to examine the effect of pressure on the mixture. At low pressure, the results should be similar to those obtained using Flory's equation (2:76) which neglected the $\tilde{p}\tilde{v}$ term.

Using the generalised version of Flory's theory, McMaster[15] examined the contribution of the equation of state parameters to the miscibility of polymer blends by allowing perturbations around the base values of these parameters. He observed that the theory is capable of predicting both LCST and UCST behavior, with LCST behavior being the more common in polymer mixtures. This is in good agreement with general experimental observations. The interaction parameter can assume both positive and negative values, and both LCST and UCST behavior exist together only over a small range of positive X_{12} values. Above this range, the two critical points meet to form an hour-glass shaped phase boundary. Of the equation of state parameters, the most important parameter affecting the miscibility is the thermal expansion coefficient which affects most of the other equations involved, though other parameters do affect the shape and extent of the phase

boundary curves, but to a smaller extend. Less than four percent difference in the thermal expansion coefficients must be observed if two polymers are to be compatible with each other at high molecular weights. However, McMaster's attempt to support his theoretical observations qualitatively with experimental evidence met with less success. Except for the LCST behavior observed, the effects of the other equation of state contributions were not obvious. Using the solvent-probe technique of inverse chromatography, Olabisi[52] observed an LCST behavior in the polyvinylchloride-polycaprolactone system and showed that the bimodality observed in that system could be a result of the odd combinations of large differences in the pure component properties (usually resulting in immiscibility according to MCmaster) and a large negative interaction parameter (favouring compatibility).

Using equation 2:87 Chai[47] simulated the spinodal behavior of the same polymer mixture as that of McMaster using McMaster's data. Like Flory, he neglected the translational motion term that was considered by McMaster. The general trend of the observations using this equation was similar to those of McMaster, except that the temperature range observed for the spinodal is now much more realistic and the dependence of the spinodal on molecular weight and thermal expansion coefficient is reduced.

Though the equation of state is an improvement over the Flory-Huggins theory in many respects, it has its own inherent difficulty in that numerous data are required for computing the various equations giving the spinodal, binodal as well as the ratio s_2/s_1, on which various equation of state parameters

so sensitively depend. This ratio cannot be accurately determined at present. The aim of the present work is to investigate whether the heats of mixing of oligomeric systems might help to shed some light on various aspects of these two major theories.

CHAPTER 3

DESCRIPTION OF CALORIMETER AND LIGHT SCATTERING TURBIDIMETER.

3:1. Description of calorimeter.

The overall design of the calorimeter was based on a National Bureau of Standards[53] model designed for solution work, modified in various aspects to suit the needs for measuring the heats of mixing of oligomers. It is a batch-type, heat conduction calorimeter which depends on the measurement of a temperature change. In general, a heat conduction calorimeter consists of a calorimeter compartment or cell surrounded by a heat flow device which, in turn, is surrounded by a heat sink (or block). The heat sink is kept at a constant temperature by one or more constant temperature jackets. The heat flow device consists of multiple-junction, serially connected thermocouples (also called Peltier or thermoelectric cells) between an inner face in good contact with the calorimeter cell and an outer face in good contact with the heat sink. The general construction of the calorimeter is shown in figures 3:1 and 3:2 which show a side cross-sectional view with a loaded cell and an end cross-sectional view. The detailed specifications of each component will be outlined below. In deciding the modifications required, the following factors were taken into considerations:

a) the viscosities of the oligomers as compared to those of aqueous or organic solutions,

b) the low thermal conductivities of the oligomers in general,

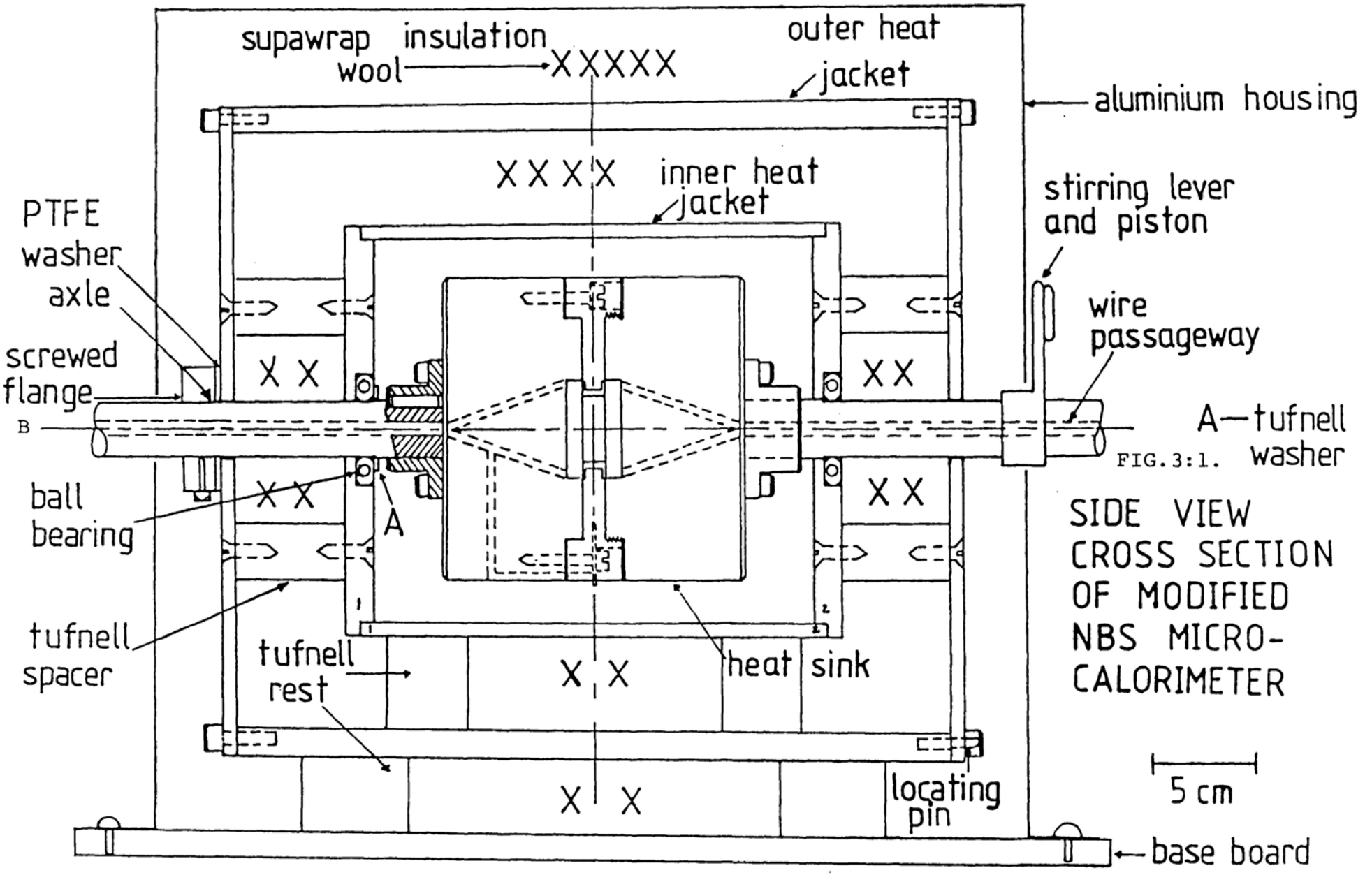


FIG.3:1. SIDE VIEW CROSS SECTION OF MODIFIED NBS MICRO-CALORIMETER

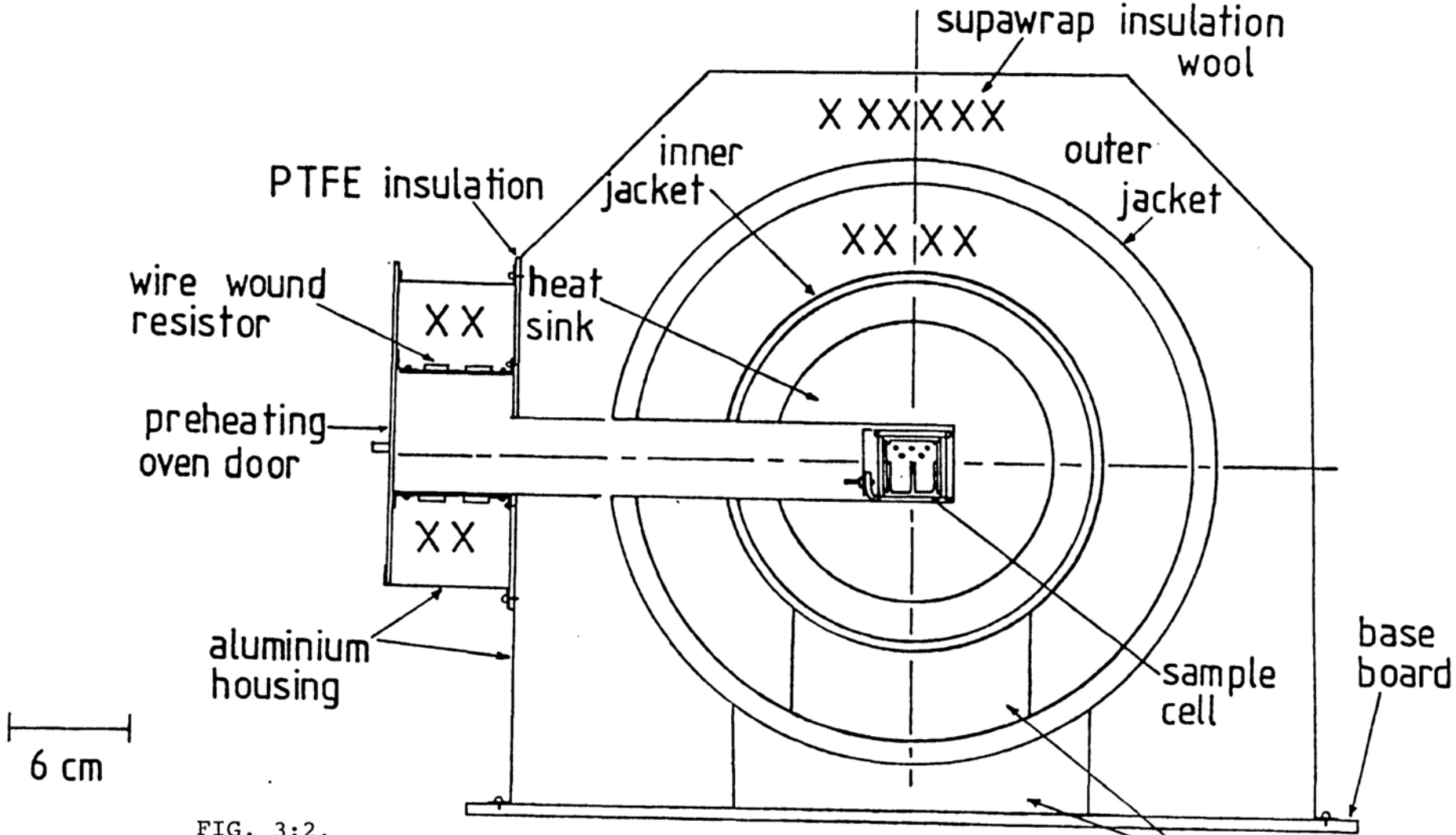


FIG. 3:2.

MICROCALORIMETER—END VIEW CROSS SECTION

c) the temperature of the phase boundaries would necessitate experiments to be carried out at temperatures above room temperatures and

d) the quantity of heat involved in the reactions will probably be small.

3:1.1. The outer heat jacket.

The outer heat jacket is made up of an aluminium cylinder 13 inches long with a 12 inches outer diameter, ½ inch thick walls and ¼ inch thick end-plates.The end-plates are secured to the cylinder by eight evenly spaced allen-type screws. Locating marks and two dowel pins at each end ensure correct repositioning of the end-plates after removal. The axle of the central heat sink passes through the end-plates via appropriately sized holes. A vertical rectangular cut-out on the side, at the mid-point of the cylinder length facilitates side loading of the calorimeter(reaction) cell into and out of the heat sink.

The outer heat jacket is heated by nichrome resistance tapes bifilar wound around the cylinder on top of mica tapes which act as electrical insulators. Bifilar winding is necessary to prevent stray magnetic fields from being set up by the current flowing through the nichrome tape. This is important because should such magnetic fields be set up, then stray e.m.f. could be generated when the heat sink is rotated and the wires in it cut across these fields. The nichrome tapes were secured with fibre glass tapes. The jacket sits on two tufnell rests which were secured to the base board by bolts.

3:1.2. The inner heat jacket.

The inner heat jacket is also made up of an aluminium cylinder 8½ inches long with a 7½ inches outer diameter, ¼ inch thick walls and ½ inch thick end-plates, through which the axle of the central heat sink also passes via push-fitted bearings countersunk into the end-plates. Half of the thickness of each end-plate was countersunk into the inside of the inner heat jacket by a lip. The end-plates of both the inner and outer heat jackets were joined at each end by four tufnell rods and countersunk screws so that both end-plates could be removed as a single unit. One end has the bearing countersunk on the inside of the inner jacket end-plate while the bearing at the other end is countersunk on the outside as shown. The central heat sink unit can only be removed from the end where the bearing is countersunk on the outside of the end-plate, together with the single end-plate unit at that end. The axle was tapered slightly at various appropriate sections to facilitate this removal and subsequent reassembly. A vertical rectangular cut-out at the half-way point in line with the cut-out in the outer heat jacket provides for cell loading via an aluminium guide. The opening of the guide is closed by a plug of perspex wound with fibre glass insulation. This removable plug ensures rapid loading of the calorimeter cell. Similar to the outer heat jacket, the inner heat jacket is heated by means of nichrome resistance tapes with similar electrical insulation and securing arrangements. It is supported by two circular, segmental tufnell rests which sit inside the outer heat jacket. The space in between the jackets are filled with Supawrap 100 loft insulating material to act as heat insulators.

3:1.3. The central heat sink unit.

In order to obtain good precision, accuracy and high sensitivity, the heat sink unit must be kept at a fairly constant temperature, preferably to within a micro-degree. This entails that the heating jacket temperatures be regulated to within point one of a milli-degree. Apart from this, the heat sink unit should also be large enough so that the small amounts of heat introduced or extracted by the calorimeter cell will not alter the heat sink temperature too significantly. This was done by using a cylindrical aluminium block 5½ inches long and 5½ inches in diameter. It is machined out in five parts, the shape of each part being as shown in the enlarged diagram in figure 3:3. The inner faces of the end-pieces have their outer edges lipped by 5/16 inch to enable the central piece to have an extruding lip. This was done to ensure non-slippage inthe vertical plane and better surface contact. The inner surfaces of the end-pieces also each have a rectangular hollow (1.61 inches wide×2.25 inches long×0.3125inch deep) machined out in the center to accomodate the heat flow detecting units.

The thickness of the thinner part of the center I-shaped piece depends on the thickness of the cell used. The surfaces adjacent to the detecting unit front copper plates were also lipped to isolate the front copper plates from the rest of the heat sink. This is to ensure that the heat is conducted into or out of the calorimeter cell via the thermoelectric units only. A rectangular hollow in the center part of this piece, in line with the cut-outs in the jackets accomodates the fully assembled calorimeter cell. The cell is push-fitted

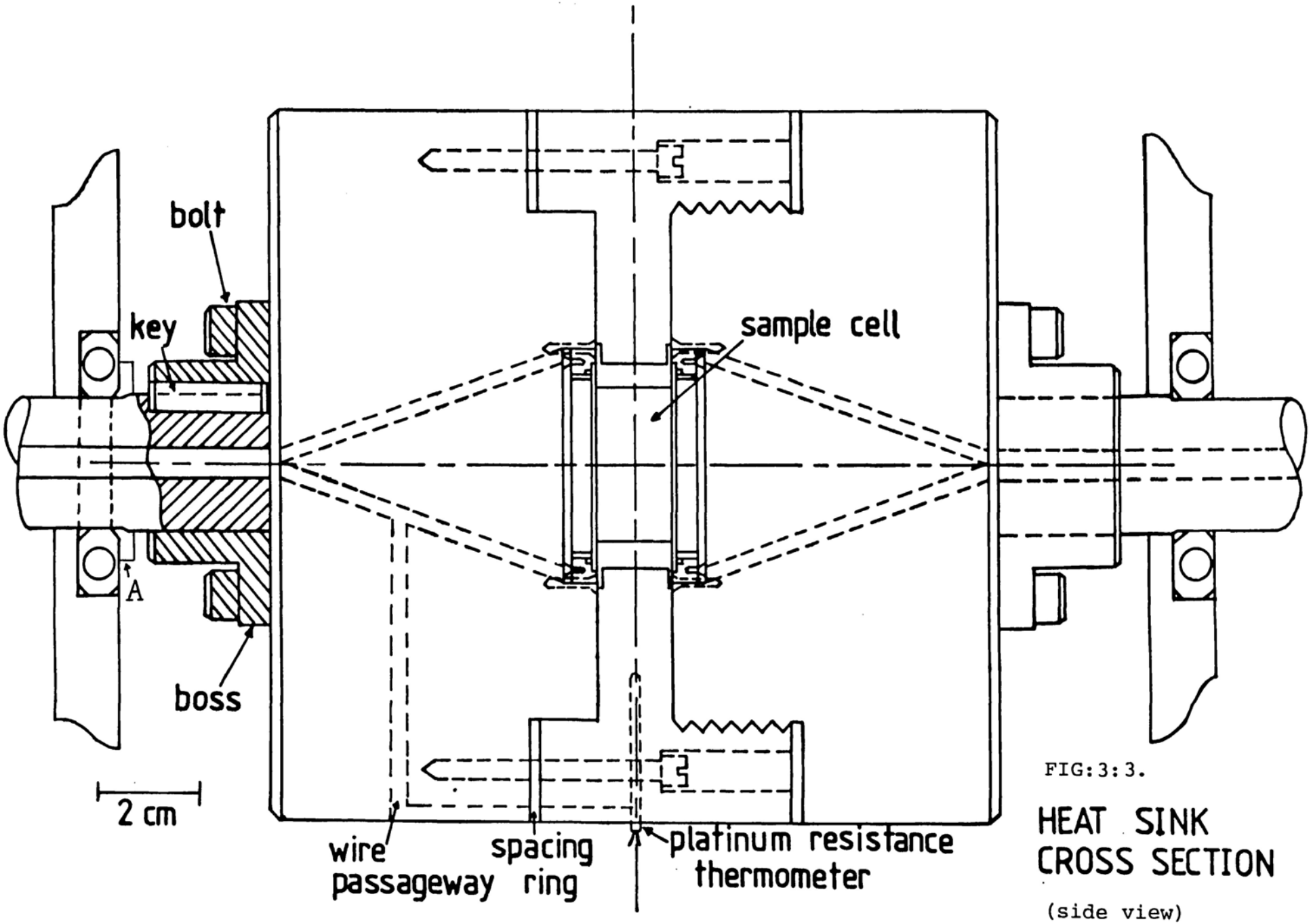


FIG:3:3.

HEAT SINK
CROSS SECTION

(side view)

into the space and is isolated from the rest of the heat sink as described later (see section 3:1.5), but in good contact with the front copper plates of the heat detecting units on both sides. To enable thicker or thinner cells to be used, the thickness of the two spacing rings on either side of the center piece could be altered, so that more or less sample could be used, but within the limit of the heat sink unit being able to be accommodated within the space of the two end-plates. The three pieces to the left were held together by two countersunk aluminium bolts. The spacing ring to the right of the center piece was held in place by the right side end-piece screwed onto the center piece via threads tapped as shown. For good thermal contact of all mating surfaces, the surfaces were ground and polished and smeared with a thin layer of heat sink compound (aluminium oxide grease).

The tufnell axle is connected at each side by means of araldite glue at the end of the axle and a key in the aluminium annular boss. The annular boss is attached at each end to the heat sink by three equally spaced allen screws. A guiding tufnell washer A between the annular boss and the inside of the inner jacket end-plate and a fixed flange at B outside the outer jacket end-plate ensures correct alignment of the cut-outs in the jackets and heat sink during assembly. Inclined passageways through the heat sink unit and the center of the axle length provide for wires from the heat detecting units to be led out at both ends. Teflon insulated wires were used inside the calorimeter due to the high temperature used (up to 100 ^{0}C). The temperature of the block is measured by a BS 1904 (1964) 38.5 ohm range platinum resistance thermometer in conjunction with a decade resistance box. The thermometer

is placed just above the calorimeter cell and as near to the center of the heat sink as possible, in order to evenly dissipate the slight heating (1μW) caused by the resistance.

3:1.4. The heat flow detecting units.

Each unit consists of four thermoelectric modules (Cambion model 801-3960-01) each of dimensions 0.85 inch long×0.66 inch wide×0.21 inch thick, arranged in a rectangular array and joined in series. Each module consists of nine thermocouple junctions made of semi-conducting materials, approximately point one inch cube in size, joined in series and electrically insulated by ceramic plates. These modules are sandwiched inside a tufnell frame and between two copper plates as shown in figure 3:4, with contact surfaces smeared with heat sink compound. The back copper plate and the tufnell frame have the same dimensions as the hollow they lie in, except for their thicknesses, which together equal the depth of the hollow. The back copper plate is attached to the tufnell frame by countersunk screws. Holes in the corners allow wires to be led out to the passageways in the heat sink unit. The front copper plate is recessed into the frame and glued down with araldite glue which was placed in the second recess in the tufnell frame.

The whole unit is held in place in the heat sink unit by allen bolts at the junction between the outer edges of the tufnell frame and the edges of the rectangular hollow of the heat sink end-pieces, with semi-circular recesses in the outer edges of the tufnell frame for the allen bolt heads. Care was taken to ensure that the bolt heads do not come into contact

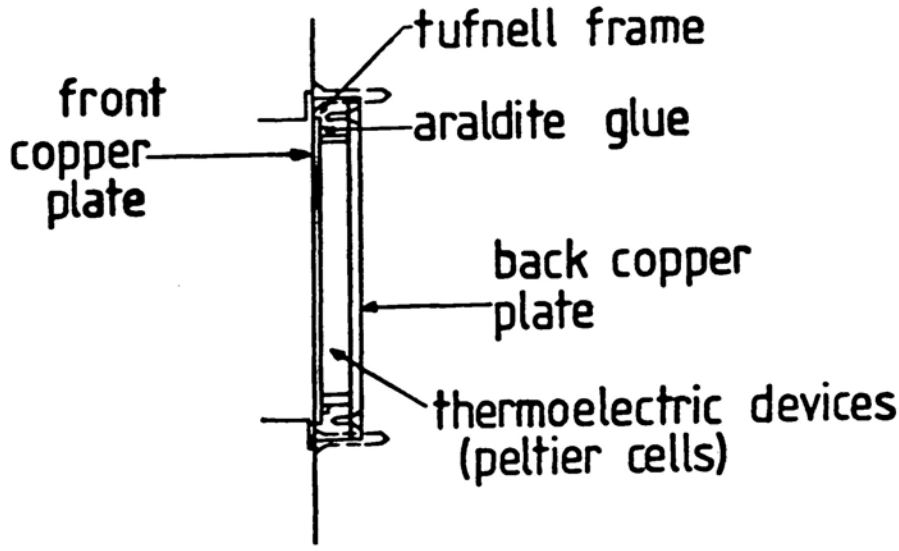


FIG.3.4. HEAT SINK—HEAT DETECTION UNIT

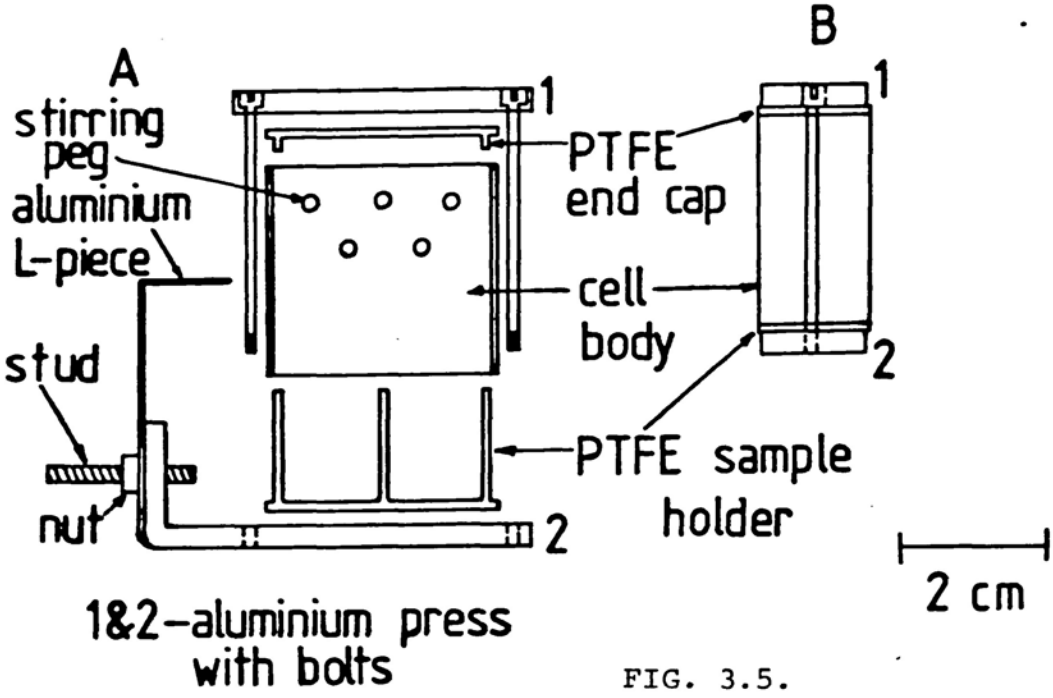


FIG. 3.5.

A EXPLODED CROSS SECTIONAL VIEW OF CELL COMPONENTS

B SIDE VIEW OF ASSEMBLED CELL

with the front copper plate which is isolated from the rest of the heat sink by the lip in the center piece of the heat sink block and the tufnell frame, except through the semi-conducting material of the thermoelectric modules. The thermoelectric modules are capable of withstanding temperatures up to 120 ^{0}C.

3:1.5. Calorimeter cell.

The calorimeter cell is made up of four parts. Figures 3:5a and 3:5b shows an exploded side view cross-section and an end view of an assembled cell. The main part of the cell body is made out of number 16 aluminium waveguide tubes with wall thickness of about one millimeter. The finished cell body measures 28mm in length, 30mm in width and 15mm in thickness externally. The samples are contained in a two compartment PTFE rectangular sample holder which is inserted into the lower half of the main cell body during assembly. It has a wall thickness of 1mm and a 1mm lip all round the bottom. This lip acts as a seal as well as a heat insulator to isolate the main cell body from the rest of the assembly and the heat sink. One corner of the sample holder is cut so that when the complete cell is assembled, the inside of the cell is opened to the atmosphere. This is to prevent a pressure build up inside the cell which could cause leakages, especially at high temperatures. This also ensures that all measurements are carried out at atmospheric pressure. The top half of the main cell body is sealed by an end-cap(PTFE), also with a lip all round it for the same purpose as the lip round the sample holder.

When assembled, the cell components are held in place by the aluminium press and bolt arrangement as shown, to prevent leaking. The press is smaller in width than the main cell body thickness, so that when assembled, the sides of the main cell body protrude outwards compared to the press. This was done to prevent the press from coming into contact with the front copper plate of the heat detection units. Insertion of the cell into the heat sink is via a long rod which is screwed onto the stud and nut arrangement on the bottom part of the press and a passageway that leads from the outside through the heat jackets. The inverted L-shaped piece helps to act as a draught excluder during the mixing process. Aluminium rods, embedded across the top half of the main cell body serve to break up the flow and assist in conducting the heat from the middle of the sample to the side of the cell. The construction of the cell in this way enables ease of weighing in the sample and ease of cleaning of the cell.

When completely assembled, the whole calorimeter is enclosed in an aluminium housing which is secured to a base-board by screws. The housing is made in three pieces, held together by self-tapping screws. The two end-pieces, each with an appropriate cut-out for the central axle, could be easily removed to allow access to the end-plates of the heat jackets. The space in between the outer jacket and the housing is filled with Supawrap insulation. The middle housing piece has a cut out, in line with the other cut-outs, for cell loading. Continuous stirring after inverting the cell is achieved by means of a stirring lever mounted on the axle and a variable speed motor (5-25 rpm) with a mounted driving

piston. The connectors for the wires from the calorimeter and those from the control equipment are mounted on the baseboard.

3:1.6. Preheating Oven.

A preheating oven was constructed on the outside of the calorimeter at the cell-loading entrance. This consists of four quarter inch thick aluminium pieces held together by four corner pieces to form a rectangular hollow 10 cm long, 5½ cm. high and 6½ cm. deep mounted on a 1 cm. thick PTFE rectangular piece 8 inches long and 6 inches wide which acts as a heat insulator between the oven and the calorimeter housing. The oven is heated by several wire wound resistors mounted on all four sides. The complete oven unit is enclosed in an aluminium housing which is mounted on the rectangular PTFE piece by means of a lip and countersunk screws. The front of the oven is closed by a sliding tufnell door for ease of cell movement. The space in between the oven and its housing is packed with Supawrap insulation. The oven with its housing is mounted onto the calorimeter housing by means of self-tapping screws via the lip in the oven housing and the backing PTFE piece as shown in figure 3:2. The advantage of placing the oven unit at the cell-loading entrance is that the temperature around the entrance will be at the same temperature as the outer heat jacket and the cell temperature does not alter significantly during loading. This helps to reduce equilibration time.

3:1.7. Temperature and temperature control of calorimeter.

The temperature control unit is a two term controller containing

a) a thermistor controller for the inner heat jacket,

b) a differential controller for the outer heat jacket and

c) a differential controller for the pre-heating oven.

The temperature of the inner heat jacket is controlled by a thermistor buried in the jacket with heat sink compound. A thermistor is used due to its sensitivity to temperature changes. A platinum resistance thermometer is also buried in this jacket and used in conjunction with another platinum resistance thermometer buried in the outer heat jacket for differential temperature control, as explained below. Over a three hour period, the stability of the temperature is within $0.001^{0}C$, as measured by the calibrated deviation meter on the control unit.

The outer heat jacket temperature is detected by a platinum resistance thermometer used in a common bridge with the platinum resistance thermometer of the inner heat jacket. The common bridge is off set by $2^{0}C$, in terms of resistance, so that the temperature of the outer jacket is controlled at a temperature $2^{0}C$ below that of the inner heat jacket. The stability of the outer heat jacket temperature is within $0.01^{0}C$ over a three hour period.

The temperature control unit contains several power switches for each jacket, depending on the temperature range used. Due to the greater power required by the larger outer jacket and the greater heat loss, it is regulated by a triac burst-firing controller using the mains voltage. The inner heat jacket is regulated by a 20 volts transistor current controller for maintaining the preset temperature and the voltage may be increased to 60 volts for rapid heating e.g. on changing temperature. The pre-heating oven controller

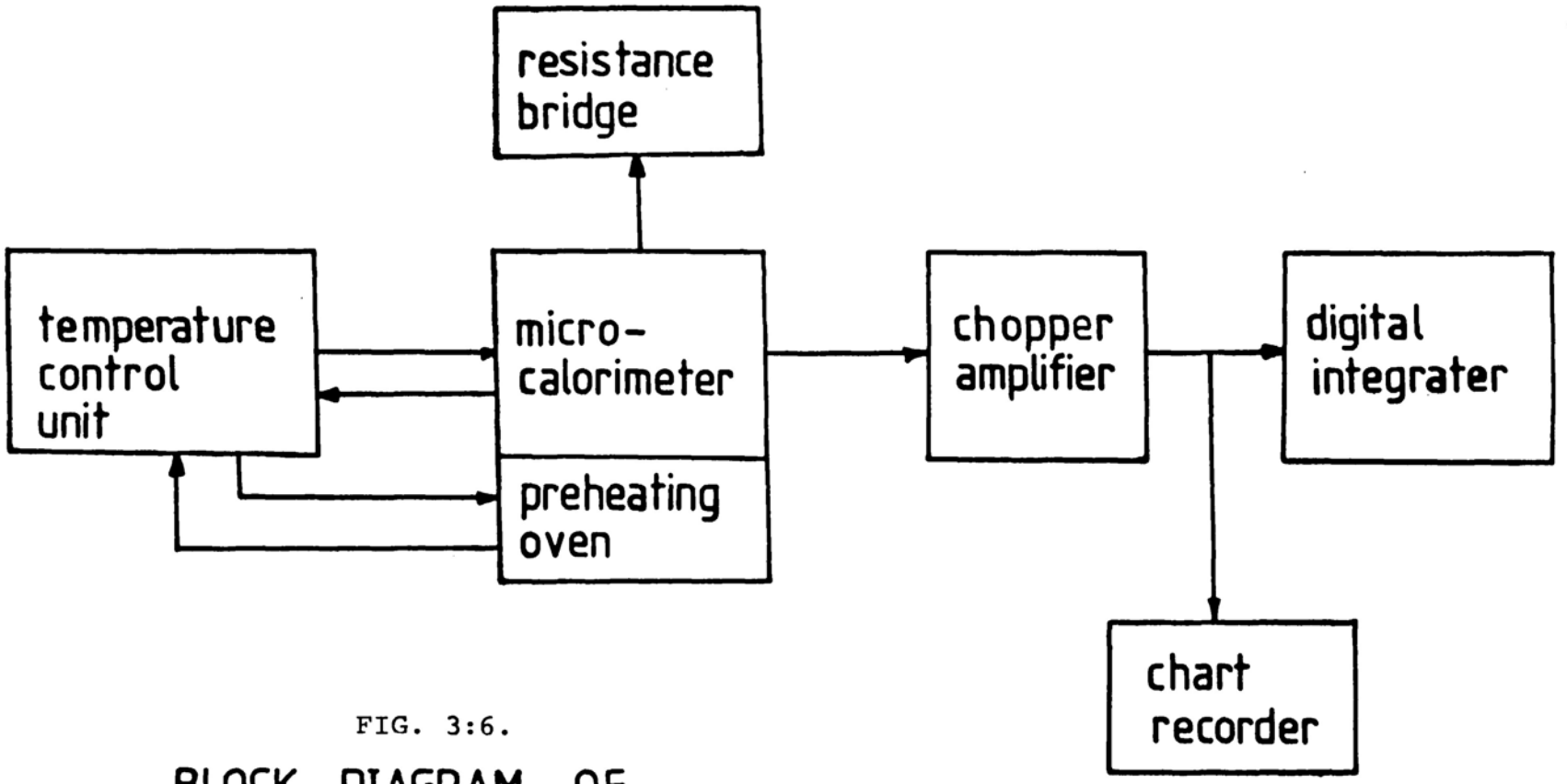


FIG. 3:6.

BLOCK DIAGRAM OF MICROCALORIMETER ELECTRONICS

works in the same way as that of the outer heat jacket and is controlled to the same temperature. Ultimately, the overall temperature of the various components is determined by the temperature of the inner jacket.

3:1.8. Signal detection.

The signal from the thermoelectric modules is passed through a chopper amplifier due to the small magnitude of the DC signal. The amplified signal is then fed into a chart recorder where an analogue plot of mV versus time t is obtained and also through a voltage to frequency converter. The converted frequency signal is then passed through a digital integrator. The digital integrator is a frequency counter where the signal could be passed over various variable dividers preset by push button controls. The counts are displayed on a four digit counter with an overflow lamp. The signal is earthed at the input of the amplifier. Figure 3:6 is a block diagram showing the various units of the complete calorimeter.

3:2. Light scattering turbidimeter.

The light scattering turbidimeter works on the criterion of optical clarity for polymer blends whose components have large refractive indices differences. When light waves fall on such a blend, they are

a) either transmitted through the compatible, transparent blend or

b) scattered by the phase separated species,

unless the phase separation has occured to such an extent that the incident light is greatly attenuated. By monitoring the intensity of the scattered light as a function of temperature at a fixed angle, information about the cloud point of the

system can be obtained at a fixed concentration. By varying the concentrations of the blend samples observed, a cloud point curve or phase boundary is obtained. Refinements to the results so obtained can be made if the angular dependence of the system is known. However, in most cases, the angular dependence can be neglected and the cloud points observed for the system at a fixed angle can be considered as close to the cloud points of the system observed at zero angle.

The light scattering turbidimeter described below is one that monitors the 45^0 scattered intensities of four samples held in a heat sink whose temperature is controlled either in an upward or downward direction over specific time periods. Using the appropriate types of cell, both solid and liquid samples can be used. The angle of 45^0 was chosen for the ease of construction comparable with maximising scattered intensity. Figure 3:7 is a block diagram of the turbidimeter, together with its data logging system.

3:2.1. Sample holder.

The sample holder can accomodate four samples in cylindrical cells for each experimental run. It is an aluminium block 10 inches long, 5 inches wide and 3.7 inches high, split into two halves with the bottom edge of the back half bevelled for the 45^0 light passageway construction. Figure 3:8 shows a side view cross-section of the two halves joined together by bolts to form the complete unit inside the thermal insulation and heat shield. Figure 3:9 shows a plan of the turbidimeter while figure 3:10 shows a front view of the back half of the block with the various half slots and passageway openings.

The straight through light passageway is 12mm. in diameter

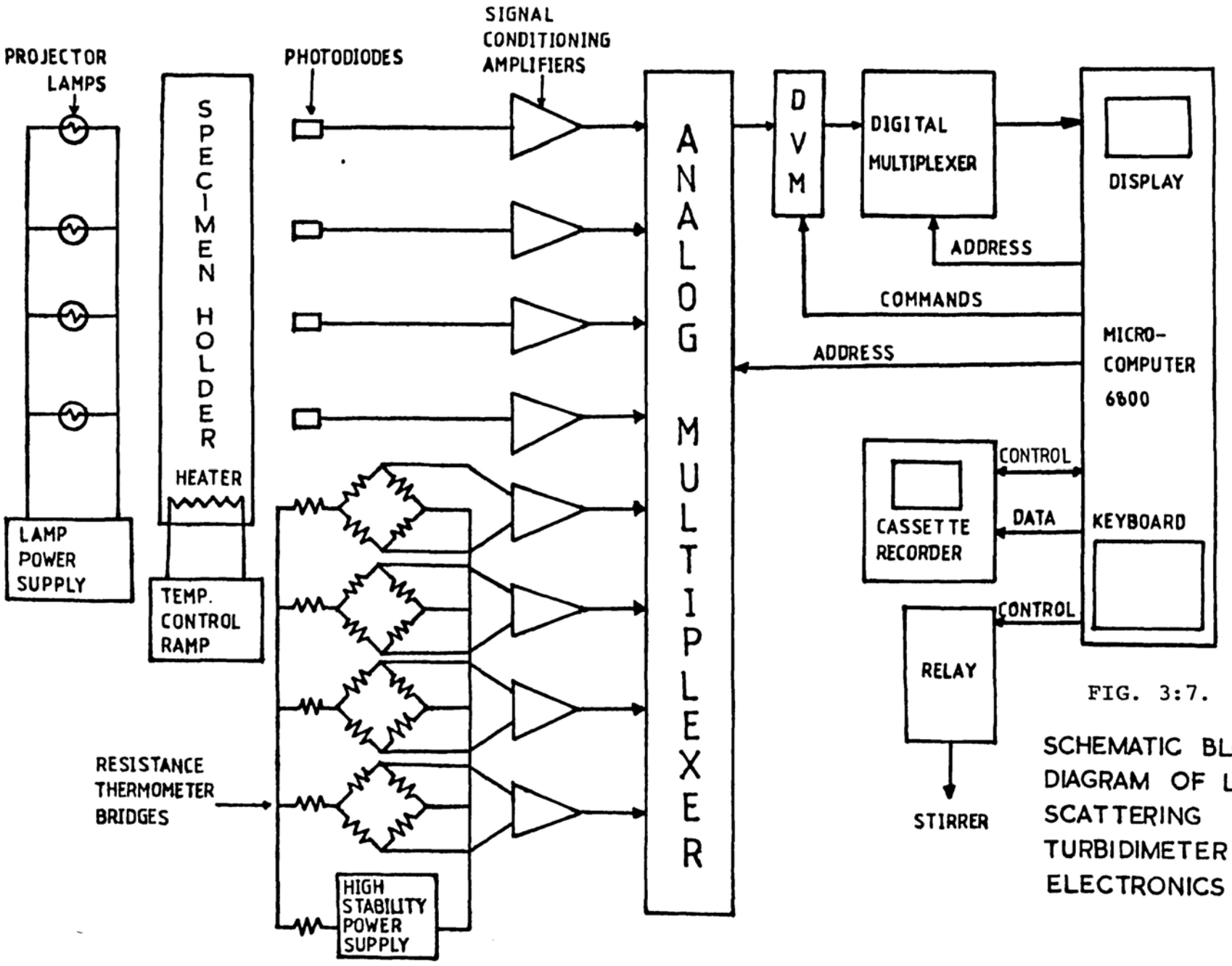


FIG. 3:7.

SCHEMATIC BLOCK DIAGRAM OF LIGHT SCATTERING TURBIDIMETER ELECTRONICS

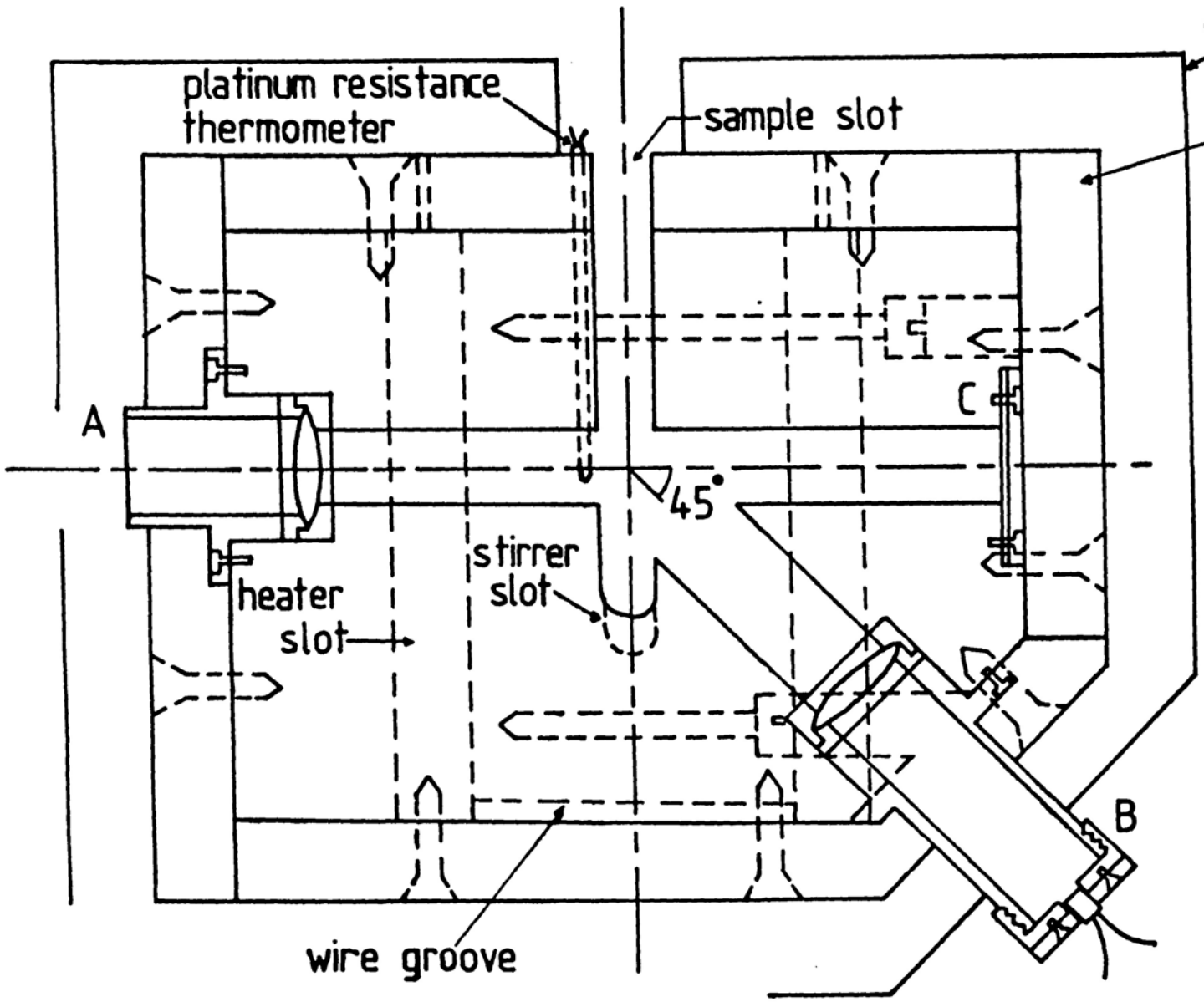


FIG. 3:8

SIDE VIEW CROSS SECTION OF LIGHT SCATTERING TURBIDIMETER SAMPLE HOLDER

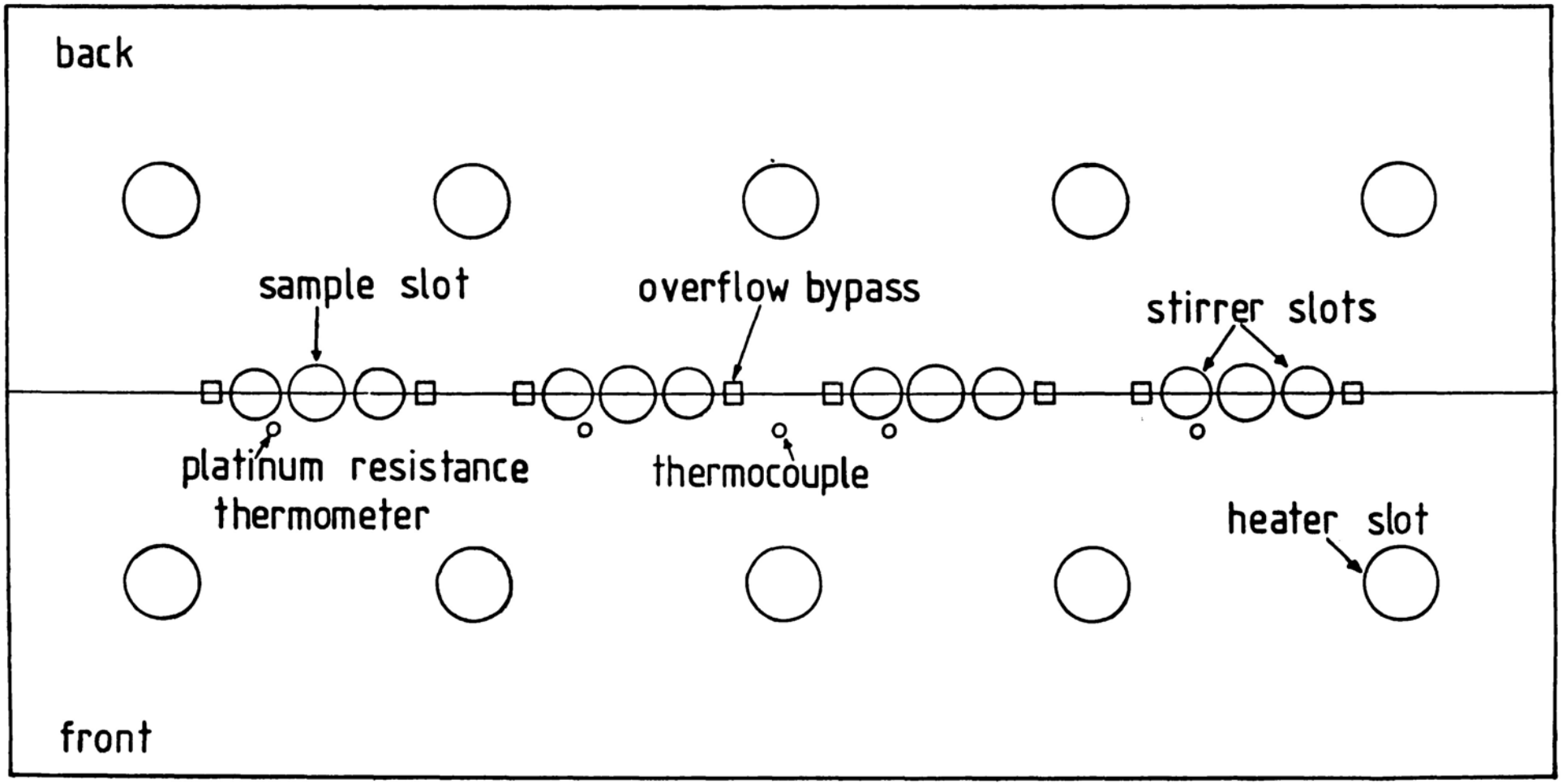


FIG. 3.9. L. S. TURBIDIMETER PLAN

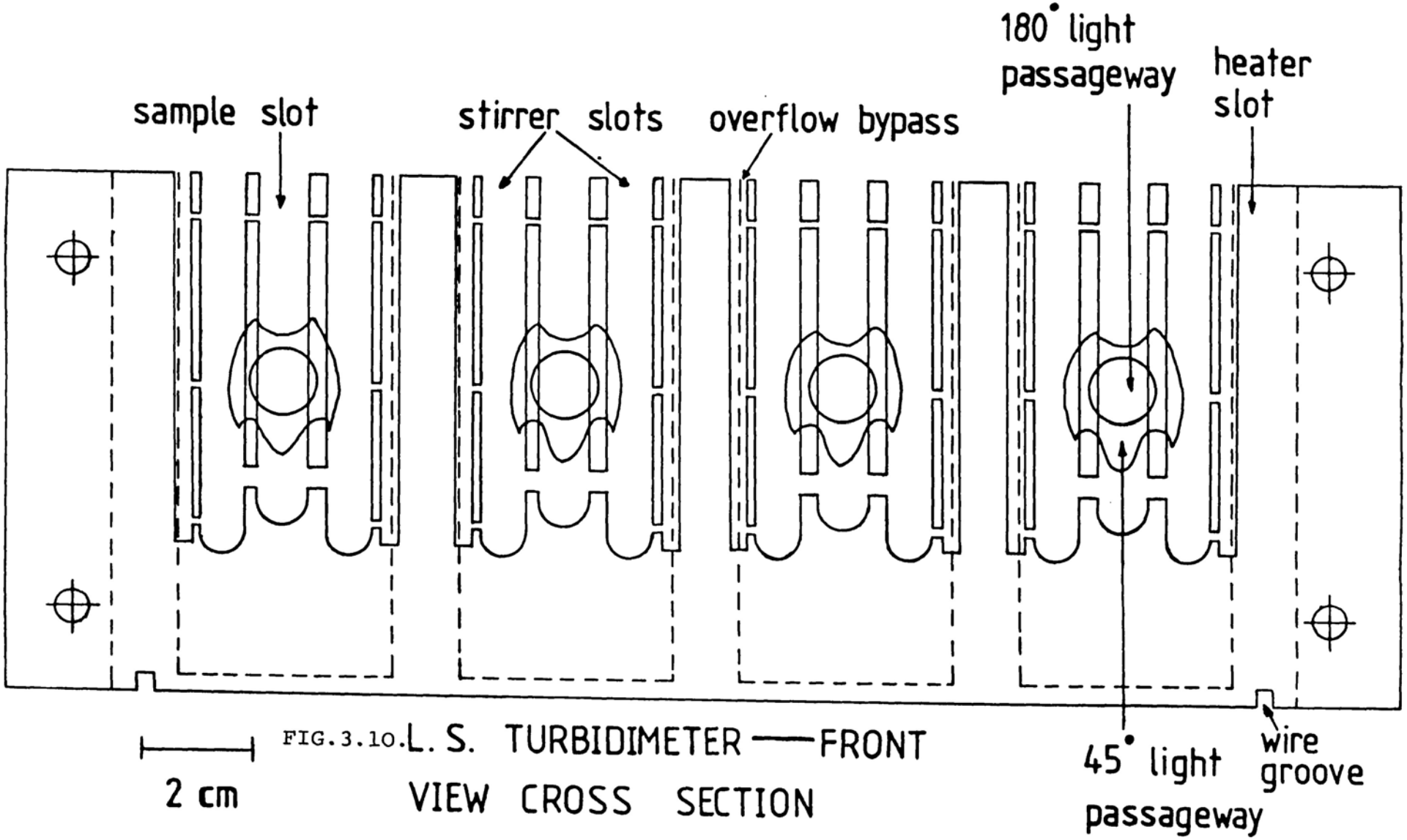


FIG. 3.1o. L. S. TURBIDIMETER — FRONT

and 1½ inches below the top of the block. At the front of this passageway is the object lens mounted in its holder and placed at a distance 2 inches from the center of the sample. The light transmitted through the sample is trapped at the back of the straight through passageway by an aluminium cap blackened on the inside. The 45^0 scattered light passageway is 15 mm. in diameter sealed by the photodiode assembly and image lens assembly as shown in the diagram. The center of the sample and the photodiode element are placed equidistant from the image lens, at its focal plane (2 inches).

Equally spaced along the meeting surfaces of the two halves are the sample slots with their accompanying stirrer and overflow bypass slots. The sample slots are 9 mm. in diameter and 6½ cm. deep, of which 1½ cm. is below the floor of the passageway. This amount of dead volume is required in order to ensure that the 1 cm. long stirrer inside the sample is out of the way of the beam when scattered intensity readings are taken (see section 3:2.7). The stirrer slots are 8 mm. in diameter and 7 cm. deep. The overflow bypass slots are 2 mm. square and 7 cm. deep. All the slots are linked by horizontal grooves cut in the appropriate places as shown.

In front of each sample slot and as close to it as is possible, is a slot 1½ cm. deep to accomodate a platinum resistance thermometer. A similar sized hole in the middle of the block is used for the hot junction of the thermocouple used to control the temperature of the block. Equally spaced around both halves are 12 mm. diameter slots which hold wire-wound resistors serving as heaters. Grooves at the bottom surface of the block facilitates wiring of the heating system.

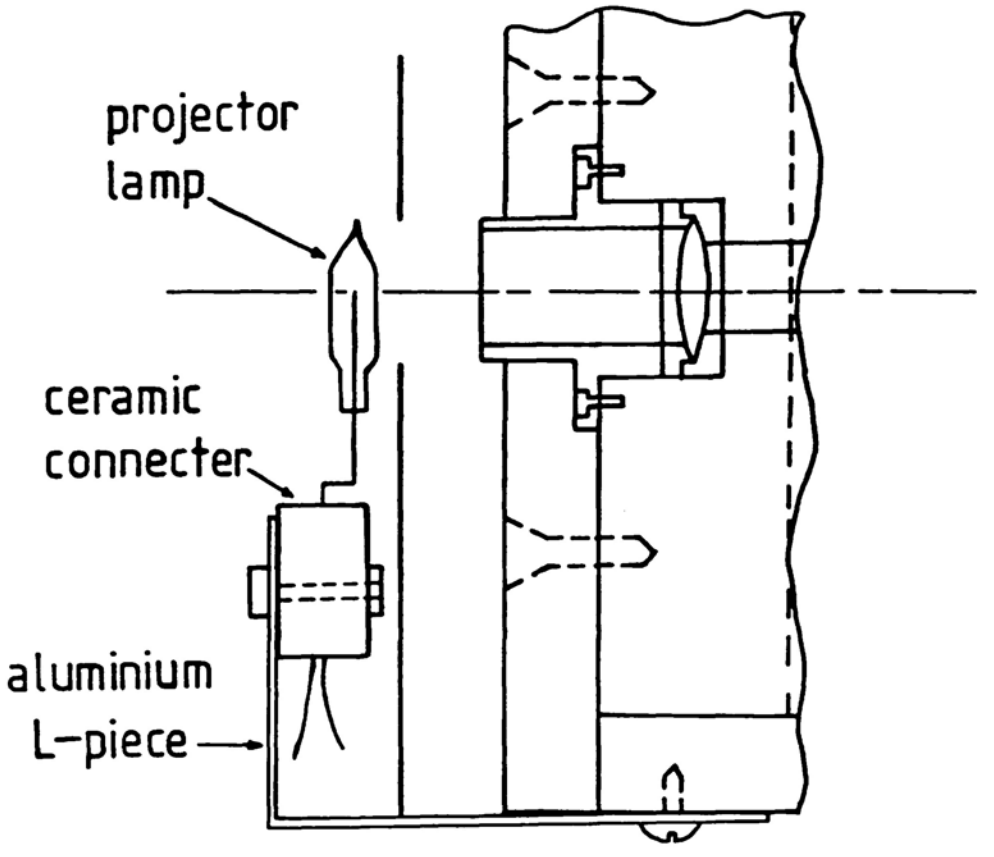
3:2.2. Constant light source.

The light sources used are four 50 watt tungsten filament projector lamps connected in series to a 12-18 volt stabilised power supply. The lamps are mounted on ceramic connector blocks held on L-shaped aluminium pieces as shown in figure 3:11. The L-shaped pieces are held to the bottom of the block insulation. Adjustment of the position of the filament with respect to the center of and distance to the lens is by means of screws and grooves in both arms of the L-shape piece.

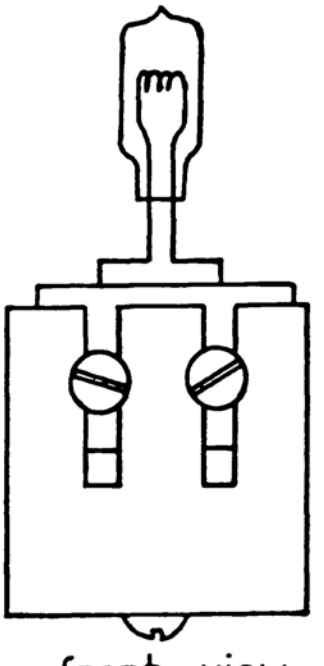
3:2.3. Lens and photodiode assemblies.

Figures 3:12a and 3:12b show exploded cross-sectional views of the two respective assemblies. The two inches focal length lens has a diameter of 2 cm. and is mounted in a PTFE lens holder. The lens holder consists of two circular PTFE pieces 24 mm. in diameter with a 18mm. diameter hole in each. Each inside surface is concaved to accomodate the lens which is sandwiched in between. The piece with the 2 mm. protruding lip is 2 mm. thick at its thinnest section while the other piece is of the same dimension in all respects, except for the 2 mm. instep on the edge instead of the lip. The whole lens mounting (assembly) is held in place in the recess of the sample block by aluminium tubes secured to the block by flanges and countersunk screws. Both the objective and image lenses are mounted in the same way, except that the image lens mounting has a longer aluminium tube section which is threaded at the open end to hold the photodiode assembly.

The photodiode is held in a circular PTFE disc 3 mm. thick and 2½ cm. in diameter, secured by countersunk screws onto the outside base of the cup-shaped PTFE piece screwed



(A) side view



(B) front view

FIG. 3:11.

LAMP
HOLDER
ASSEMBLY

2 cm

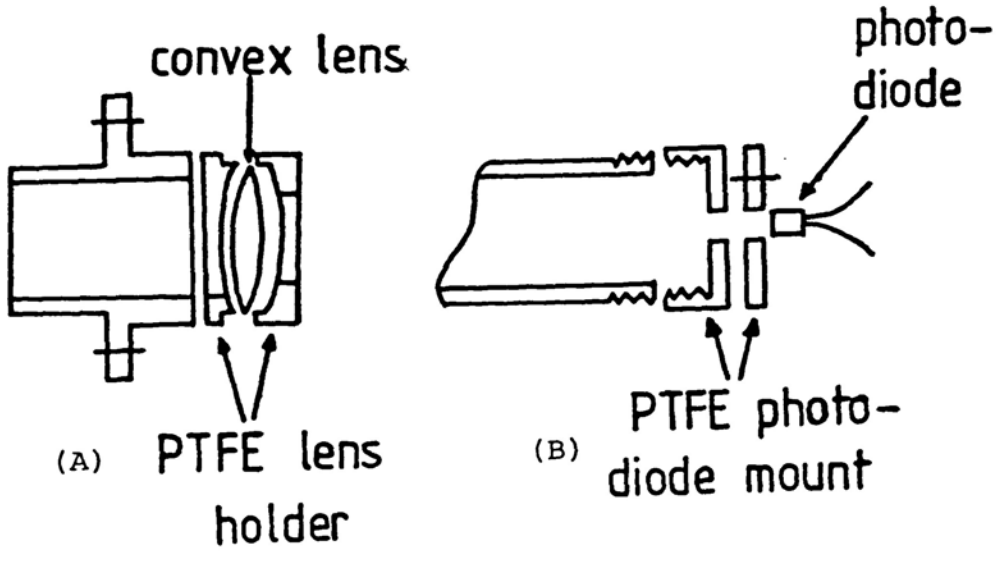


FIG. 3:12. (A) LENS ASSEMBLY AND (B) PHOTODIODE ASSEMBLY.

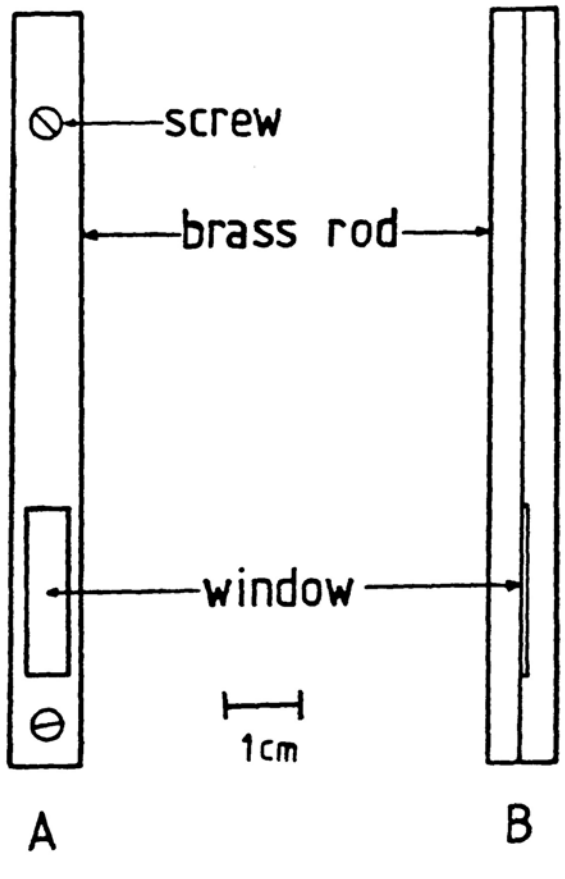


FIG. 3:13.

SOLID
SAMPLE
CELL

A-front view

B-side view

onto the aluminium tube of the lens mounting. Mounting of the photodiode in this way facilitates fine adjustment of the distance of the photodiode element from the lens. As the photodiode assembly tends to get hot at high temperatures, a piece of aluminium can be attached to the PTFE disc to conduct some heat away and hence preserve photodiode performance. The light source, sample and photodiode element are placed at the focal planes of both lenses so that the incident and scattered beams are focussed as an intense spot on the sample and photodiode element respectively. This arrangement was found to be more favourable than having both these beams parallel because the intensity of the scattered light measured in the latter case is very much reduced.

3:2.4. Sample cells.

Liquid samples are sealed in Pyrex glass tubes after degassing. The tubes have an external diameter of 9 mm. and a length of 11 cm. when sealed. An iron nail 1 cm. long inside the sample acts as a follower for magnetic stirring. The level of the sample must be at least 3½ cm. from the bottom of the tube. Assuming a density of 1 gm/cm^3 for most polymers/oligomers, about 0.9 gm. total of the mixture is usually sufficient to ensure this.

Solid samples are sandwiched in thin film forms in brass cells, one of which is shown in figure 3:13. It is a brass cylindrical rod with dimensions similar to those of the glass tubes. The two halves are held together by countersunk screws. One half has a recess to accomodate the sample, and a window in each half, in line with the straight through passageway, allows for transmission of the incident and scattered light.

Holding the sample in this way helps to reduce sample buckling as well as allowing room for sample expansion during heating.

3:2.5 Stirring of liquid samples.

The stirring of liquid sample is achieved by the piece of iron nail inside the sample acting as a magnetic follower, and cylindrical bar magnets 2 cm. long, moving up and down the stirrer slots. The magnets are crimped onto connector rods screwed onto a T-piece. The T-piece is connected to a windscreen wiper motor controlled by a relay working in conjunction with the microcomputer. The horizontal grooves connecting the stirrer and sample slots enable the magnets to act on the nail, since that aluminium is a non-magnetic material. Provision has been made for index matching of the glass cells, if required. Mating surfaces can be sealed with PTFE gaskets. The overflow bypass slots facilitate the displacement of the index matching liquid due to the movements of the stirrers.

3:2.6. Temperature control and measurement.

The aluminium block is heated by ten wire-wound resistors joined in a series-parallel combination arrangement incorporating a thermal fuse set for 300^{0}C. It is controlled by a three term mains triac burst firing (zero-switching) temperature control ramp which utilises a copper-constantan thermocouple for temperature sensing. The starting (or reference) temperature of the control ramp is set by means of a range switch and a multiturn potentiometer. This reference temperature can be offset by a digitally generated ramp. Various time periods and temperature ranges can be preset on the ramp, enabling the rate of temperature change to be

controlled. The direction of the temperature change can also be chosen i.e. allowing controlled heating or cooling runs. The temperature of each cell is measured by platinum resistance thermometers placed parallel to and as close to the samples as possible in the block. The use of four thermometers helps to avoid the problem of eliminating the temperature gradient of the large aluminium block.

To minimise the temperature gradient of the block and to prevent large heat losses, it is enclosed in half inch thick syndanode thermal insulating slabs. However, even with the insulating jacket, it was found that the heat loss at high temperatures was still quite substantial. An aluminium heat shield was therefore added to reflect the heat loss back to the block. A fan is provided for rapid cooling of the block.

3:2.7. Data logger and controller.

The photodiodes and platinum resistance thermometers each have their own signal conditioning amplifiers for the 2 volts full scale digital voltmeter. Each signal goes to an analogue multiplexer which switches one input at a time to the digital voltmeter. A microcomputer selects the analogue channel to be scanned, after which the digital voltmeter is commanded to convert the signal from analogue to digital. When the conversion is complete, the digital binary coded decimal signal is multiplexed into computer memory. Data is assembled from all the channels scanned (a pre-set number), processed and formatted by programmed software control, after which it is fed out to a digital cassette recorder. The formatting is to put into ASCII code recognition characters, spacings,

line feed, etc. to make the cassette tape compatible with readers and other software on larger college facilities, including the end-of-file marks.

An additional control signal is provided to activate the stirrer via a relay. The relay is controlled by programmed software such that when stirring stops a few seconds before readings are taken, the magnets are at the bottom of the stirrer slots. This is to ensure that the nail has sufficient time to settle to the bottom of the sample. This is necessary to prevent it from contributing to the scattered intensities. Besides stirring intervals, data acquisition intervals are also selected by software control. Both intervals have a maximum of 9999 seconds.

3:2.8. Software control.

This consists of two programs coded 6000 and 6040.

a) Program 6000: This facilitates manual stepping through of the various channels. Each channel is displayed in turn on the panel indicator and the channel readings on the digital voltmeter. Odd number channels indicate intensity readings while even number channels indicate temperature readings in Kelvin. This program is necessary in order to provide a manually controlled display of what is occuring in each channel before commencing the experiment proper or when optical alignment is required. This secondary program must be executed before entering the main program, otherwise the secondary program (6000) loop will be in operation and columns of FFFFs will be recorded onto the cassette tape instead of the required data, if the main program is entered directly.

b) Main program 6040: The first part of the main program is a cassette handling routine for rewinding the cassette, winding off of the cassette leader tape etc. It also checks the status of the recorder. The second part of the program is for experimental identification. The first thirty characters are used for this. This selects stirring intervals, data acquisition intervals,the number of channels to be scanned (in consecutive order) plus any other identification code desired such as sample numbers, channel numbers corresponding to the sample numbers in them, date of experiment, etc. These are put onto the tape and the interval clock started.

During the experiment, the elapsed time is continuously displayed on the panel indicator, except when readings are transferred onto the tape when the channel number scanned is displayed. Intensities are written onto the tape as they are, but temperature readings are converted by software routine to Kelvin. Data is formatted as shown in appendix C in tabulated form, together with the elapsed time.

The experiment can be terminated at any time and a choice is provided for either another experiment to be carried out with new identification data fed in or old data used, or the file closed by an end-of-file mark added onto the tape for the tape-reader. The tape is then rewound. Both end-of-file marks for the thermiset and digistore readers are put onto the tape.

CHAPTER 4.

EXPERIMENTS AND RESULTS.

4:1. Calorimeter characteristics.

In a well designed heat conduction calorimeter, the output voltage of the thermoelectric cells is a measure of the rate at which heat is transferred from the reaction cell to the heat sink or vice-versa. A calorimeter experiment using this type of calorimeter is then a continuous measurement of the thermoelectric cell output voltage as a function of time (analogue measurements) or at fixed sampling intervals(for digital sampling). These measurements can be divided into three parts, namely

a) the fore period

b) the reaction period and

c) the after period.

The fore and after periods involve no heat exchange. Ideally, this implies that the mean of the measured voltages is zero and any fluctuations about this mean is due to the noise of the circuit. The reaction period commences with the initiation of the reaction or electrical heating, and the accompanying heat effect is detected as a heat flow across the thermoelectric cells corresponding to a change in the thermoelectric cell output voltage. The direction of heat flow (and hence the direction of the voltage change) depends on the nature of the heat effect of the reaction i.e. exothermic or endothermic. On completion of the reaction or electrical heating, the output voltage will decay exponentially to the after period baseline, which ideally, should be identical to the fore period baseline.

4:1.1. The quality of baseline.

The quality of the baseline or thermoelectric cell output voltage readings in the absence of heat effects is an indication of the absence of electrical or thermal interference and is a measure of the noise of the circuits. In general, the quality of the baseline of the calorimeter constructed is good over the time periods of the experiments. For a 1 mV full scale deflection (f.s.d.) of the chart recorder (equivalent to gain setting E on the amplifier), the base line drift over a two hour period is less than 15 μV while at a full scale deflection of 10 μV, the drift is less than 0.5 μV, as this is in the limit of resolution of the amplifier used. The drift of the baseline can be attributed to the pressure exerted on the thermoelectric units by the push-fit cell, as witnessed by the almost negligible drift observed when the heat sink is unloaded. Large deviations from electrical zero could be attributed to (a) liquid leakage from the cells, (b) severe thermal disturbances of the heat sink due to loss of temperature control or improper closing of the cell loading guide passage-way and (c) occasional humming from other heavy electrical equipment picked up by the chart recorder from the main supply.

4:1.2. Sensitivity, heat flow and time constant of the calorimeter[54].

When a temperature difference exists between the inner and outer faces of the heat flow units, heat is conducted across the heat flow units, and the flow across is proportional to the output voltage. The constant of proportionality F, is called the calibration constant of the calorimeter and is given by

the formula,

$$F = h / \varepsilon_0 \qquad 4:1$$

where h is the thermal conductivity of a single thermocouple pair and ε_0 is the thermoelectric coefficient of the thermocouple material. If h_0 is the thermal conductivity of the materials, then

$$h = h_0 a/\ell \qquad 4:2$$

where ℓ is the length of the thermocouple material and a the cross-sectional area. Thus F determines the sensitivity of the calorimeter since 1/F gives the volts output per watt of input power. The sensitivity of the calorimeter is therefore independent of the number of thermocouple junctions used.

The number of thermocouple junctions used, however, is important in order to

a) cover the surface of the reaction cell uniformly to ensure complete conduction of heat through the thermocouples only and

b) to obtain the time constant required for the calorimeter.

The rate of heat flow w_i through a single thermocouple path is given by

$$w_i = h_i(\theta_c - \theta_b)_i \qquad 4:3$$

where h_i is the thermal conductivity of the ith. path and $(\theta_c - \theta_b)_i$ the temperature difference between the reaction cell surface and the block at the point i. The voltage v_i generated by the thermocouple of thermoelectric constant ε_{0i} is

$$v_i = \varepsilon_{0i}(\theta_c - \theta_b)_i \qquad 4:4$$

From equations 4:1, 4:3 and 4:4, the calibration for path i, f_i, is given by

$$f_i = h_i/\varepsilon_{0i} = w_i/v_i \qquad 4:5$$

therefore,

$$w_i = f_i v_i \qquad 4:6$$

The total heat flow from the reaction cell is

$$W = \Sigma w_i = \Sigma f_i v_i \qquad 4:7$$

If all f_i are equal and the thermocouples are serially connected, then

$$V = \Sigma v_i \qquad 4:8$$

and

$$F = f_i = \text{constant} \qquad 4:9$$

and equation 4:6 becomes

$$W = FV \qquad 4:10$$

For semi-conducting materials, ε_{0_i} are equal and fluctuations in F are usually due to variations in ℓ_i due to the small path lengths involved. In order to maintain a similar temperature profile of the surface to the thermoelectric cells in each experiment (due to the non-uniform generation of heat in the reaction cell), they are sandwiched between copper plates which are in good thermal contact with the calorimeter cell walls and the heat sink.

If the heat content of the calorimeter cell is altered instantaneously, the output voltage V will alter rapidly from the baseline, reach a peak and then decay exponentially back to the baseline voltage. To a first approximation, the voltage decay is given by

$$V = V_0 \exp(-t/\tau) \qquad 4:11$$

where τ is the time constant of the calorimeter given by

$$\tau = C_p/nh \qquad 4:12$$

where C_p is the heat capacity of the reaction cell and contents, n is the number of thermocouple junctions and h as before. This

time constant determines the length of time required for an experimental run. For example, to measure the heat involved with an accuracy of 0.1%, the voltage must decay to 0.1% of its maximum value. This involves 6.9τ or 10 half-response times (which is defined as the time required for the signal to decay to half its maximum value).

To obtain small τ values, C_p should be kept as small as possible and the conduction to the block, nh, as large as is practical. Since h has to be small to give good sensitivity to the calorimeter, a large number of thermocouple junctions n is helpful. Since the sensitivity of the microcalorimeter could not be altered short of replacing the modules, efforts were concentrated instead on reducing the time constant of the calorimeter. The results of these efforts will be discussed in the next chapter.

4:1.3. Electrical calibrations and calculation of areas.

The calibration cell used for electrical calibrations of the oligomeric systems examined is similar to the cells used in the actual experiments, except that instead of the PTFE sample holder, it had two PTFE end-caps. It contained a 100 ohm (±0.02%) Muirhead wire-wound resistor immersed in a 50/50 mixture of the system under investigation. The leads from the resistor were led out via a hole near the top on the side of the calorimeter cell exposed to the opening of the oven after loading. Current was fed into the resistor from a 0.02% current calibrator over a time period measured by a stop-watch. The power input P is

$$P = I^2R \qquad 4:13$$

where I is the current and R is the resistance, while the

energy input is

$$E = I^2Rt \qquad 4:14$$

where t is the time of current input.

In the electrical calibration runs carried out, the analogue plots of output voltage versus time were observed to have the same fore and after baseline. Theoretically, the total heat of the reaction, Q, is proportional to the area A bounded by the peak and the extrapolated baseline from that before to that after the reaction. Hence,

$$Q = FA \qquad 4:15$$

where F is the calibration constant defined previously. A plot of Q versus A would be a straight line passing through the origin and of gradient F. The area A is obtained by weighing the cutout of a tracing of A on high quality tracing paper and the weight converted to area from a known weight-area relationship of the tracing paper used. A plot of integrator counts versus energy is also obtained. Knowing F, the energy involved in an experimental run can then be obtained. However, because of the time constants for the various systems used are different as a result of vastly differing thermal conductivities and thermal capacities, the heat loss from the two sides of the calorimeter cell not in contact with the heat flow units would be different. Hence to use the same calibration constant for all the systems would lead to corrections that are difficult to determine. To overcome this,electrical calibrations for each oligomeric system used were carried out. Tables 4:1, 4:2a, 4:2b and 4:3 show the results of the electrical calibrations for the distilled water, methoxylated(polyethylene-oxide-polypropylene oxide) and polystyrene-polybutadiene systems respectively, carried out at the temperatures indicated.

The contents of tables 4:1 to 4:3 are shown graphically in figures 4:1 to 4:3. The methoxylated(polyethylene oxide-polypropylene oxide) calibration plot at 30.1^{0}C is used for subsequent measurements of the same system at higher temperatures since the thermal conductivities and thermal capacities of this system are assumed to vary only slightly with temperature. The calibration constants obtained for the various systems illustrate the discrepancies mentioned above.

Table 4:1

Results of electrical calibration of distilled water at 30.0^{0}C. Chart recorder full scale deflection is 1 mV.

Run no.	Input power/W	Heating time/s	Heat input/J	Area /cm^2	Int.read. /×200	F/(J/cm^2) ×10^{-2}
W_1	0.99998	2.6	2.5999	40.45	4415	6.4274
W_2	0.99998	1.5	1.5000	24.49	2526	6.1249
W_3	0.99998	3.4	3.3999	53.21	5745	6.3896
W_4	0.99998	1.0	1.0000	16.63	1779	6.0132

Average calibration constant = 6.2388 (±0.2018) 10^{-2}J/cm^2.

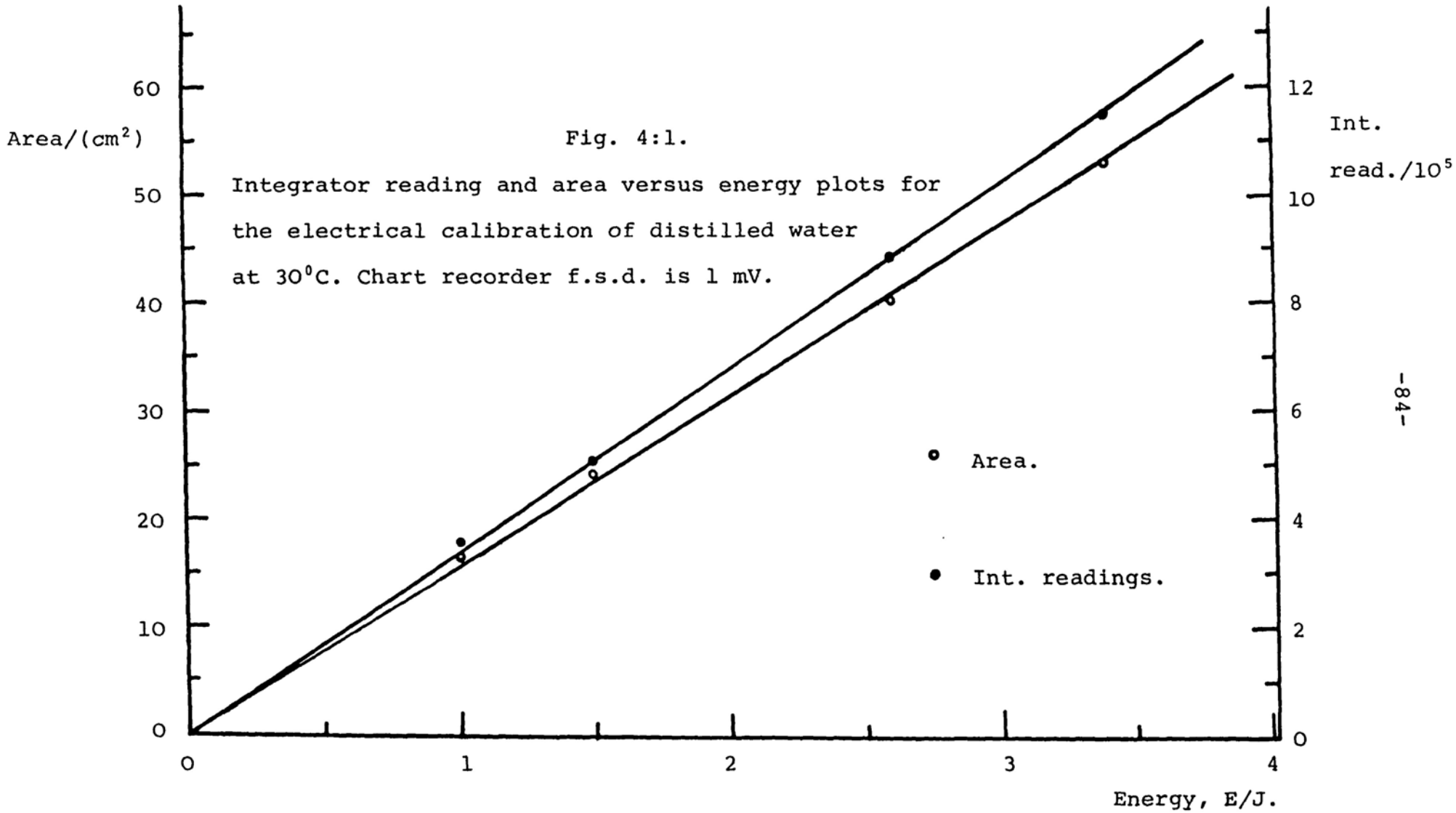


Fig. 4:1.

Integrator reading and area versus energy plots for the electrical calibration of distilled water at 30°C. Chart recorder f.s.d. is 1 mV.

Table 4:2a

Electrical calibration of the methoxylated(polyethylene oxide-polypropylene oxide) system at 30.1°C for energy above 1J. Chart recorder f.s.d. is 1 mV.

Run no.	Input power/ $(10^{-2}W)$	Heating times/s	Heat input/J	Area /cm^2	Int. read. /(×500)	Cal. constant $F/(J/cm^2)\times10^{-2}$
$80A_1$	0.25	40.2	10.05	147.7	6915	6.804
$80A_2$	4.0	25.1	1.004	14.6	653	6.877
$80A_3$	12.5	40.2	5.025	74.9	3340	6.709
$80A_4$	11.56	58.0	6.705	97.8	4244	6.856
$80A_5$	1.323	40.4	0.5343	7.7	335	6.939
$80A_6$	12.25	65.6	8.036	116.2	5099	6.916
$80A_7$	12.5	40.1	5.0125	73.8	3260	6.792
$80A_8$	5.0176	41.0	2.057	30.6	1305	6.722
$80A_9$	7.508	43.1	3.2336	45.6	1938	7.096
$80A_{10}$	10.24	40.0	4.096	60.7	2483	6.748
$80A_{11}$	12.25	37.4	4.5815	65.5	2773	6.995
$80A_{12}$	12.25	50.0	6.125	88.9	3864	6.890
$80A_{13}$	7.563	40.1	3.033	44.8	1934	6.770
$80A_{14}$	10.24	40.1	4.096	60.9	2670	6.726
$80A_{15}$	10.24	40.2	4.116	61.8	2675	6.660
$80A_{16}$	18.06	50.4	9.104	135.9	6138	6.700
$80A_{22}$	12.25	40.9	5.010	73.10	3195	6.854
$80A_{23}$	20.25	43.0	8.7075	129.6	5530	6.719
$80A_{24}$	23.52	53.0	12.467	184.9	12000	6.743

Average calibration constant = $6.817(\pm0.1145)\times10^{-2}J/cm^2$.

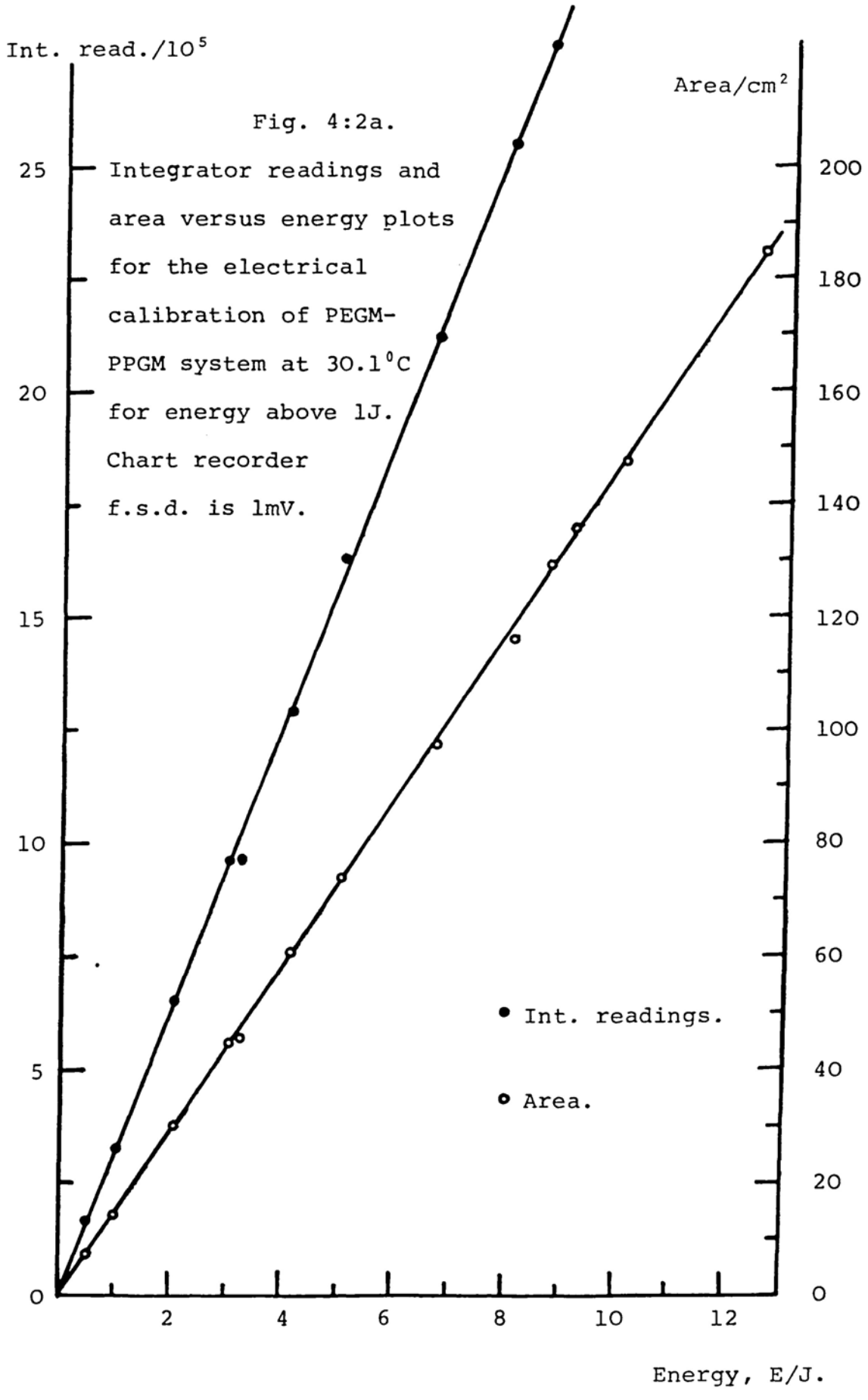


Fig. 4:2a.
Integrator readings and area versus energy plots for the electrical calibration of PEGM-PPGM system at 30.1°C for energy above 1J. Chart recorder f.s.d. is 1mV.

Table 4:2b

Electrical calibration of the methoxylated(polyethylene oxide-polypropylene oxide) system at 30.1^{0}C for energy below 1J. Chart recorder f.s.d. is 100 μV

Run number	Input power/ (10^{-3}W)	Heating times/s	Heat input/J	Area /cm^2	Int. read. /(×500)	Cal. constant F/(J/cm^2)×10^{-3}
80A$_2$	40.000	25.1	1.004	146.1	6462	6.872
80A$_5$	13.230	40.4	0.5343	76.98	3346	6.941
80A$_{17}$	10.000	38.9	0.3890	57.43	2508	6.773
80A$_{18}$	6.4000	41.0	0.2624	37.76	1696	6.949
80A$_{19}$	6.4000	26.3	0.1680	23.58	1045	7.125
80A$_{20}$	16.900	39.8	0.6730	97.79	4300	6.882
80A$_{21}$	20.736	39.9	0.8270	122.2	5300	6.768

Average calibration constant = 6.901(±0.122)×10^{-3}J/cm^2.

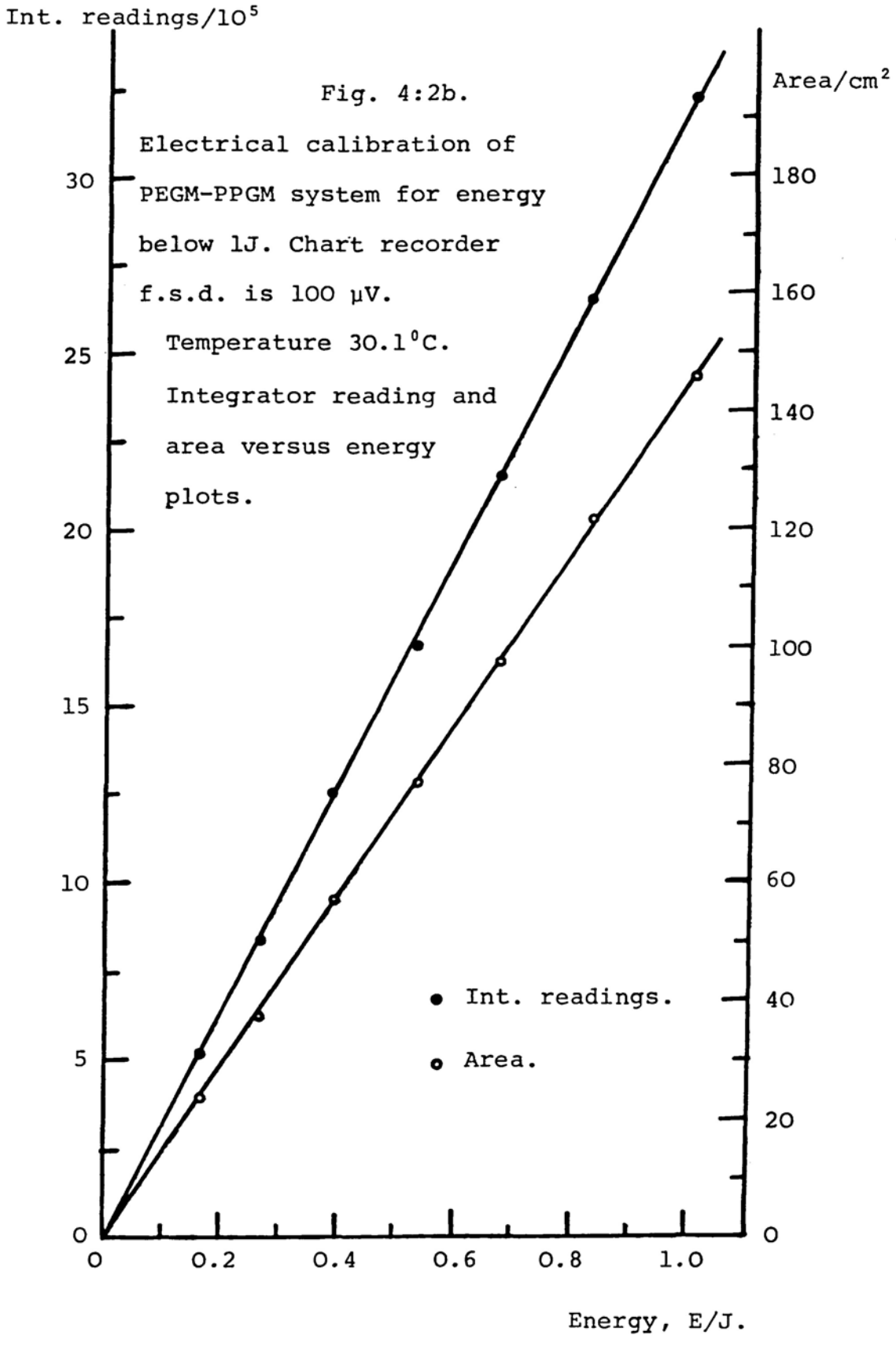


Fig. 4:2b.

Electrical calibration of PEGM-PPGM system for energy below 1J. Chart recorder f.s.d. is 100 μV.

Temperature 30.1°C.

Integrator reading and area versus energy plots.

Table 4:3.

Electrical calibration of the polystyrene(1010)-polybutadiene(960) system at 70.1°C. Chart recorder full scale deflection is 100 μV.

Run number	Input power/ (10^{-3}W)	Heating times/s	Heat input/J	Area /cm^2	Int. read. /(×500)	Cal. constant F/(J/cm^2)×10^{-3}
PS_1	30.25	220.1	0.6650	102.5	4415	6.488
PS_2	2.500	365.5	0.9137	142.9	6032	6.394
PS_3	2.500	210.0	0.5250	81.8	3387	6.418
PS_4	1.600	200.1	0.3200	48.9	2149	6.544
PS_5	2.025	565.0	1.1441	176.3	7563	6.490
PS_6	2.500	600.0	1.5000	233.5	9854	6.424

Average calibration constant = 6.460 (±0.057)×10^{-3}J/cm^2.

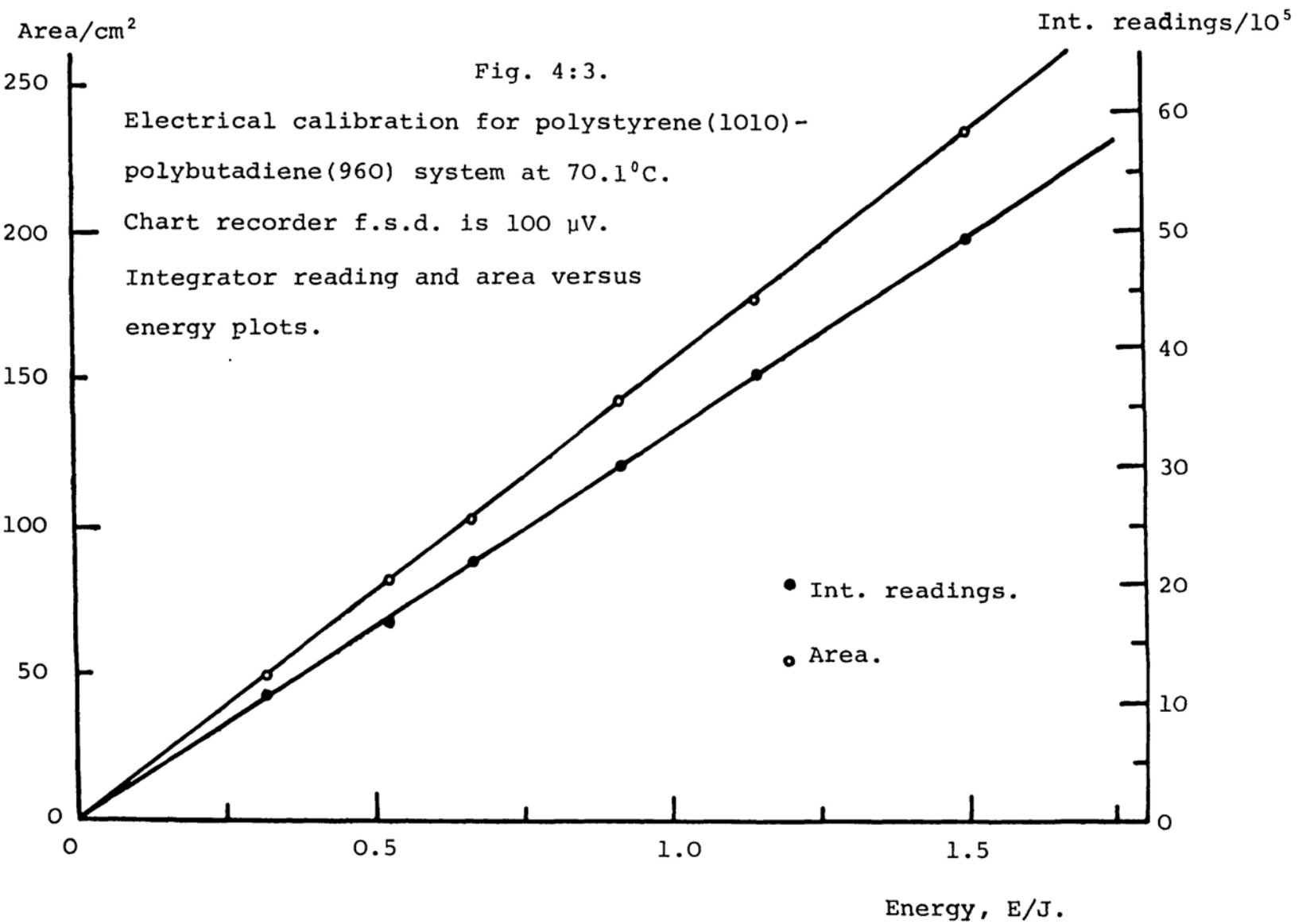


Fig. 4:3.

Electrical calibration for polystyrene(1010)-polybutadiene(960) system at 70.1°C.

Chart recorder f.s.d. is 100 μV.

Integrator reading and area versus energy plots.

4:2. Materials.

The materials used for the chemical test of the calorimeter and the heats of mixing were procured from various sources. Their characterisation, as quoted by the manufacturers, were checked, where possible. The methods of sample preparation are outlined below.

4:2.1. Hydrochloric acid and sodium hydroxide solutions.

The neutralisation of an acid by a base is used as a chemical test for the calorimeter due to its good documentation. The HCl and NaOH parent solutions were volumetric solutions bought from BDH Chemical Company. The 0.1M HCl vial meant for a total volume of 500 ml. was instead diluted with distilled water to one liter to give a 0.05M solution. The 1M NaOH vial was diluted to 500 ml., of which 5 ml. was extracted and diluted to 100 ml. to give a 0.05M solution. Assuming the 0.05M HCl solution to be accurate after dilution, the NaOH solution was titrated against it using phenolpthalein as indicator. The molarity of the NaOH solution was determined to be 0.04925M in this manner.

4:2.2. Oligomeric polystyrene.

The oligomeric polystyrene sample of number average molecular weight 1010 (designation PS 1010) was obtained from Polymer Laboratory with a quoted polydispersity of less than 1.1. This was checked by gel permeation chromatography(g.p.c.) to ensure that the polydispersity was narrow and that the molecular weight was accurate enough for our purpose.

4:2.3. Oligomeric Polybutadiene.

Oligomeric samples of polybutadiene of number average molecular weights 960 and 2350 (designations PBD 960 and PBD 2350 respectively) were purchased from Goodyear Chemical Company with polydispersities of less than 1.2 and 1.1 respectively. The stated number average molecular weights were determined by vapour phase osmometry and both samples contain 0.5% wt./wt. butylated hydroxytoluene antioxidant. Both samples were used without checking. The microstructures of the samples, as given by the manufacturer, are listed in table 4:4.

Table 4:4.

Microstructures of polybutadiene samples.

PBD 960		PBD 2350	
Microstructure (NMR)		Microstructure (IR)	
	mole %		weight %
Trans 1,4	49	Trans 1,4	53
Cis 1,4	36	Cis 1,4	41
Vinyl 1,2	15	Vinyl 1,2	6

4:2.4. Oligomeric polyethylene oxide and polypropylene oxide.

Several samples of polypropylene glycol of molecular weights 400, 1000, 1500 and 2000 and a sample of polyethylene glycol of molecular weight 600, all with narrow polydispersities were obtained from Shell Chemicals. The α-ω hydroxy ended oligomers were methoxylated following the method adopted by Booth[55] et al. The methoxylated samples were dried on a vacuum line ($<10^{-3}$mm. Hg) for a week followed by another week in a

vacuum oven at 40°C. The degree of methoxylation was checked by infra-red spectroscopy. The absence of the broad band about 3500 cm^{-1} due to OH stretching was deemed to be a sign of complete methoxylation (> 99% conversion). The absence of the characteristic band at 1640 cm^{-1} due to unbonded water was used as an indication that the product was dried.

Gel permeation chromatography was used to check that the molecular weights quoted by the manufacturer were accurate to within a monomer unit. All g.p.c. showed a narrow band with molecular weight distributions of less than 1.1. The second batch of polyethylene glycol methoxylated used for some of the runs at 70.1°C however, showed slight traces of incomplete methoxylation. The samples used, their molecular weights and designations are shown in table 4:5,

Table 4:5.

Parent sample	molecular weight.	designation	methoxylated designation.
Polyethylene glycol	600	PEG 600	PEGM 600
Polypropylene glycol	400	PPG 400	PPGM 400
Polypropylene glycol	1000	PPG 1000	PPGM 1000
Polypropylene glycol	1500	PPG 1500	PPGM 1500
Polypropylene glycol	2000	PPG 2000	PPGM 2000

4:3. Methods of loading reaction cell.

The reaction cell was cleaned after each run either with detergent and distilled water or solvent followed by detergent and water, depending on the materials previously used. For aqueous solutions, the former method was used while the latter was used for oligomers. After the cell parts have been

carefully washed, they are flushed with acetone and then dried in an oven at 120°C for two hours before being loaded with samples for the next run.

4:3.1. Loading of samples.

(A). Aqueous solutions (HCl/NaOH reaction).

Known volumes of these solutions could be pipetted or syringed into the two compartments of the PTFE sample holder. Alternatively the PTFE holder could be weighed before and after each loading. In the neutralisation chemical test carried out, 1 ml. of the hydrochloric acid solution was introduced via a grade B Pyrex burette and 1.2 ml. of sodium hydroxide solution introduced by means of a 2 ml. grade B pipette graduated in tenths of a milliliter. This slight excess of NaOH was used in all the runs. This was done so that the HCl concentration is the limiting concentration.

(B). PEGM-PPGM samples.

The dry PTFE sample holder was weighed and the samples syringed in. The sample holder was weighed after each loading to determine the amount of each component used. Depending on the concentrations of the mixture used in each run, the lesser component was always placed in the compartment without the corner cut. This was done to ensure that, on inverting and re-inverting the cell during mixing, at least all the samples of the lesser component was involved in the mixing process. In general, a total mixture of between 1 to 1.5 gram was used for each run.

(C). PS-PBD samples.

Due to the viscosity of the polystyrene sample, it cannot be pipetted into the sample holder, even at elevated temperatures. Instead, a freezing technique was employed. The sample was heated in its container at 50°C until it flowed reasonably well. A thin glass rod, rounded at the ends, was dipped into the sample and withdrawn with some PS attached at the end. Liquid nitrogen was then poured into the compartment of a pre-weighed sample holder into which the PS sample was to be introduced. The PS at the end of the glass rod was then dipped into the liquid nitrogen where it become brittle and fractured. The fractured pieces settled to the bottom of the compartment and the liquid nitrogen was evaporated off. When most of the liquid nitrogen had evaporated off, the compartment containing the PS was carefully closed with a piece of tissue held in place by a finger. The holder was then quickly turned over to empty any pieces of PS which may have jumped into the next compartment during the fracturing process, and the compartment given a quick blast of air. The sample holder was then wiped on the outside to remove the moisture condensed and placed in an oven at 120°C for half an hour to dry before weighing. The amount of PS to be withdrawn on the end of the glass rod could be gauged fairly accurately after a few attempts.

The PBD samples used were fluid enough to be pipetted directly into the compartments. The main disadvantage in weighing in the PS sample in the way described is that the moisture trapped inside the sample on evaporating the liquid nitrogen might not be completely eliminated by the drying process. Drying to constant weight could be adopted, but the time scale might be a serious hindrance. This minor

disadvatage has to be borne with, in view of the ease and cleanliness of introducing the sample into the compartment.

4:3.2. Cell assembly after sample loading.

After the samples have been loaded into the sample holder, the holder was inserted into the bottom half of the main cell body. This was done in such a way that the corner that has been cut is always adjacent to the side of the cell facing the oven opening after insertion of the complete cell into the heat sink. Identification marks on all pieces of the same cell ensured that all the various components of that cell were assembled in the same manner each time that cell was used. Loading of the sample holder into the main cell body in this way is necessary so that on inverting and re-inverting the reaction(calorimeter) cell during mixing, the contents of the cell will flow back into the compartments without leakages. For more fluid samples, this re-inverting must not be done too rapidly, otherwise leakages of cell contents via the cut-outs will occur.

After the sample holder had been inserted, the remaining open end of the main cell body was sealed by the PTFE end-cap. The whole cell assembly was then placed in the aluminium press and the press slightly tightened. The main cell body within the press is then adjusted with the aid of a straight edge so that when inserted into the heat sink, there is an air gap between the side of the press and the front copper plates of the heat flow units. This was necessary to ensure that the heat flow path from the cell to the heat sink and vice-versa was through the thermoelectric modules only. After the cell

had been adjusted, the press was tightened completely so that the lips of the PTFE pieces act as seals and thermal insulation at both ends.

4:4. Experimental runs.

The assembled cell and press was placed in the pre-heating oven to pre-equilibrate the cell. After 15 minutes, the cell was transferred into the heat sink via the stud on the press and a long rod for final temperature equilibration. After the transference, the cell guide passageway was plugged up completely and the oven door closed. The amplifier gain was then chosen (A to L). Equilibration times varied, depending on the amplifier gain chosen. On a gain of E (1 mV f.s.d.) about 30 minutes was sufficient while at a setting of G (100 μV fsd.) about 1.5 hours was required to obtain a stable baseline. At a setting of H (30 μV fsd.) or higher, overnight equilibration was required.

4:4.1. Actual run.

After the required base line stability was attained, the deflection meter on the amplifier and the chart recorder were both zeroed by means of the offset and zero control knobs at the back of the amplifier/integrator and on the chart recorder respectively. The digital integrator was reset and the divider factor chosen. The temperature of the heat sink was noted via the decade resistance box. The digital integrator was then started and the run initiated by inverting and re-inverting the heat sink through 180^0 five times. This was necessary to ensure that any sample stuck to the walls of the sample holder was mixed. The speed at which these inversions

were carried out depended on the viscosities of the samples involved. After the final inversion, the heat sink was attached to the motor and axle arrangement so that the heat sink could be mechanically rocked slowly to and fro at an angle of 45^0 to the vertical. This rocking motion was maintained until a steady after period baseline was obtained. In general, a baseline shift will be seen to occur. Efforts to reduce or eliminate this baseline shift will be outlined in the discussion chapter.

At the end of the run, the stirring mechanism was detached and the heat sink returned to the starting position, and then inverted again to ensure that there was no further reaction. The integrator was stopped, the reading noted and the integrator reset. The heat sink was returned once more to the starting position and left in that position, whereby the fore period baseline would be attained after a short period (usually about 20 minutes). When this had occured, the integrator was started again, the heat sink inverted and attached to the stirring mechanism as before. This will induce the same baseline shift to occur as in the actual run. When sufficient length of the baseline shift had been obtained to cover the area under the curve (i.e. from the fore to the after period baselines) the stirring was stopped and the cell removed. The next pre-equilibrated cell was then loaded into the heat sink. The used cell was washed and dried after discarding the samples.

Should any leakages be seen to have occured, the copper plates of the heat flow units can be wiped via the cell insertion rod and a long piece of Kimwipe tissue. Care should be taken to ensure that the leads from the heat flow units are connected in the correct way for the nature of the reaction

under investigation i.e. exothermic or endothermic.

4:4.2. Run time and calculation of Area under the curve.

The operation time of each run depends on the thermal conductivities and viscosities of the samples under investigation. For aqueous systems, the reaction was completely over in less than 10 minutes from initiation of the run. For the methoxylated glycol systems, each run averages about 35 minutes, while for the PS-PBD system, each run averages 1¼ hours. Hence, taking into account the time required to do the baseline shift, about 7 runs are possible for aqueous solutions in an 8 hour period with an amplifier gain of E or lower. For the glycol systems, about 5 runs are possible with a gain of F while for the PS-PBD system, about 3 runs are possible at a gain of H.

In general, the temperature of the heat sink does not alter significantly. After the fourth run in the methoxylated glycol systems,the block temperature falls by about $0.1^{0}C$. This fall in temperature could partially be avoided if longer equilibration times were used i.e. the run rate reduced.

The area under the curve was obtained by tracing the plot on tracing paper and then superimposing the baseline shift on the plot. The tracing was cut out, weighed and the area obtained as in the case outlined in the electrical calibration. To obtain the integrator reading for the run, the integrator reading of the baseline shift was subtracted from the integrator reading of the actual run at the point where the after period baseline met the baseline shift. The amount of heat involved during the mixing was then obtained from the integrator counts-energy plot obtained from the

electrical calibration of the system concerned.

4:4.3. Blank heat effects.

Blank heat effects were measured by loading both the sample holder compartments with the same sample and executing a normal run. Polypropylene glycol was used. The heat effect observed was very small, in the region of a few hundred μJ. As this is almost in the limit of resolution of the amplifier used and well within experimental errors, this correction was neglected in the heats of mixing reported. Apart from the extremely small value involved, this omission was justified by the fact that partial correction had already been applied as a result of applying the baseline shift super-position.

4:5. Results.

The results of the chemical test and the heats of mixing of the various systems are given below under the conditions stated. Heats of mixing values are experimentally measured values and $-T\Delta S_m$ values are calculated from the Flory-Huggins ideal entropy contribution (equation 2:16). Molecular weights used are the rounded values quoted in the designation of each component.

4:5.1. HCl-NaOH chemical test.

The results of the heats of neutralization runs carried out at 30°C are shown in table 4:6. The energy measured in each run was normalised to per mole of HCl as shown in column 3. Column 4 is a correction applied to convert the data[56] to 25°C. Column 5 is a correction for the heats of dilution to standard state (infinite dilution) for the relative apparent molal enthalpies and heat capacities of the reactants and

products using the method of Pitzer[57] and the tabulated data of Parker[56] at 25°C. The final result in column 6 is the internal energy of ionization of water at 25°C.

Table 4:6.

Results of heats of neutralization measurements at 30°C.

Run no.	Measured heat/J	$-\Delta U$/ (kJ/mole)	Corrections to: (a) 25°C/ (kJ/mole)	(b) std.state (kJ/mole)	$-\Delta U_o$/ (kJ/mol.)
C_1	2.790	55.80	1.07	-0.535	56.335
C_2	2.795	55.90	1.07	-0.535	56.435
C_3	2.740	54.80	1.07	-0.535	55.335

Volume of HCl used in all 3 runs = 1.0 cm^3.

Volume of NaOH used in all 3 runs = 1.2 cm^3.

Average $-\Delta U_o$ = 56.040 (±0.608) kJ/mole.

Best literature value[56] = 55.810 (±0.100) kJ/mole.

The result measured on this calorimeter differed from the best literature value by 1%. Since the chemicals used in these tests were not subjected to extreme precautions and the BDH degree of purity was accepted, these results indicate that the accuracy of the calorimeter certainly is estimated to be about 1%.

4:5.2. Chain length compatibility.

Chain length compatibility was investigated by measuring the heats of mixing of PPG 400 with PPG of the other three molecular weights as a function of concentration of PPG 400 at 30^0C , as well as the heats of mixing of PPGM 400 with PPGM 1500. The results obtained were normalised to unit gram of the total mixture, as were all subsequent heat of mixing results. Volume fractions of the components were obtained using the specific volume data of Booth[55] et al. Tables 4:7 to 4:10 show the tabulated results obtained for the systems indicated at the top of each table. PPG 400 and PPGM 400 were used as component 1 where relevant with a chain length of 7.

Figures 4:4 to 4:6 show plots of the various tabulated quantities against PPG 400 (or PPGM 400) concentrations used. Dotted curves are experimental curves (where shown) while bold curves are drawn where possible to produce smooth curves within experimental errors. The errors incurred in the heats of mixing are 5% and 8% for the glycols and the methoxylated systems respectively. The percentage error in the glycol system is estimated as described later (see section 4:5.3). The percentage error for the methoxylated components is larger due to the high sensitivity of the amplifier used as a consequence of the small energies involved.

Table 4:7.

Results of PPG 400-PPG 1025 system at 30.1(±0.1) ^{0}C. Ref. wt.=1g total mixture.

Run number GOH	W_2/ (g)	W_1/ (g)	$n_2 \times 10^4$/ (moles)	ϕ_2	$n_1 \times 10^4$/ (moles)	ϕ_1	Δh_m/ (J/g) (meas.)	$-T\Delta S_m$/ (J/g) (cal.)	Δg_m/ (J/g) (cal.)	χ_{12} ($g \times 10^2$)
33	0.5076	0.4924	4.9522	0.5087	12.3100	0.4913	0.383	-3.050	-2.667	3.465
34	0.4100	0.5900	4.0000	0.4110	14.7500	0.5890	0.333	-2.865	-2.532	3.112
35	0.6150	0.3850	6.0000	0.6161	9.6250	0.3839	0.333	-3.056	-2.723	3.182
36	0.4573	0.5427	4.4615	0.4584	13.5675	0.5416	0.369	-2.975	-2.606	3.362
38	0.3379	0.6621	3.2966	0.3388	16.5525	0.6612	0.294	-2.626	-2.332	2.970
39	0.2218	0.7782	2.1639	0.2226	19.4550	0.7774	0.234	-2.055	-1.821	3.062
41	0.2699	0.7301	2.6332	0.2707	18.2525	0.7293	0.276	-2.320	-2.044	3.165
42	0.7446	0.2554	7.2644	0.7454	6.3850	0.2546	0.287	-2.741	-2.454	3.417
43	0.8036	0.1964	7.8400	0.8043	4.9100	0.1957	0.227	-2.450	-2.223	3.257
44	0.6257	0.3743	6.1044	0.6267	9.3575	0.3733	0.336	-3.044	-2.708	3.246
45	0.7737	0.2263	7.5483	0.7744	5.6575	0.2256	0.265	-2.611	-2.611	3.427
46	0.6753	0.3247	6.5883	0.6763	8.1175	0.3237	0.333	-2.958	-2.625	3.437
47	0.5719	0.4281	5.5795	0.5730	10.7025	0.4270	0.384	-3.080	-2.696	3.548

W_2=Wt. of PPG 1025 used. n_i= no. of moles component i. (cal.)=calculated values.

W_1=Wt. of PPG 400 used. ϕ_i= vol. fraction of comp. i. (meas.)=measured values.

Degree of polymerisation of PPG 400= 7.

Table 4:8

Results of PPG 400-PPG 1500 system at 30.1(±0.1)°C. Ref. wt.= 1g of total mixture.

Run number GOH	W_2/ (g)	W_1/ (g)	$n_2 \times 10^4$/ (moles)	ϕ_2	$n_1 \times 10^4$/ (moles)	ϕ_1	Δh_m/ (J/g) (meas.)	$-T\Delta S_m$/ (J/g) (cal.)	Δg_m/ (J/g) (cal.)	χ_{12} ($g \times 10^2$)
23	0.1961	0.8139	1.3073	0.1868	20.3475	0.8132	0.318	-1.614	-1.296	4.740
24	0.3497	0.6503	2.3313	0.3508	16.2575	0.6492	0.518	-2.387	-1.869	5.146
25	0.4476	0.5524	2.9840	0.4488	13.8100	0.5512	0.551	-2.677	-2.126	5.037
26	0.5307	0.4693	3.5380	0.5314	11.7325	0.4686	0.550	-2.806	-2.256	4.998
27	0.6519	0.3481	4.3460	0.6530	8.7025	0.3470	0.570	-2.789	-2.219	5.683
28	0.7697	0.2303	5.1313	0.7706	5.7575	0.2294	0.451	-2.474	-2.023	5.760
29	0.5765	0.4235	3.8433	0.5778	10.5875	0.4222	0.573	-2.833	-2.260	5.307
30	0.8694	0.1306	5.7960	0.8700	3.2650	0.1300	0.303	-1.883	-1.580	6.044
31	0.4398	0.5602	2.9320	0.4410	14.0050	0.5590	0.551	-2.659	-2.108	5.055
32	0.1258	0.8742	0.8387	0.1263	21.8550	0.8737	0.215	-1.182	-0.967	4.413

W_2= wt. of PPG 1500. n_i=no. of moles of comp. i. (cal.)=calculated values.

W_1= wt. of PPG 400. ϕ_i=vol. fraction of comp. i. (meas.)=measured values.

Degree of polymerisation of PPG 400=7.

Table 4:9.

Results of PPG 400-PPG 2000 system at 30.1(±0.1)°C. Ref. wt. = 1g . of total mixture.

Run number GOH	W_2/ (g)	W_1/ (g)	$n_2 \times 10^4$/ (moles)	ϕ_2	$n_1 \times 10^4$/ (moles)	ϕ_1	Δh_m/ (J/g) (meas.)	$-T\Delta S_m$/ (J/g) (cal.)	Δg_m/ (J/g) (cal.)	χ_{12} (g $\times 10^2$)
2	0.5411	0.4589	2.7055	0.5547	11.4725	0.4453	0.776	-2.742	-1.966	6.909
3	0.3411	0.6589	1.7055	0.3539	16.4725	0.6461	0.679	-2.261	-1.582	6.599
4	0.5974	0.4026	2.9870	0.6109	10.0650	0.3891	0.692	-2.767	-2.075	6.377
5	0.8647	0.1353	4.3235	0.8621	3.3825	0.1379	0.423	-1.851	-1.428	8.219
6	0.4570	0.5430	2.2850	0.4711	13.5750	0.5289	0.761	-2.614	-1.853	6.742
8	0.7536	0.2464	3.7680	0.7640	6.1600	0.2360	0.653	-2.498	-1.845	7.862
9	0.6965	0.3035	3.4825	0.7082	7.5875	0.2918	0.690	-2.659	-1.969	7.276
10	0.6246	0.3754	3.1230	0.6378	9.3850	0.3622	0.714	-2.757	-2.043	6.759
11	0.1233	0.8767	0.6165	0.1295	21.9175	0.8705	0.290	-1.084	-0.794	5.789
12	0.2497	0.7503	1.2485	0.2458	18.7575	0.7542	0.516	-1.776	-1.260	6.341
13	0.6581	0.3419	3.2905	0.6707	8.5475	0.3293	0.703	-2.725	-2.022	6.948

W_1=wt. of PPG 400 used. n_i= no. of moles of comp. i. (cal.)=calculated values.

W_2=wt. of PPG 2000 used. ϕ_i= vol. fraction of comp. i. (meas.)=measured values.

Degree of polymerisation of PPG 400=7.

Table 4:10.

Results of PPGM 400-PPGM 1500 system at 30.1(±0.1)°C. Ref. wt. = 1g . total of mixture.

Run number (4/15)	W_1/ (g)	W_2/ (g)	$n_1 \times 10^4$/ (moles)	ϕ_1	$n_2 \times 10^4$/ (moles)	ϕ_2	Δh_m/ (J/g) $\times 10^{-3}$	$-T\Delta S_m$/ (J/g) (cal.)	Δg_m/ (J/g) (cal.)	χ_{12} (g $\times 10^4$)
1	0.3574	0.6426	8.9350	0.3652	4.2840	0.6348	-9.99	-2.7601	-2.7601	-9.9795
2	0.6521	0.3479	16.3025	0.6598	2.3193	0.3402	-12.63	-2.3397	-2.3523	-12.9030
3	0.5448	0.4552	13.6200	0.5268	3.0347	0.4732	-11.93	-2.7735	-2.7854	-10.4880
4	0.8307	0.1693	20.7680	0.8354	1.1287	0.1646	-7.94	-1.4552	-1.4631	-13.1605
5	0.4090	0.5910	10.2250	0.4173	3.9400	0.5827	-10.52	-2.7896	-2.8001	-10.0042

W_1=wt. of PPGM 400 used. n_i=no. of moles of comp.i. (cal.)=calculated values.

W_2=wt. of PPGM 1500 used. ϕ_i=vol. fraction of comp. i.

Degree of polymerisation of PPGM 400= 7.

Fig 4:4.

Heat of mixing (Δh_m) and entropy of mixing ($-T\Delta S_m$) versus PPG 400 volume fraction plots for PPG-PPG system at 30.1°C.

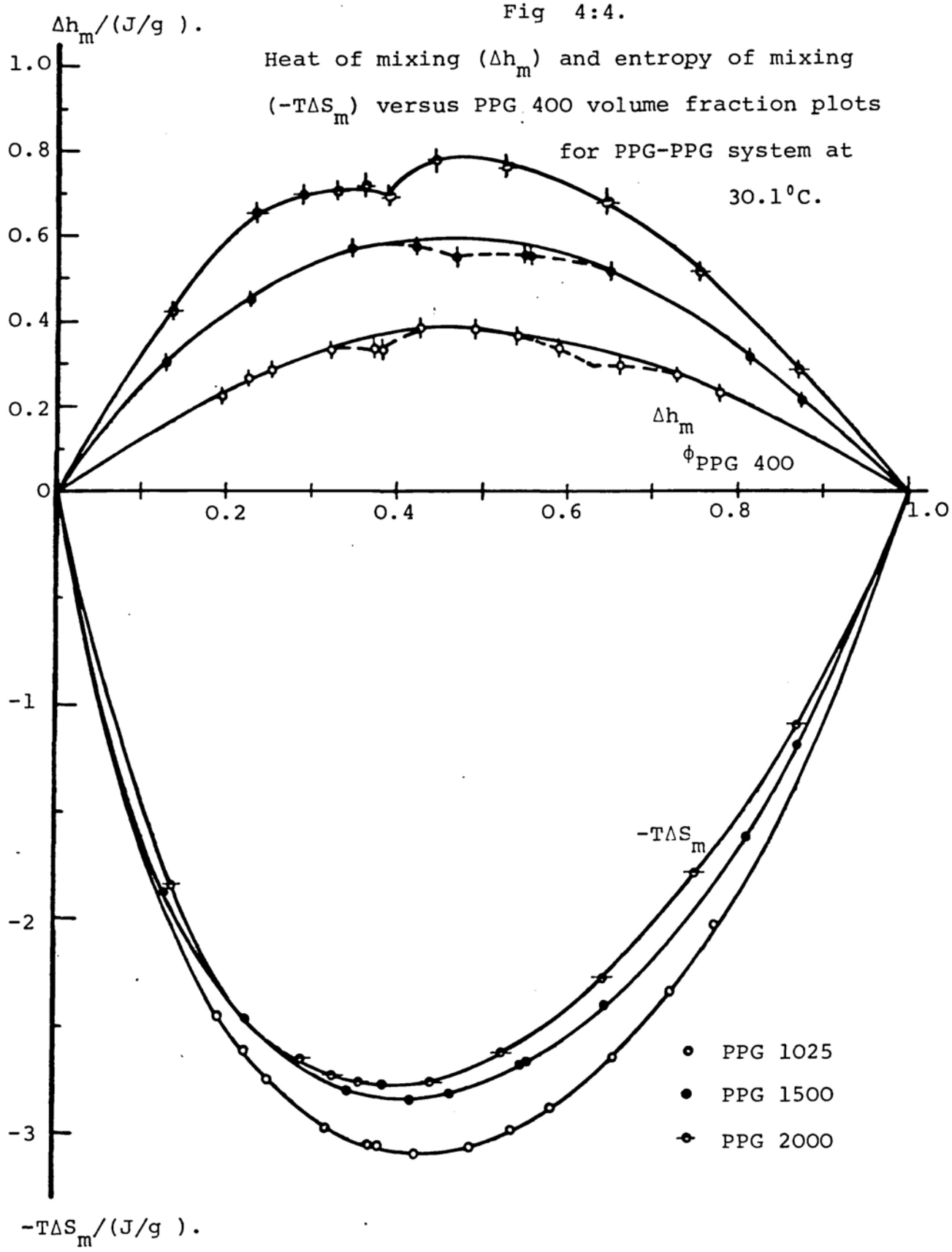
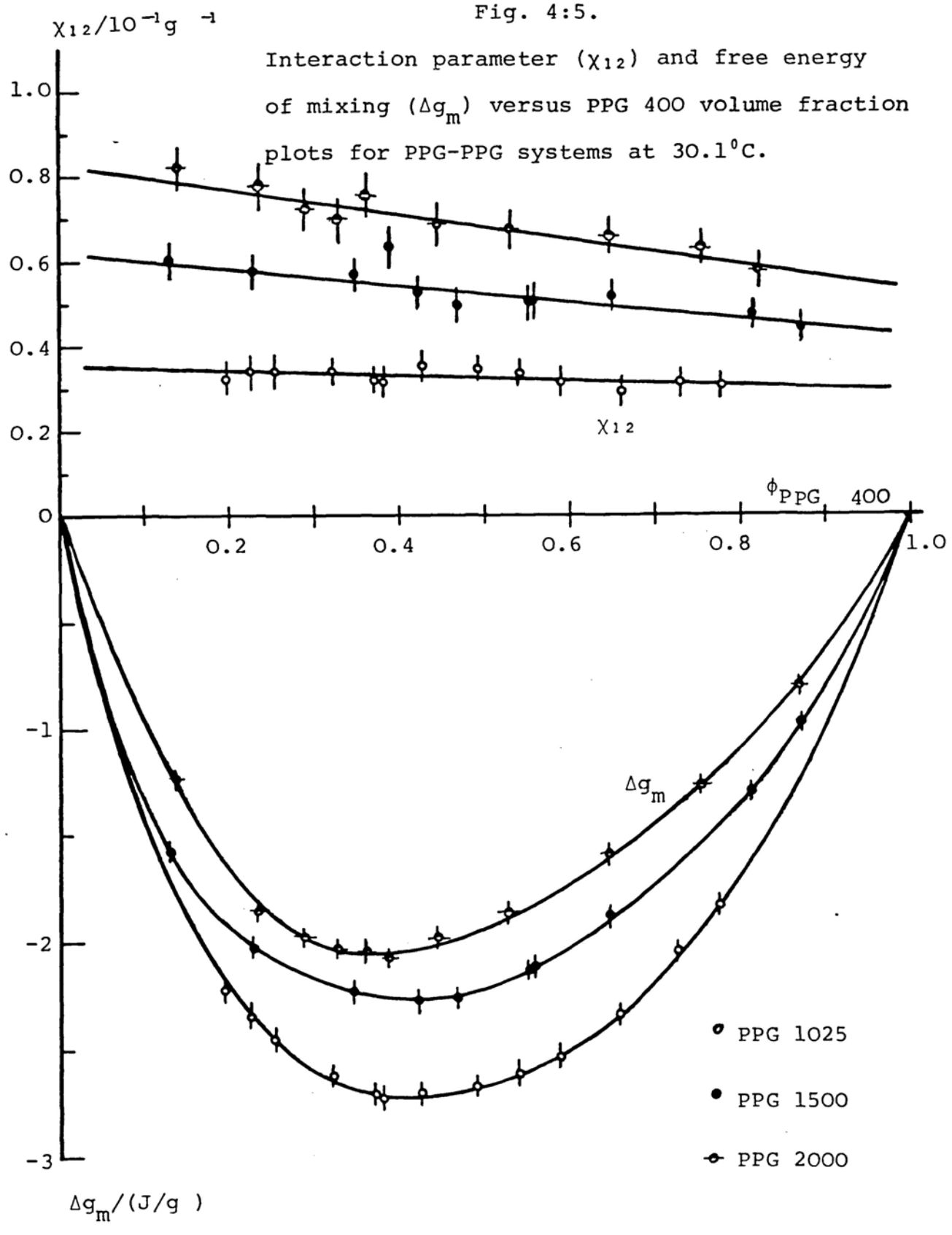


Fig. 4:5.

Interaction parameter (χ_{12}) and free energy of mixing (Δg_m) versus PPG 400 volume fraction plots for PPG-PPG systems at 30.1°C.



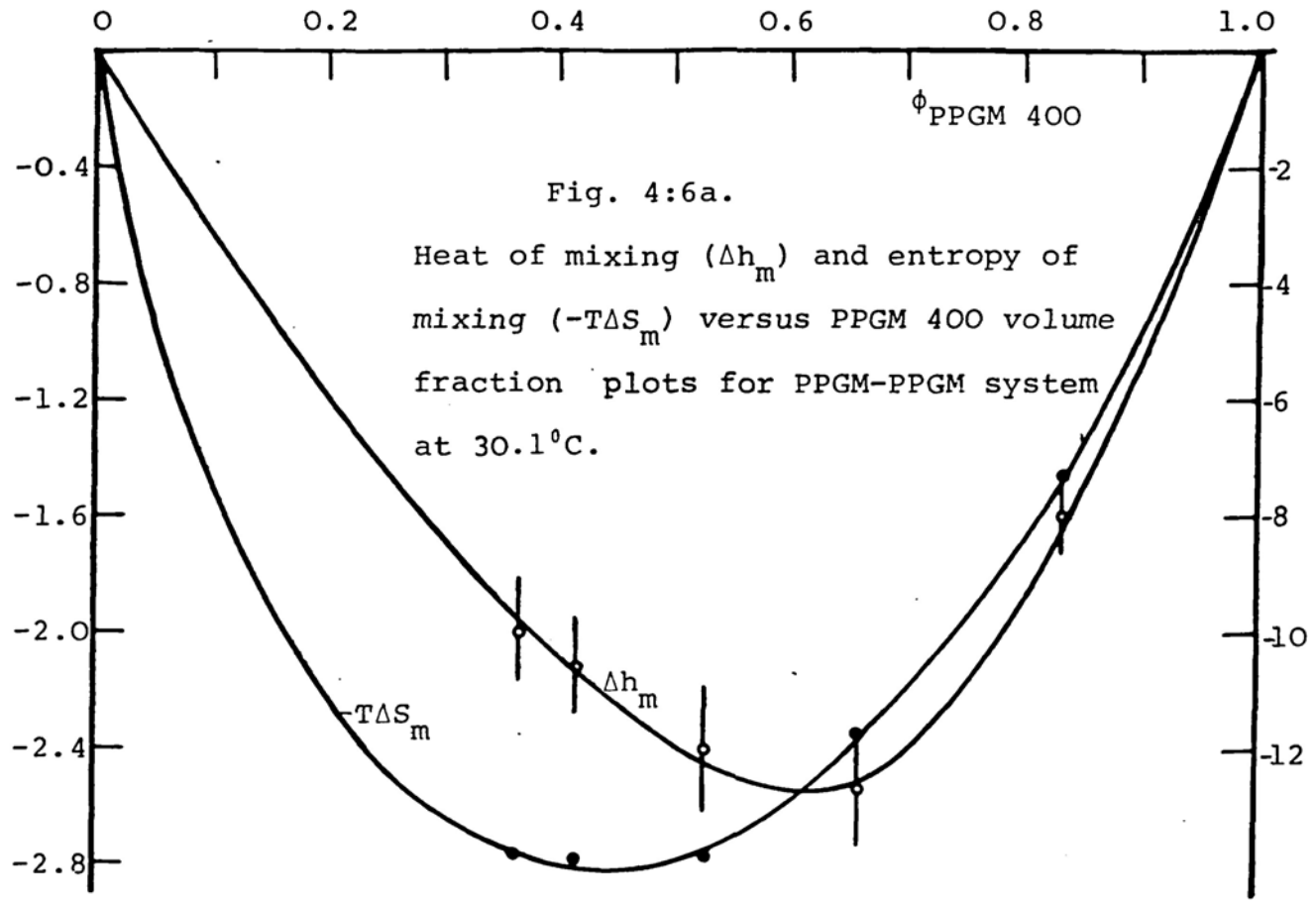


Fig. 4:6a.

Heat of mixing (Δh_m) and entropy of mixing ($-T\Delta S_m$) versus PPGM 400 volume fraction plots for PPGM-PPGM system at 30.1°C.

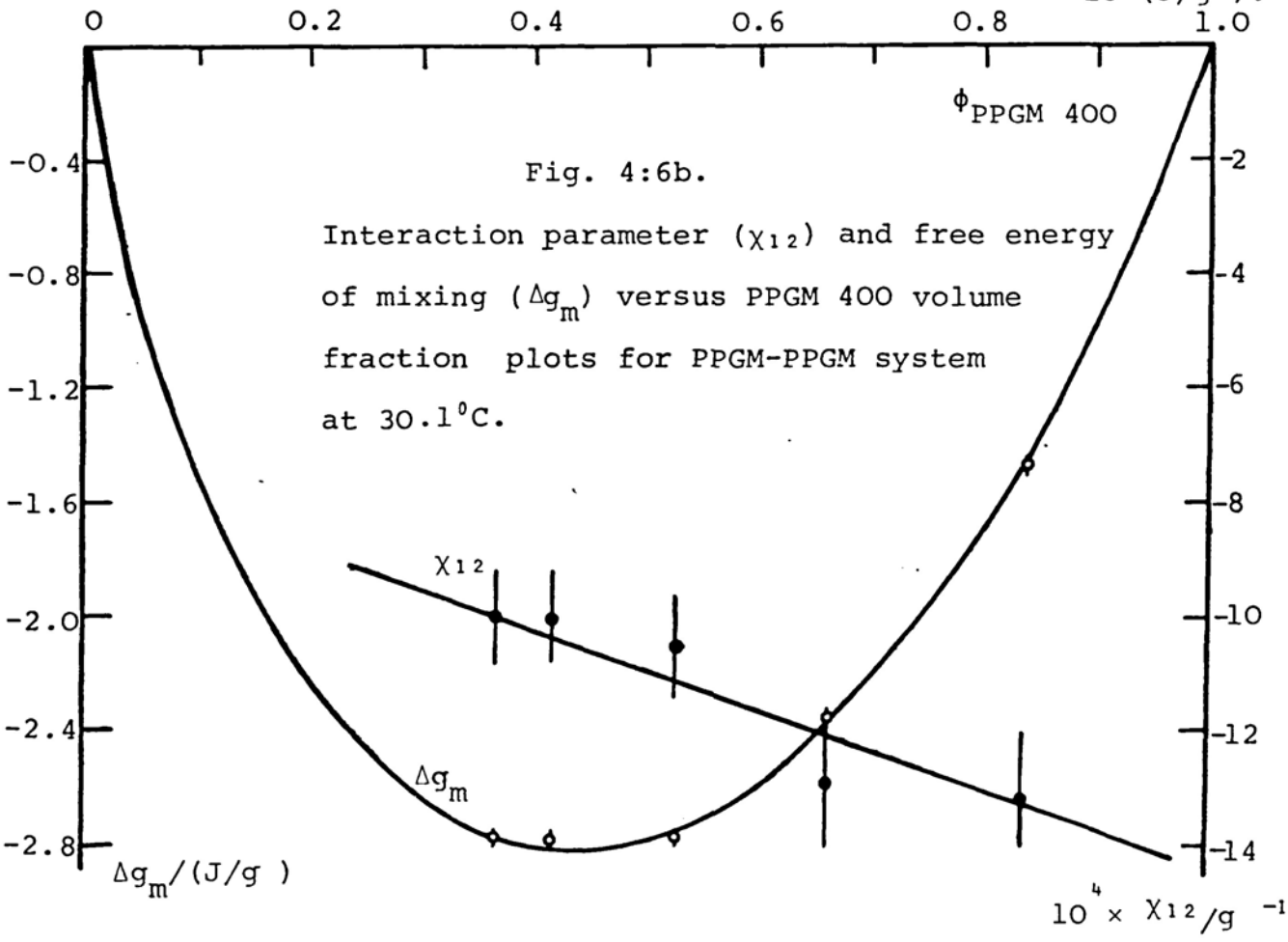


Fig. 4:6b.

Interaction parameter (χ_{12}) and free energy of mixing (Δg_m) versus PPGM 400 volume fraction plots for PPGM-PPGM system at 30.1°C.

4:5.3. PEGM-PPGM system.

The heats of mixing of PEGM 600 with PPGM of various molecular weights were measured at three temperatures, namely, 30.1, 50.1 and 70.1°C. In order to test the reproducibility of the results obtained, several runs were made at 30.1°C for the PEGM 600-PPGM 2000 system at a fixed concentration. Table 4:11 shows the results of these runs.

Table 4:11.

Results of reproducibility runs at 30.1°C.

ϕ_1 = 0.488, ϕ_2 = 0.512 (PEGM 600 = component 1)

Run number	TBS_1	TBS_2	TBS_3	TBS_4	TBS_5
Δh_m/(J/g)	0.778	0.799	0.784	0.828	0.792

Average Δh_m = 0.796(±0.020) J/g

As can be seen, the value of any single run could be safely estimated to within an error of ±3%. To test the accuracy of tracing and cutting the area under the peak using tracing paper, it was found that tracing and cutting out the same peak several times showed a deviation of less than 1% of subsequent attempts from that of the first attempt. In general, the accuracy of the heats of mixing could be taken to be within ±4% for energies above 0.1 J/g , while the accuracy below 0.1 J/g is estimated to be within ±8% due to the larger baseline shift observed owing to the higher sensitivity required of the amplifier.Tables 4:12 to 4:22 show the results obtained for the various binary PEGM-PPGM systems investigated at the temperatures indicated at the topof each table. Figures 4:7 to 4:12 show the results in graphical form. PEGM 600 is component 1 with a degree of

polymerisation of 14. Volume fractions were obtained using the specific volume data of Booth[55] et al and Tripathi[13]. The heat of mixing results at 70.1°C were obtained from a new batch of PEGM 600, except for the PEGM 600* curve, which appears to show slight traces of incomplete methoxylation. This is reflected in the lower endothermal heats of mixing. The PEGM 600* curve was obtained using the batch of completely methoxylated PEGM 600 used in previous measurements.

Table 4:12.

Results of PEGM 600-PPGM 400 system at 30.1(±0.1)°C. Ref. wt= 1g . of total mixture.

Run number 6/4M	W_2/ (g)	W_1/ (g)	$n_2 \times 10^4$/ (moles)	ϕ_2	$n_1 \times 10^4$/ (moles)	ϕ_1	Δh_m/ (J/g)	$-T\Delta S_m$/ (J/g) (cal.)	Δg_m/ (J/g) (cal.)	χ_{12} (g)
1	0.5135	0.4865	12.8375	0.5429	8.1083	0.4571	2.550	-3.578	-1.028	0.1641
2	0.6165	0.3835	15.4125	0.6441	6.3917	0.3559	2.430	-3.374	-0.944	0.1672
3	0.3409	0.6591	8.5225	0.3679	10.9850	0.6321	2.315	-3.419	-1.104	0.1623
4	0.2563	0.7437	6.4075	0.2795	12.3950	0.7205	1.989	-3.084	-1.095	0.1626
5	0.1522	0.8478	3.8050	0.1680	14.1300	0.8320	1.481	-2.367	-0.886	0.1767
6	0.7399	0.2601	18.4975	0.7620	4.3350	0.2380	2.130	-2.837	-0.707	0.1827
7	0.8448	0.1552	21.1200	0.8597	2.5867	0.1403	1.390	-2.086	-0.696	0.1771
8	0.4425	0.5574	11.0625	0.4719	9.2900	0.5281	2.495	-3.590	-1.095	0.1612

W_1=wt. of PEGM 600 used. n_i=no. of moles of comp. i. (cal.)=calculated values.

W_2= wt. of PPGM 400 used. ϕ_i=vol. fraction of comp. i.

Degree of polymerisation of PEGM 600 used for calculating χ_{12} = 14.

Table 4:13.

Results of PEGM 600-PPGM 1000 system at 30.1(±0.1)^{0}C. Ref. wt.= 1g . of total mixture.

Run number 6/10M	W_2/ (g)	W_1/ (g)	$n_2 \times 10^4$/ (moles)	ϕ_2	$n_1 \times 10^4$/ (moles)	ϕ_1	Δh_m/ (J/g)	$-T\Delta S_m$/ (J/g) (cal.)	Δg_m/ (J/g) (cal.)	χ_{12} (g)
1	0.3624	0.6376	3.6240	0.3836	10.6267	0.6164	2.322	-2.172	0.150	0.1614
2	0.5693	0.4307	5.6930	0.5914	7.1783	0.4086	2.550	-2.374	0.176	0.1702
3	0.6765	0.3235	6.7650	0.6960	5.3917	0.3040	2.357	-2.237	0.120	0.1779
4	0.4840	0.5160	4.8400	0.5066	8.6000	0.4934	2.582	-2.362	0.220	0.1679
5	0.1650	0.8350	1.6500	0.1779	13.9167	0.8221	1.525	-1.406	0.119	0.1745
6	0.8333	0.1667	8.3330	0.8456	2.7783	0.1544	1.620	-1.661	-0.041	0.1954
7	0.2925	0.7075	2.9250	0.3116	11.7917	0.6884	2.160	-1.970	0.190	0.1665

W_1= wt. of PEGM 600 used. n_i= no. of moles of comp. i. (cal.)=calculated values.

W_2= wt. of PPGM 1000 used. ϕ_i=vol. fraction of comp. i.

Degree of polymerisation of PEGM 600 = 14.

Table 4:14.

Results of PEGM 600-PPGM 1500 system at 30.1(±0.1)°C. Ref. wt.= 1g . of total mixture.

Run number 6/15M	W_2/ (g)	W_1/ (g)	$n_2 \times 10^4$/ (moles)	ϕ_2	$n_1 \times 10^4$/ (moles)	ϕ_1	Δh_m/ (J/g)	$-T\Delta S_m$/ (J/g) (cal.)	Δg_m/ (J/g) (cal.)	χ_{12} (g)
1	0.4224	0.5776	2.8160	0.4431	9.6267	0.5569	2.303	-1.999	0.304	0.1530
2	0.3737	0.6263	2.4913	0.3936	10.4383	0.6064	2.209	-1.902	0.307	0.1523
3	0.5939	0.4061	3.9593	0.6140	6.7683	0.3860	2.305	-2.111	0.194	0.1571
4	0.6904	0.3096	4.6027	0.7081	5.1600	0.2919	2.050	-2.003	0.047	0.1589
5	0.8333	0.1667	5.5553	0.8447	2.7783	0.1553	1.541	-1.541	-0.001	0.1859
6	0.1848	0.8152	1.2320	0.1978	13.5867	0.8022	1.533	-1.258	0.275	0.1616
7	0.5296	0.4704	3.5307	0.5505	7.8400	0.4495	3.383	-2.112	0.271	0.1564

W_1= wt. of PEGM 600 used. n_i= no. of moles of comp. i. (cal.)=calculated values.

W_2= wt. of PPGM 1500 used. ϕ_i=vol. fraction of comp. i.

Degree of polymerisation of PEGM 600 = 14.

Table 4:15.

Results of PEGM 600-PPGM 2000 system at 30.1(±0.1)°C. Ref. wt. = 1g . of total mixture.

Run number 6/20M	W_2/ (g)	W_1/ (g)	$n_2 \times 10^4$/ (moles)	ϕ_2	$n_1 \times 10^4$/ (moles)	ϕ_1	Δh_m/ (J/g)	$-T\Delta S_m$/ (J/g) (cal.)	Δg_m/ (J/g) (cal.)	χ_{12} (g)
3	0.3548	0.6452	1.7740	0.3737	10.7533	0.6263	1.917	-1.709	0.208	0.1351
4	0.7147	0.2853	3.5735	0.7310	4.7550	0.2690	1.733	-1.857	-0.124	0.1412
5	0.2229	0.7771	1.1145	0.2373	12.9517	0.7627	1.514	-1.289	0.225	0.1396
6	0.6344	0.3656	3.1720	0.6530	6.0933	0.3470	1.985	-1.967	0.018	0.1413
7	0.5066	0.4934	2.5330	0.5270	8.2233	0.4730	2.127	-1.961	0.166	0.1390
8	0.8357	0.1643	4.1785	0.8466	2.7383	0.1534	1.303	-1.470	-0.167	0.1592
9	0.1437	0.8563	0.7185	0.1541	14.2717	0.8459	1.099	-0.941	0.158	0.1416
10	0.5532	0.4468	2.7660	0.5732	7.4467	0.4268	2.129	-1.987	0.142	0.1413
11	0.5258	0.4742	2.6290	0.5460	7.9033	0.4540	2.098	-1.975	0.123	0.1377
12	0.4283	0.5717	2.1415	0.4483	9.5283	0.5517	1.966	-1.862	0.104	0.1304
13	0.4502	0.5498	2.2510	0.4704	9.1633	0.5296	1.993	-1.897	0.096	0.1310
14	0.5254	0.4746	2.6270	0.5455	7.9100	0.4545	2.057	-1.974	0.083	0.i3i5
15	0.4507	0.5493	2.2535	0.4709	9.1550	0.5291	1.962	-1.897	0.065	0.1289

W_1=wt. of PEGM 600 used in each run. n_i=no. of moles of comp. i. (cal.)=calculated values.

W_2= wt. of PPGM 2000 used in each run. $_i$=vol. fraction of comp. i.

Degree of polymerisation of PEGM 600 =14.

Table 4:16.

Results of PEGM 600-PPGM 1000 system at 50.1(±0.1)°C. Ref. wt.=1g . of total mixture.

Run number 10M50	W_2/ (g)	W_2/ (g)	$n_2 \times 10^4$/ (moles)	ϕ_2	$n_1 \times 10^4$/ (moles)	ϕ_1	Δh_m/ (J/g)	$-T\Delta S_m$/ (J/g) (cal.)	Δg_m/ (J/g) (cal.)	χ_{12} (g)
1	0.6736	0.3264	6.7360	0.6922	5.4400	0.3078	2.090	-2.389	-0.299	0.1475
2	0.4873	0.5127	4.8730	0.5088	8.5450	0.4912	2.245	-2.518	-0.273	0.1372
3	0.3871	0.6129	3.8710	0.4077	10.2150	0.5923	2.152	-2.371	-0.219	0.1373
4	0.2583	0.7417	2.5830	0.2752	12.3617	0.7248	1.940	-1.965	-0.025	0.1516
5	0.8162	0.1838	8.1620	0.8287	3.0633	0.1713	1.541	-1.865	-0.324	0.1613
6	0.1500	0.8500	1.5000	0.1613	14.1667	0.8387	1.278	-1.405	-0.127	0.1486
7	0.5957	0.4043	5.9570	0.6163	6.7383	0.3837	2.295	-2.510	-0.215	0.1469
8	0.2725	0.7275	2.7250	0.2899	12.1250	0.7101	2.098	-2.022	-0.076	0.1586

W_1=wt. of PEGM 600 used in each run. n_i=no. of moles of comp. i. (cal.)=calculated values.

W_2=wt. of PPGM 1000 used in each run. ϕ_i=vol. fraction of comp. i.

Degree of polymerisation of PEGM 600 = 14.

Table 4:17.

Results of PEGM 600-PPGM 1500 system at 50.1(±0.1)°C. Ref. wt.= 1g . of total mixture.

Run number 15M50	W_2/ (g)	W_1/ (g)	$n_2 \times 10^4$/ (moles)	ϕ_2	$n_1 \times 10^4$/ (moles)	ϕ_1	Δh_m/ (J/g)	$-T\Delta S_m$/ (J/g) (cal.)	Δg_m/ (J/g) (cal.)	χ_{12} (g)
1	0.5509	0.4491	3.6727	0.5714	7.4850	0.4286	1.983	-2.257	-0.274	0.1232
2	0.3116	0.6884	2.0773	0.3294	11.4733	0.6706	2.001	-1.852	0.149	0.1407
3	0.4345	0.5655	2.8967	0.4550	9.4250	0.5450	2.085	-2.151	-0.066	0.1292
4	0.6877	0.3123	4.5847	0.7053	5.2050	0.2947	2.044	-2.139	-0.095	0.1480
5	0.1658	0.8342	1.1053	0.1777	13.9033	0.8223	1.342	-1.244	0.098	0.1444
6	0.8491	0.1509	5.6607	0.8594	2.5150	0.1406	1.174	-1.557	-0.383	0.1444
7	0.6300	0.3700	4.2000	0.6498	6.1667	0.3508	2.081	-2.224	-0.143	0.1381
8	0.5980	0.402o	3.9867	0.6178	6.7000	0.3822	2.070	-2.248	-0.178	0.1329
9	0.5530	0.4470	3.6867	0.5734	7.4500	0.4266	2.066	-2.257	-0.191	0.1285

W_1= wt. of PEGM 600 used. n_i=no. of moles of comp. i. (cal.)=calculated values.

W_2= wt. of PPGM 1500 used. ϕ_i=vol. fraction of comp. i.

Deg. of poly. of PEGM 600 = 14.

Table 4:18.

Results of PEGM 600-PPGM 2000 system at 50.1(±0.1)^{0}C. Ref. wt.= 1g of total mixture.

Run number 20M50	W_2/ (g)	W_1/ (g)	$n_2 \times 10^4$/ (moles)	ϕ_2	$n_1 \times 10^4$/ (moles)	ϕ_1	Δh_m/ (J/g)	$-T\Delta S_m$/ (J/g) (cal.)	Δg_m/ (J/g) (cal.)	χ_{12} (g)
1	0.4464	0.5536	2.2320	0.4651	9.2267	0.5349	1.829	-2.021	-0.192	0.1133
2	0.3277	0.6723	1.6385	0.3441	11.2050	0.6554	1.735	-1.742	-0.007	0.1194
3	0.7524	0.2476	3.7620	0.7662	4.1267	0.2338	1.686	-1.881	-0.195	0.1417
4	0.6593	0.3407	3.2965	0.6761	5.6783	0.3239	1.845	-2.067	-0.222	0.1277
5	0.5383	0.4617	2.6915	0.5571	7.6950	0.4429	1.840	-2.107	-0.267	0.1141
6	0.1815	0.8185	0.9075	0.1930	13.6417	0.8070	1.214	-1.187	0.027	0.1225
7	0.1627	0.8373	0.8135	0.1732	13.9550	0.8268	1.196	-1.097	0.099	0.1315
8	0.2389	0.7611	1.1945	0.2530	12.6850	0.7470	1.464	-1.435	0.029	0.1212
9	0.8482	0.1572	4.2140	0.8513	2.6200	0.1487	1.158	-1.524	-0.366	0.1380
10	0.7524	0.2476	3.7620	0.7662	4.1267	0.2338	1.648	-1.881	-0.233	0.1385

W_1=wt. of PEGM 600 used. n_i= moles of comp. i. (cal.)=calculated values.

W_2=wt. of PPGM 2000 used. ϕ_i=vol. fraction of comp. i.

Deg. of poly. of PEGM 600 = 14.

Table 4:19.

Results of the PEGM 600-PPGM 1000 system at 70.1(±0.1)°C. Ref. wt.= 1g . of total mixture.

Run number 10M70	W_2/ (g)	W_1/ (g)	$n_2 \times 10^4$/ (moles)	ϕ_2	$n_1 \times 10^4$/ (moles)	ϕ_1	Δh_m/ (J/g)	$-T\Delta S_m$/ (J/g) (cal.)	Δg_m/ (J/g) (cal.)	χ_{12} (g) $\times 10^2$
1	0.5551	0.4449	5.5510	0.5756	7.4150	0.4244	1.577	-2.689	-1.112	9.248
2	0.6978	0.3022	6.9780	0.7150	5.0367	0.2850	1.401	-2.472	-1.071	9.737
3	0.4050	0.5950	4.0500	0.4252	9.9167	0.5748	1.537	-2.5560	-1.019	9.123
4	0.2174	0.7826	2.1740	0.2319	13.0433	0.7681	0.819	-1.889	-1.070	6.777
5	0.7952	0.2048	7.9520	0.8083	3.4133	0.1917	1.239	-2.092	-0.853	11.240
6	0.3135	0.6865	3.1350	0.3316	11.4417	0.6684	1.278	-2.303	-1.025	8.431
7	0.4722	0.5278	4.7220	0.4930	8.7967	0.5070	1.638	-2.658	-1.020	9.453
8	0.5945	0.4055	5.9450	0.6143	6.7583	0.3857	1.493	-2.664	-1.171	9.007
9	0.6553	0.3447	6.5530	0.6738	5.7450	0.3262	1.387	-2.575	-1.188	8.968

W_1=wt. of PEGM 600 used.
W_2=wt. of PPGM 1000 used .
Deg. of poly. of PEGM 600 = 14.

n_i=moles of comp. i.
ϕ_i=vol. fraction of comp. i.

(cal.)= calculated values.

(new batch of PEGM 600 used)

Table 4:20.

Results of PEGM 600-PPGM 1500 system at 70.1(±0.1)°C. Ref. wt.= 1g . of total mixture.

Run number 15M70	W_2/ (g)	W_1/ (g)	$n_2 \times 10^4$/ (moles)	ϕ_2	$n_1 \times 10^4$/ (moles)	ϕ_1	Δh_m/ (J/g)	$-T\Delta S_m$/ (J/g) (cal.)	Δg_m/ (J/g) (cal.)	χ_{12} (g) $\times 10^2$
1	0.4235	0.5765	2.8233	0.4431	9.6083	0.5569	1.478	-2.261	-0.783	8.689
2	0.6046	0.3954	4.0307	0.6235	6.5900	0.3765	1.289	-2.381	-1.092	7.852
3	0.5134	0.4866	3.4227	0.5334	8.1100	0.4666	1.496	-2.378	-0.882	8.655
4	0.7112	0.2888	4.7413	0.7273	4.8133	0.2727	1.259	-2.216	-0.957	9.001
5	0.2944	0.7056	1.9627	0.3113	11.7600	0.6887	1.152	-1.905	-0.753	7.876
6	0.1459	0.8541	0.9727	0.1561	14.2350	0.8439	0.511	-1.205	-0.694	5.756
7	0.4270	0.5730	2.8467	0.4467	9.5500	0.5533	1.437	-2.268	-0.831	8.431
8	0.8391	0.1609	5.5940	0.8496	2.6817	0.1504	0.939	-1.710	-0.771	10.315

W_1= wt. of PEGM 600 used. n_i=moles of comp. i. (cal.)=calculated values.

W_2=wt. of PPGM 1500 used. ϕ_i=vol.fraction of comp. i.

Deg. of poly. of PEGM 600 = 14. (New batch of PEGM 600 used)

Table 4:21.

Results of PEGM 600-PPGM 2000 system at 70.1(±0.1)^{0}C. Ref. wt.= 1g . of total mixture.

Run number 20M70	W_2/ (g)	W_1/ (g)	$n_2 \times 10^4$/ (moles)	ϕ_2	$n_1 \times 10^4$/ (moles)	ϕ_1	Δh_m/ (J/g)	$-T\Delta S_m$/ (J/g) (cal.)	Δg_m/ (J/g) (cal.)	χ_{12} (g)$\times 10^2$
1	0.4965	0.5035	2.4825	0.5146	8.3917	0.4854	1.427	-2.202	-0.775	8.271
2	0.3496	0.6504	1.7480	0.3662	10.8400	0.6338	1.248	-1.912	-0.664	7.869
3	0.6133	0.3867	3.0665	0.6304	6.4450	0.3696	1.396	-2.235	-0.839	8.600
4	0.7865	0.2135	3.9325	0.7984	3.5583	0.2016	1.268	-1.879	-0.611	11.171
5	0.1681	0.8319	0.8405	0.1785	13.8650	0.8215	0.616	-1.191	-0.575	6.230
6	0.6822	0.3178	3.4110	0.6977	5.2967	0.3023	1.430	-2.159	-0.729	9.685
7	0.8862	0.1138	4.4310	0.8934	1.8967	0.1066	0.820	-1.354	-0.534	12.112
9	0.4972	0.5028	2.4860	0.5153	8.3800	0.4847	1.471	-2.202	-0.731	8.52 6

W_1=wt. of PEGM 600 used. n_i=moles of comp. i. cal=calculated values.

W_2= wt. of PPGM 2000 used. ϕ_i=vol. fraction of comp. i.

Deg. of poly. of PEGM 600 = 14. (New batch of PEGM 600 used).

Table 4:22.

Results of PEGM*600-PPGM 2000 system at 70.1(±0.1) ^{0}C. Ref. wt.= 1g . of total mixture.

Run number 20*M70	W_2/ (g)	W_1^*/ (g)	$n_2 \times 10^4$/ (moles)	ϕ_2	$n_1^* \times 10^4$/ (moles)	ϕ_1^*	Δh_m/ (J/g)	$-T\Delta S_m$/ (J/g) (cal.)	Δg_m/ (J/g) (cal.)	χ_{12} (g) $\times 10^2$
8	0.7864	0.2136	3.9320	0.8123	3.5600	0.2052	1.476	-1.842	-0.366	12.775
10	0.7861	0.2139	3.9305	0.7981	3.5650	0.2019	1.475	-1.881	-0.406	12.975
11	0.6587	0.3413	3.2935	0.6748	5.6883	0.3252	1.731	-2.193	-0.462	11.287
12	0.5471	0.4529	2.7355	0.5650	7.5483	0.4350	1.961	-2.239	-0.278	11.508
13	0.8703	0.1297	4.3515	0.8783	2.1617	0.1217	1.013	-1.461	-0.448	13.354
15	0.2020	0.7980	1.0100	0.2140	13.3000	0.7860	1.231	-1.358	-0.127	10.825
16	0.4094	0.5906	2.0470	0.4270	9.8433	0.5730	1.963	-2.061	-0.098	11.689
17	0.5984	0.4016	2.9920	0.6157	6.6933	0.3843	1.896	-2.241	-0.345	11.515

W_1=wt. of PEGM*600 used. n_i=moles of comp. i used. cal.=calculated values.

W_2=wt. of PPGM 2000 used. ϕ_i=vol. fraction of comp. i.

Deg. of poly. of PEGM* 600 = 14. * denotes PEGM 600 batch used at previous two temperatures.

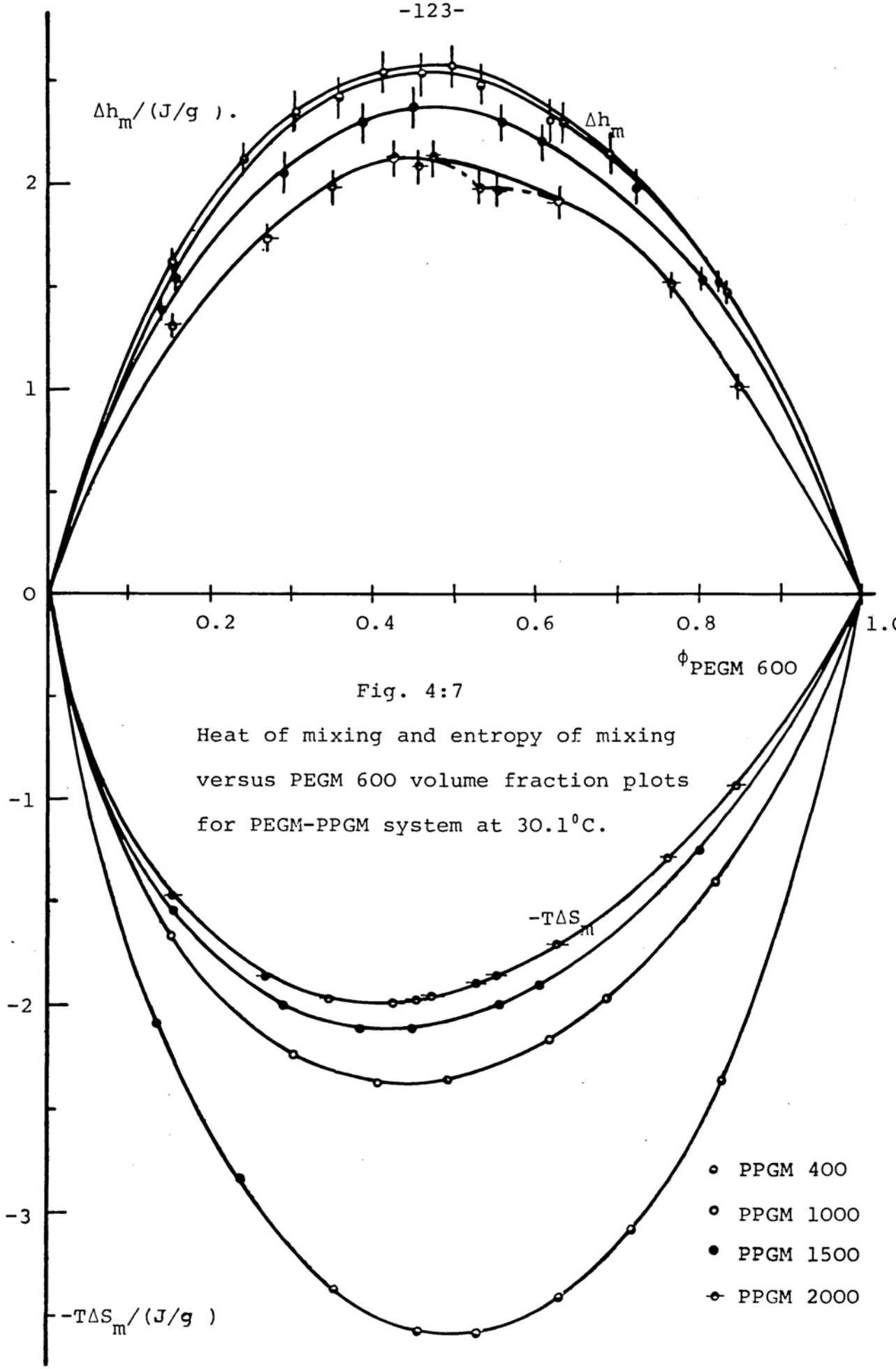
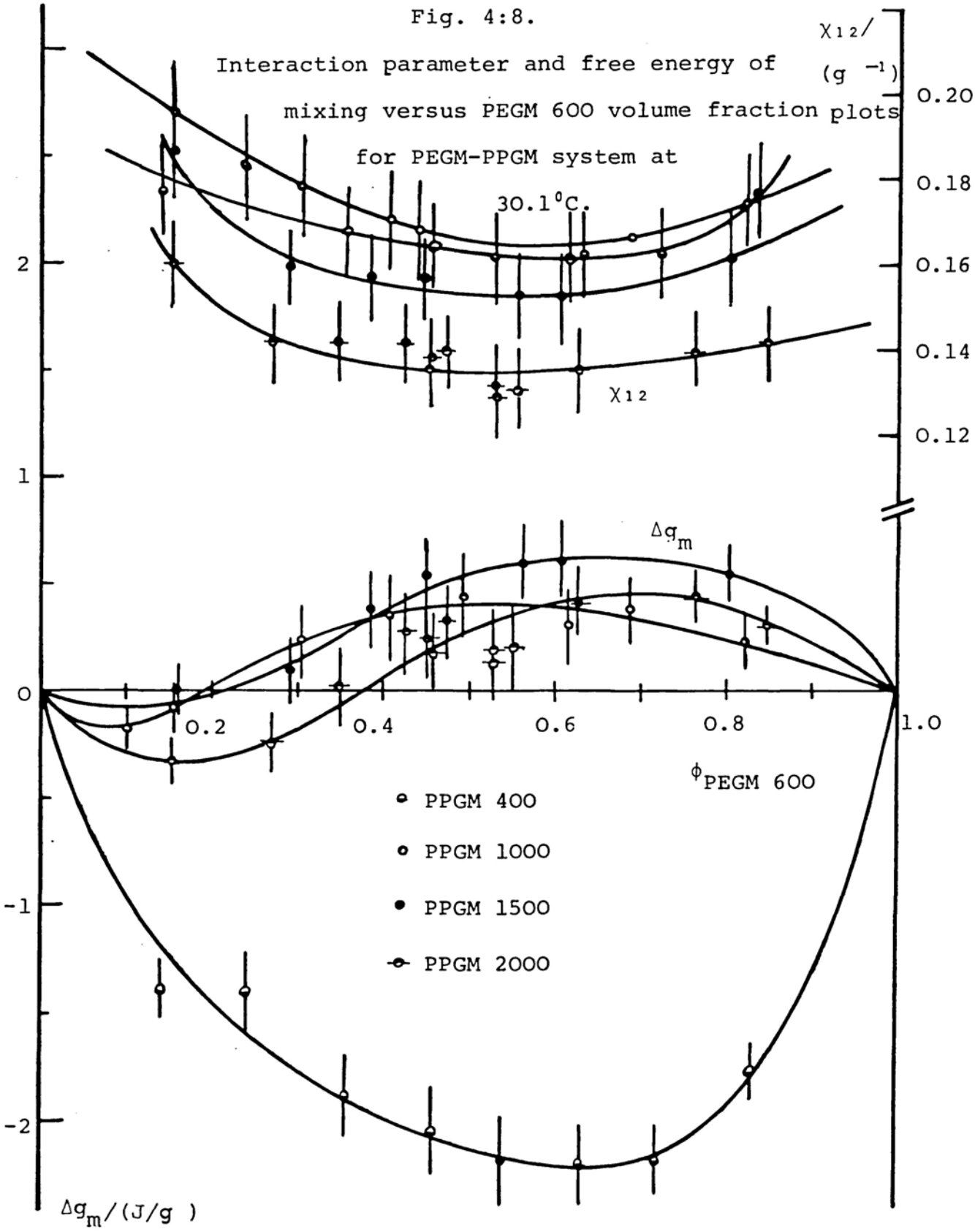


Fig. 4:7

Heat of mixing and entropy of mixing versus PEGM 600 volume fraction plots for PEGM-PPGM system at 30.1^{0}C.

Fig. 4:8.

Interaction parameter and free energy of mixing versus PEGM 600 volume fraction plots for PEGM-PPGM system at 30.1°C.



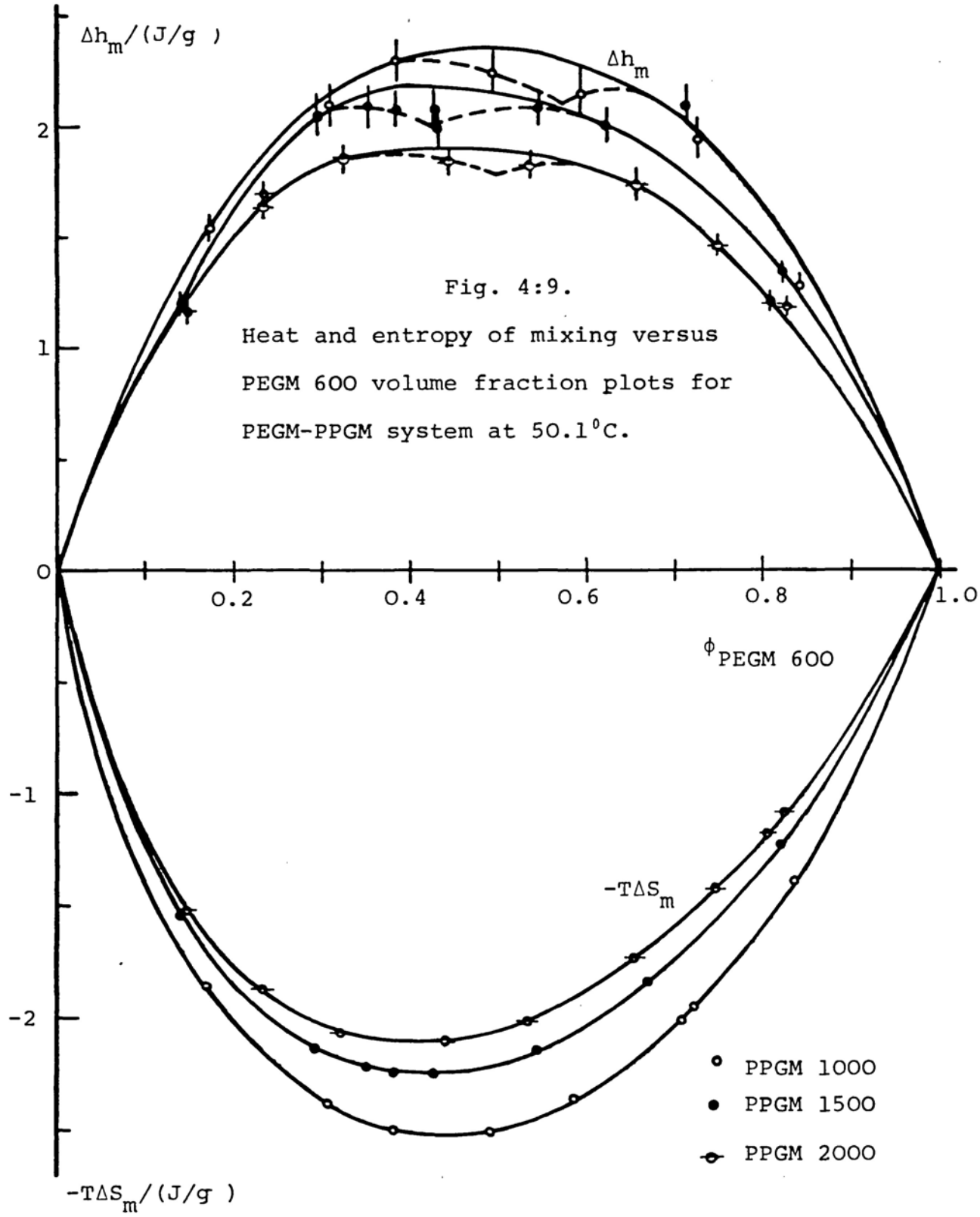


Fig. 4:9.

Heat and entropy of mixing versus PEGM 600 volume fraction plots for PEGM-PPGM system at 50.1°C.

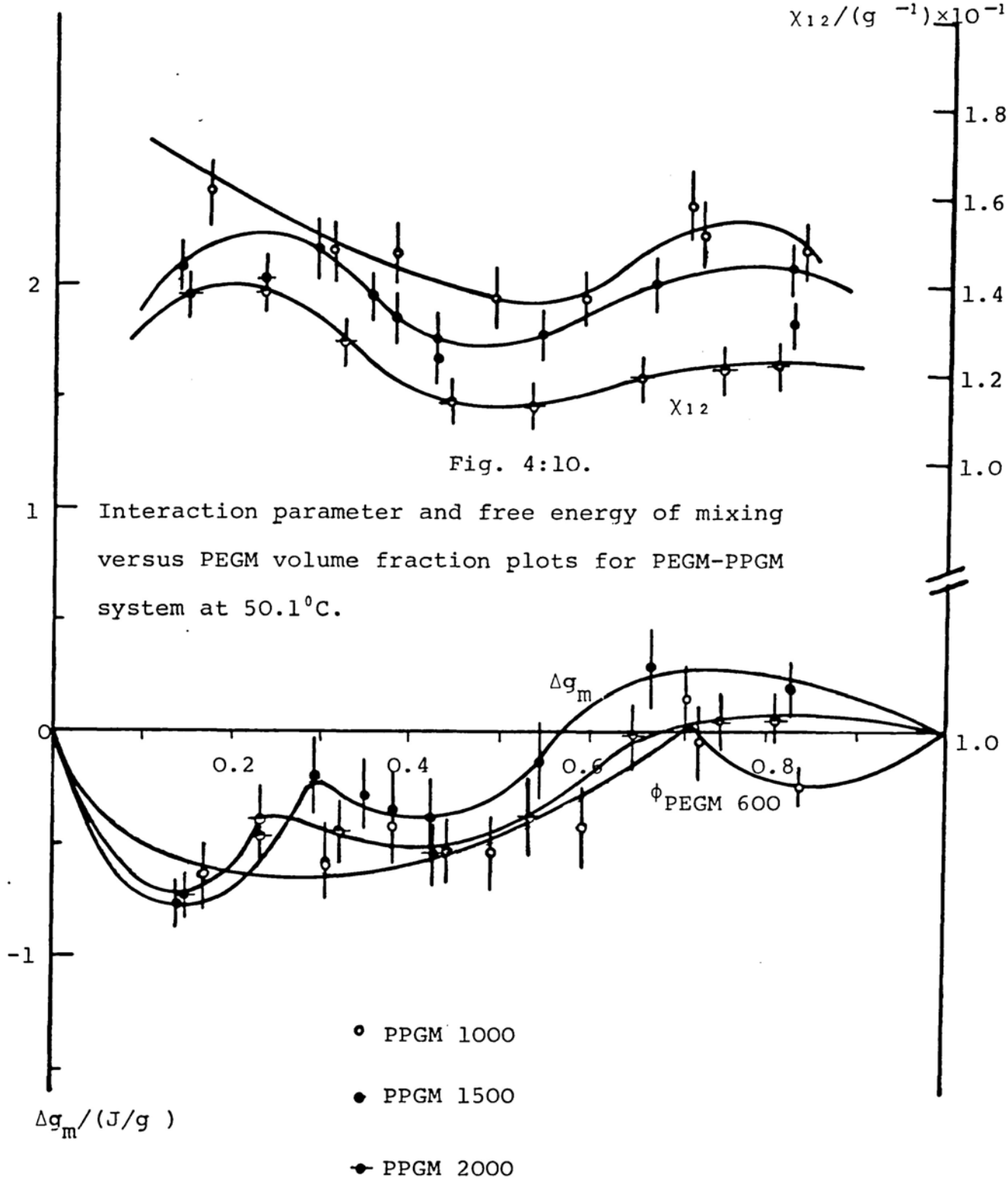


Fig. 4:10.

Interaction parameter and free energy of mixing versus PEGM volume fraction plots for PEGM-PPGM system at 50.1°C.

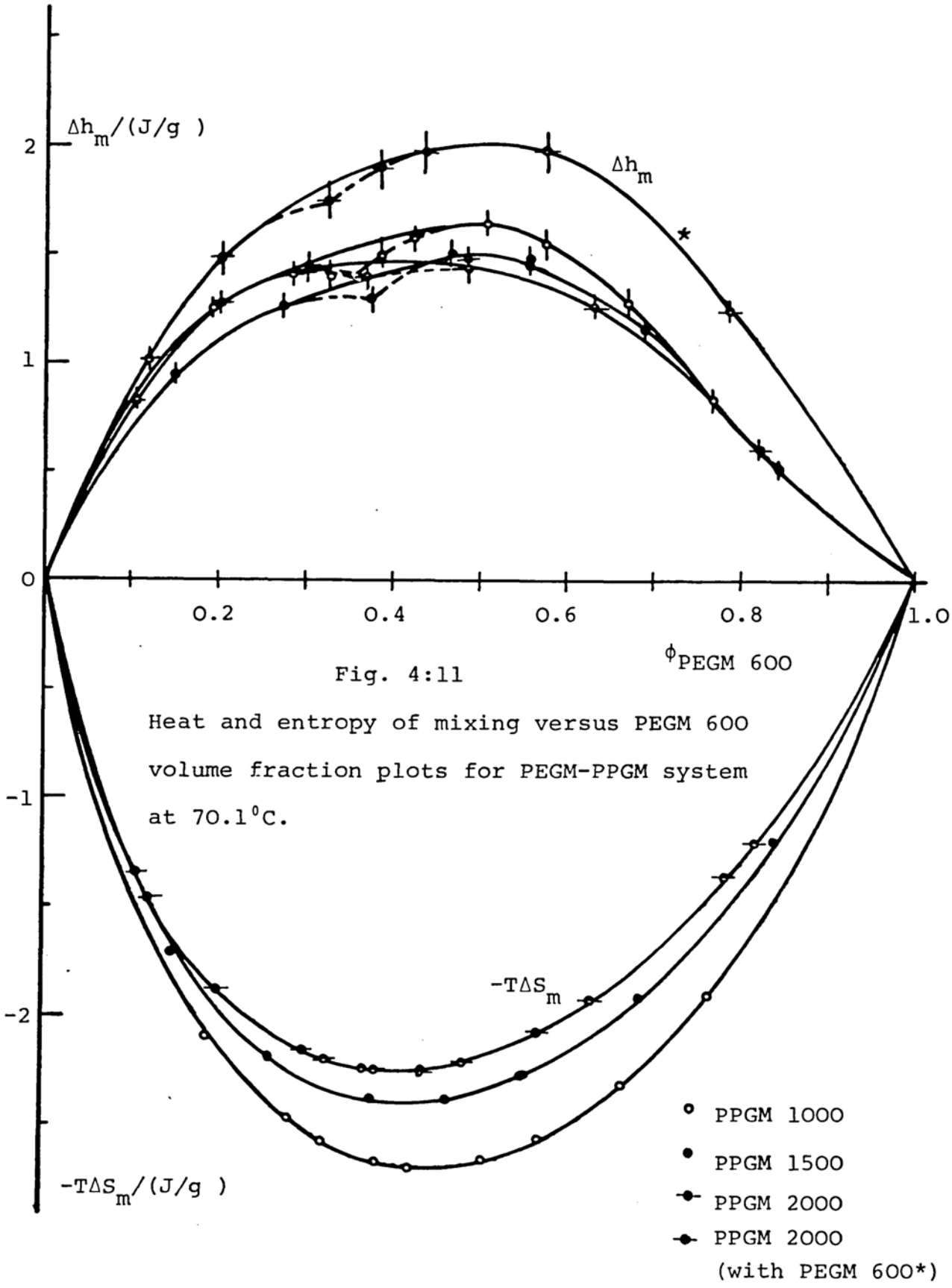


Fig. 4:11

Heat and entropy of mixing versus PEGM 600 volume fraction plots for PEGM-PPGM system at 70.1°C.

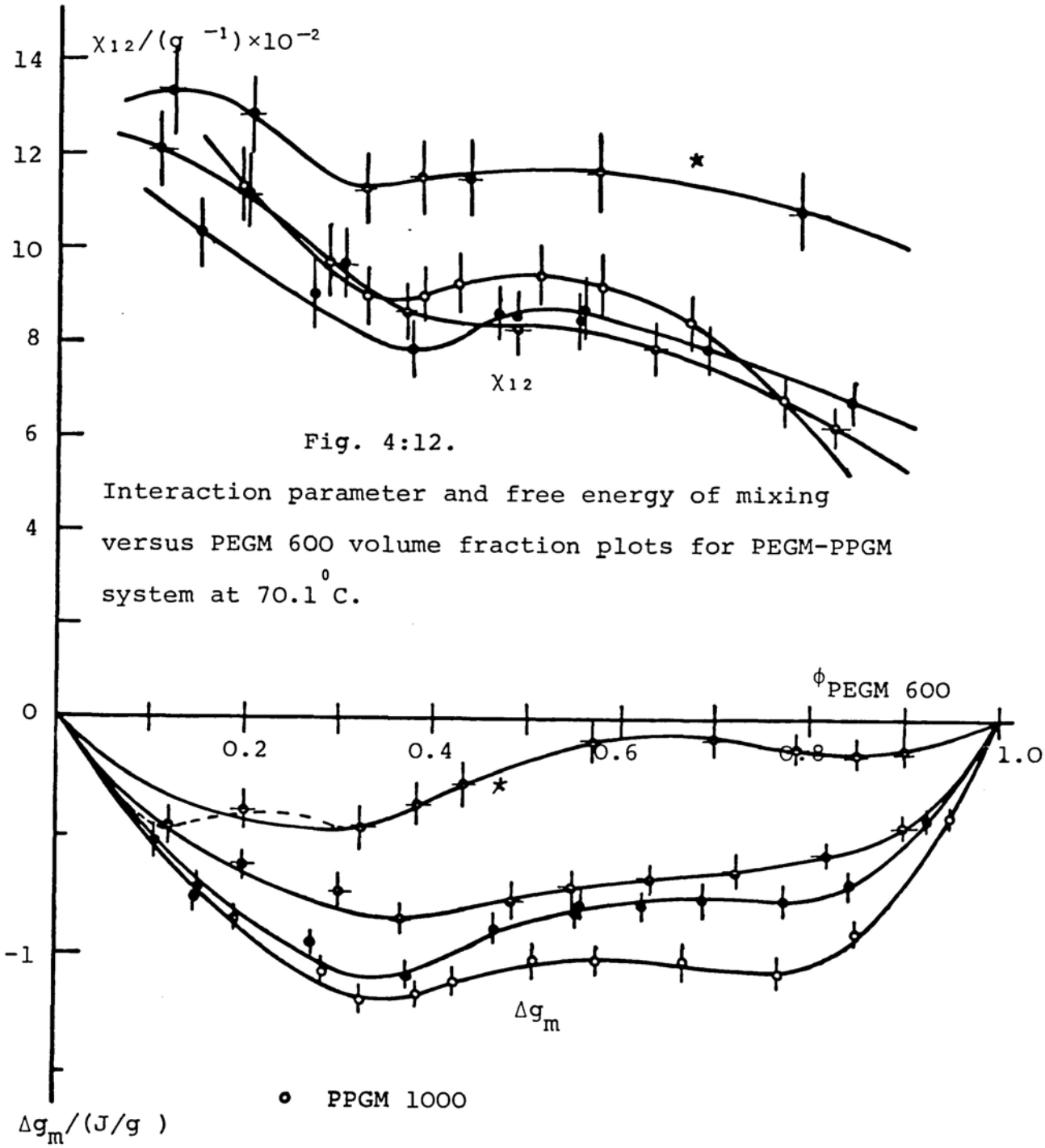


Fig. 4:12.

Interaction parameter and free energy of mixing versus PEGM 600 volume fraction plots for PEGM-PPGM system at 70.1 ^{0}C.

4:5.4. PS-PBD system at 70.1°C.

The heats of mixing of PS 1010 with samples of PBD 2350 and PBD 960 are shown in tables 4:23 and 4:24. The measurements were made at 70.1°C due to the problem of the viscosity of the PS sample at lower temperatures. PS is taken as component 1 with a degree of polymerisation of 10. Volume fractions were obtained using the specific volume data of Richardson and Savill[58]. Due to the time span and nature of each run, the error in the heats of mixing is estimated to be within the ±8% range rather than the ±5% range expected for the amount of heat involved. Figures 4:13 and 4:14 show the results in graphical form.

Table 4:23.

Results of PS 1010-PDB 2350 system at 70.1(±0.1)^{0}C. Ref. wt.= 1g . of total mixture.

Run number 23SBD	W_1/ (g)	W_2/ (g)	$n_1 \times 10^4$/ (moles)	ϕ_1	$n_2 \times 10^4$/ (moles)	ϕ_2	Δh_m/ (J/g)	$-T\Delta S_m$/ (J/g) (cal.)	Δg_m/ (J/g) (cal.)	χ_{12} (g)
1	0.5486	0.4513	5.4317	0.5086	1.9204	0.4914	1.332	-1.4379	-0.1059	0.1748
3	0.6630	0.3370	6.5644	0.6231	1.4340	0.3769	1.205	-1.2859	-0.0809	0.1706
4	0.2819	0.7181	2.7911	0.2505	3.0557	0.7495	0.955	-1.3545	-0.3995	0.1599
5	0.8269	0.1731	8.1871	0.8027	0.7366	0.1973	0.760	-0.8549	-0.0949	0.1648
6	0.1711	0.8289	1.6941	0.1496	3.5272	0.8504	0.712	-1.0819	-0.3699	0.1731
8	0.3893	0.6107	3.8545	0.3519	2.5996	0.6481	1.143	-1.4709	-0.3279	0.1603

W_1= wt. of PS 1010 used. n_i=moles of comp. i used in each run. cal=calculated values.

W_2=wt. of PBD 2350 used. ϕ_i=vol. fraction of comp. i.

Deg. of poly. of PS 1010 used in evaluating χ_{12} = 10.

Table 4:24.

Results of PS1010-PBD 2350 system at 70.1(±0.1) °C. Ref. wt.= 1 g . of total mixture.

Run number 96SBD	W_1/ (g)	W_2/ (g)	$n_1 \times 10^4$/ (moles)	ϕ_1	$n_2 \times 10^4$/ (moles)	ϕ_2	Δh_m/ (J/g)	$-T\Delta S_m$/ (J/g) (cal.)	Δg_m/ (J/g) (cal.)	χ_{12} (g)
2	0.6061	0.3939	6.0010	0.5643	4.1031	0.4357	1.286	-1.9533	-0.6673	0.1723
3	0.4849	0.5151	4.801o	0.4421	5.3656	0.5579	1.473	-2.0125	-0.5395	0.1927
4	0.8061	0.1939	7.9812	0.7777	2.0198	0.2223	0.781	-1.4399	-0.6589	0.1542
5	0.3448	0.6552	3.4139	0.3069	6.8250	0.6931	1.383	-1.8654	-0.4824	0.2048
6	0.7024	0.2976	6.9545	0.6652	3.1000	0.3348	1.214	-1.7777	-0.5637	0.1827
7	0.2405	0.7595	2.3812	0.2104	7.9115	0.7896	1.003	-1.5934	-0.5928	0.1869
8	0.1531	0.8469	1.5158	0.1321	8.8219	0.8679	0.637	-1.2327	-0.5957	0.1697

W_1= wt. of PS 1010 used. n_i=moles of comp. i used. cal.=calculated values.

W_2= wt. of PBD 2350 used. ϕ_i= vol. fraction of comp. i.

Deg. of poly.of PS 1010 = 10.

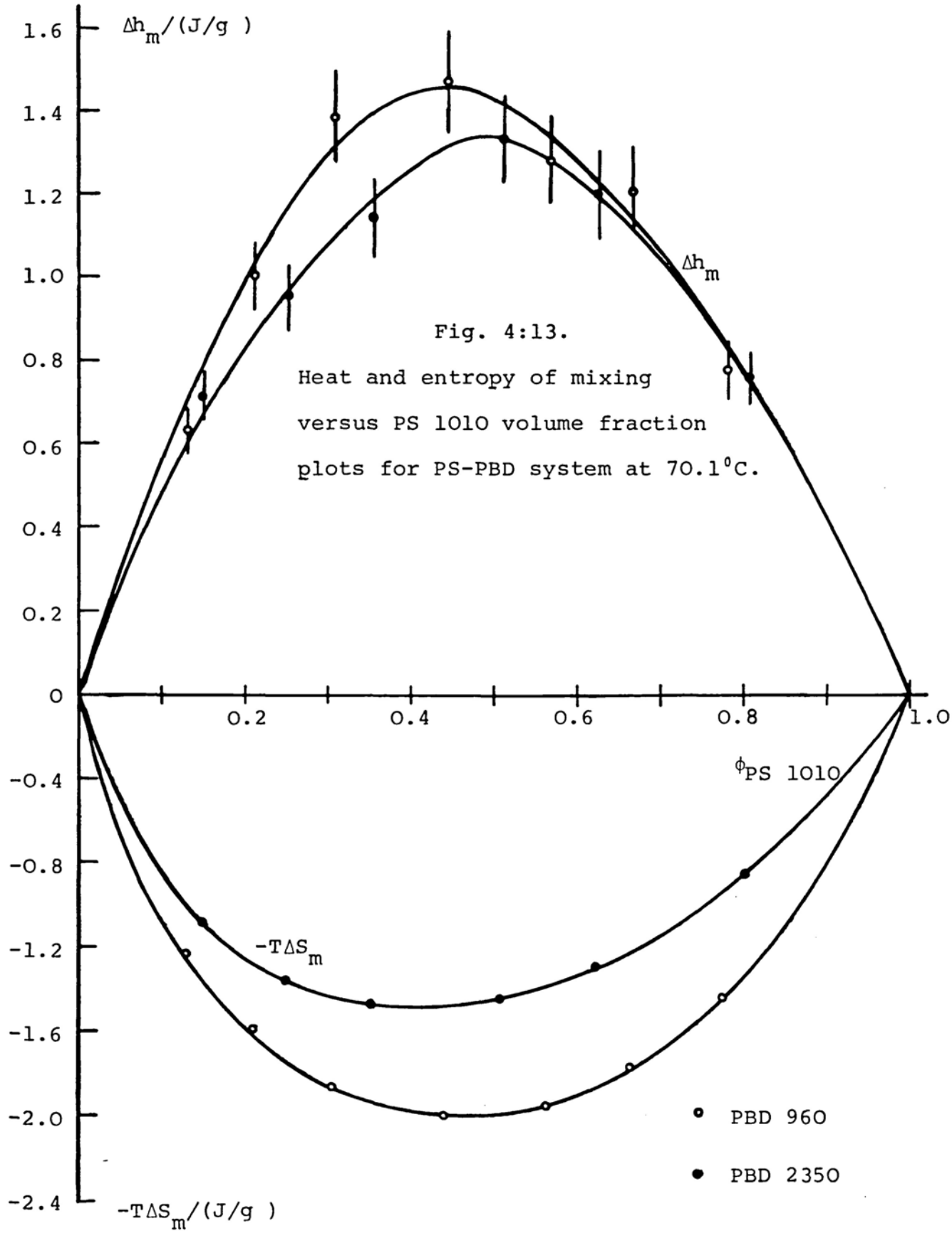


Fig. 4:13.

Heat and entropy of mixing versus PS 1010 volume fraction plots for PS-PBD system at 70.1°C.

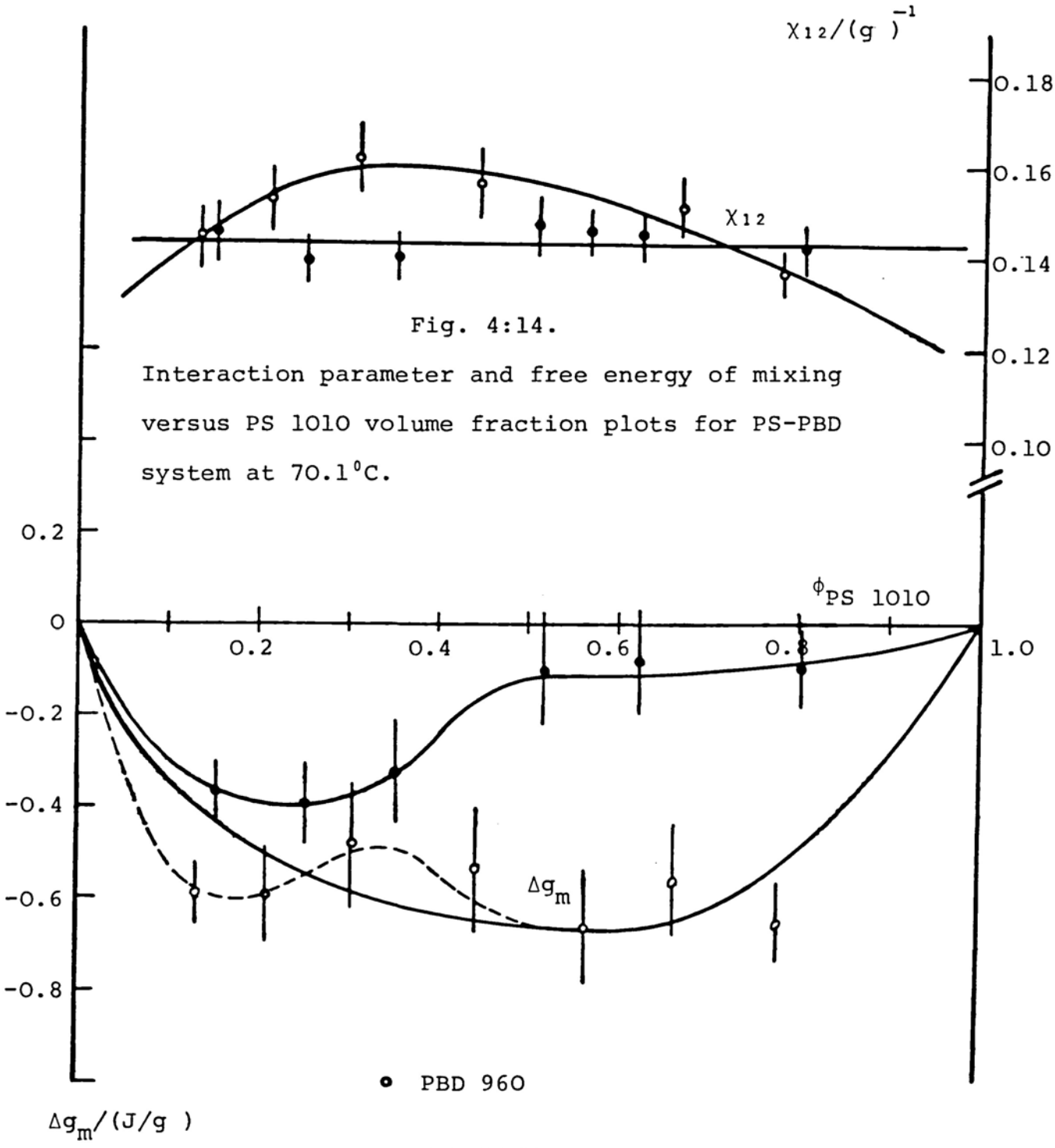


Fig. 4:14.

Interaction parameter and free energy of mixing versus PS 1010 volume fraction plots for PS-PBD system at 70.1°C.

4:6. Light scattering turbidimeter characteristics.

In a light scattering experiment on polymer blends, the intensities scattered by the samples are monitored as a function of temperature either on a heating or cooling cycle. During phase separation,the mixture will phase separate out into two phases of different compositions. For a blend exhibiting UCST behavior in a cooling cycle, this will result in an increase in the intensity of the scattered light observed at a fixed angle. As the phase separation continues on lowering the temperature further, the scattered intensity will increase further. This will continue until attenuation of the scattered light occurs, whereby the scattered light intensity will decrease to a steady level. Here the temperature at which the scattered intensity begins to increase is the cloud point for that sample. In systems exhibiting LCST behaviors the temperatures at which the scattered intensities begin to increase in a heating cycle are the cloud points of the samples. Heating cycles are preferred for systems showing LCST behaviors due to the phase transitions observed being approached from the homogeneous, single phase region. Cooling cycles are preferred for systems exhibiting UCST behaviors for the same reason.

In using a turbidimeter of the type described earlier, it is important to know the characteristics of the light source and photo detecting device as a function of temperature, as well as the temperature lag between the block temperature and the center of the sample. This is necessary to ensure that any changes in the intensities observed are due mainly to the transitions occuring in the samples as a result of

temperature changes and not due to the characteristics of the light source or detector. The experiments to determine these characteristics and the results of these determinations are described below.

4:6.1. Stability of the tungsten light source and photodiodes.

Tungsten projector lamps connected in series to a stabilised power supply were used as light sources in the turbidimeter. Photodiodes, more sensitive towards the red wavelength end of the spectrum, are used as photon detectors. To test the stability of the light sources and photodiodes, empty Pyrex glass cells similar to those used in the actual experiments were placed in the sample slots and the temperature of the block scanned upwards and downwards through a range of 150°C from room temperature. The changes in intensities scattered by the glass materials as the block temperature changes were found to vary to slightly different extents in the different channels. At low temperatures, intensity changes were negligible. Above 150°C, the intensities were found to increase by about twenty units. These increases could be attributed to the increase in photodiode dark current and changes in the refractive index of the glass with temperature. These changes in scattered intensities are negligible compared to the intensities scattered by phase separating particles which are in the region of hundreds of units. In general, when the turbidity of the sample changes rapidly with temperature, this dark current change can be neglected without seriously affecting the cloud point determination. However, where the turbidity of the sample changes

slowly with temperature, subtraction of this dark current change helps to flatten out the baseline. This would enable a sharper cloud point to be determined.

4:6.2. Temperature lag.

To investigate the temperature lag, one of the empty cells was filled with a PS-PBD oligomeric mixture while the rest were filled with PEGM-PPGM mixtures. Thermocouples were inserted inside each sample and connected to a millivoltmeter via a multiswitch. Heating runs from 30° to 130°C show a temperature lag of about 4°C at the maximum heating rate of 2°C/minute. Reducing the heating rate to 0.5°C/minute reduces the lag to about 1.5°C. Further reduction in the lag is possible if the heating rate is reduced further. For cooling runs from 130°C to room temperature, the temperature lag was observed to be less than 0.5°C above 70°C and about 0.2°C between 40°and 70°C. Hence for systems exhibiting UCST behaviors, cooling rates of less than 0.5°C/minute are required. This can easily be achieved on the temperature ramp used. For systems showing LCST behaviors, slow heating rates are recommended. The slowest heating rate possible is 5°C over 1000 minutes. These measured temperature lags are the worst possible cases as the samples were not stirred at all.

4:7. Materials.

Due to the time factor, only the PS-PBD system was examined. The PBD 2350 and PS 1010 samples were the same samples used in the heats of mixing experiments. The PS 1520 sample was prepared by Yip[12] using anionic polymerisation in the Department. The sample was characterised by g.p.c. analysis, giving a number average molecular weight of 1520

and a polydispersity of 1.1.

4:8. Sample preparation.

Due to the different physical properties of the two PS samples, different methods of sample preparation were adopted.

4:8.1. PS 1010-PBD 2350 system.

Pyrex glass tubes 9 mm. in outer diameter with a wall thickness of 1mm. were used in making the sample tubes. One end of the tube was rounded off and a B10 ground glass cone was fitted to the other end. A constriction was pulled half way up the tube such that when the tube was sealed at the constriction, the sample tube had the dimensions mentioned in section 3:2.4.

A pre-weighed, clean sample tube was immersed in liquid nitrogen and then filled with liquid nitrogen. A clean piece of copper wire was dipped into the PS 1010 sample and some PS withdrawn. This was then dipped into the liquid nitrogen inside the sample tube where it fractures and settles to the bottom of the tube. If the constriction became blocked, it was cleared using the copper wire. The sample tube was then withdrawn from the liquid nitrogen container, the liquid nitrogen in it evaporated and the whole tube dried in an oven at 120^{0}C for an hour. The tube was weighed to determine the amount of PS introduced. The process was repeated until the required amount of PS was introduced. The PBD 2350 was then pipetted in to make up the required concentration. A piece of nail was inserted into the sample to act as a stirrer.

4:8.2. PS 1520-PBD 2350 system.

The required amount of PBD 2350 was pipetted into a clean, pre-weighed tube. The PS 1520 was introduced via a glass funnel with a long stem until the required mixture concentration was attained. The nail was then inserted into the sample.

4:8.3. Degassing and sealing of samples.

The weighed samples were attached to a vacuum line via the ground glass cones and degassed at a vacuum of better than 10^{-3} torr at temperatures of 90°C and 140°C for the PS 1010-PBD 2350 and PS 1520-PBD 2350 systems respectively. During the degassing, care was taken to ensure that the mixtures did not splash up to the constrictions. The contents were stirred occasionally with a magnet to assist the degassing and to ensure that homogeneous mixtures were obtained. After a few hours of degassing at 10^{-3} torr or better, the samples were sealed off at the constrictions.

4:9. Cloud point measurements.

Preliminary cloud points of both systems were determined to the nearest 10 degrees by means of program 6000 described in the software section. The block temperature was increased in ten degrees intervals by means of the starting temperature control on the ramp. Large changes in scattered intensities, corresponding to phase separation, could then be established by visual inspection as the intensity channels are scanned through manually.

The block was then cooled and a starting temperature

established. Since the PS-PBD system exhibits UCST behavior, cooling runs were carried out. The starting temperature was selected in each run such that it was at least 15 degrees above the highest cloud point of the four samples under investigation. The samples were kept at this temperature for at least half an hour with continuous stirring to ensure that the samples were homogeneous throughout.

After half an hour of stirring, the stirrer was stopped and the experiment proper commenced by the initiation of program 6040. This enables stirring times, data acquisition intervals, the number of channels to be scanned and any other identification data to be selected and stored on tape. The cooling run and data acquisition were then started. On termination of the run, the end-of-file mark was recorded onto the tape and the tape then listed. The experiments were repeated to ensure reproducibility.

4:10. Results.

A). PS1010-PBD 2350 system.

Apart from the photodiode dark current increase as a function of temperature, no large changes in scattered intensities were observed for all concentrations examined in the temperature range 30^0 to 180^0C. Since PS-PBD systems are known to show UCST characteristics[12 13], this implies that the maximum cloud point of the system lies well below 30^0C. As the turbidimeter was not designed for temperatures below room temperature , an alternative method was used to determine the phase boundary.

This was done by cooling the sample tubes in methanol in

a dewar flask. The flask has two clear, unsilvered strips through which the samples could be observed. The methanol was stirred mechanically and cooled by passing evaporated liquid nitrogen gas through copper cooling coils immersed in the methanol. The temperature of the methanol was detected by a thermocouple placed adjacent to the samples and connected to a digital thermometer with a built-in cold junction compensator. The temperatures at which the onset of milkiness appear in the clear samples were taken to be the cloud points. Table 4:25 and figure 4:15 show the results obtained in tabular and graphical forms respectively. The phase boundary is non-symmetrical.

Table 4:25.

Cloud points of PS 1010-PBD 2350 system.

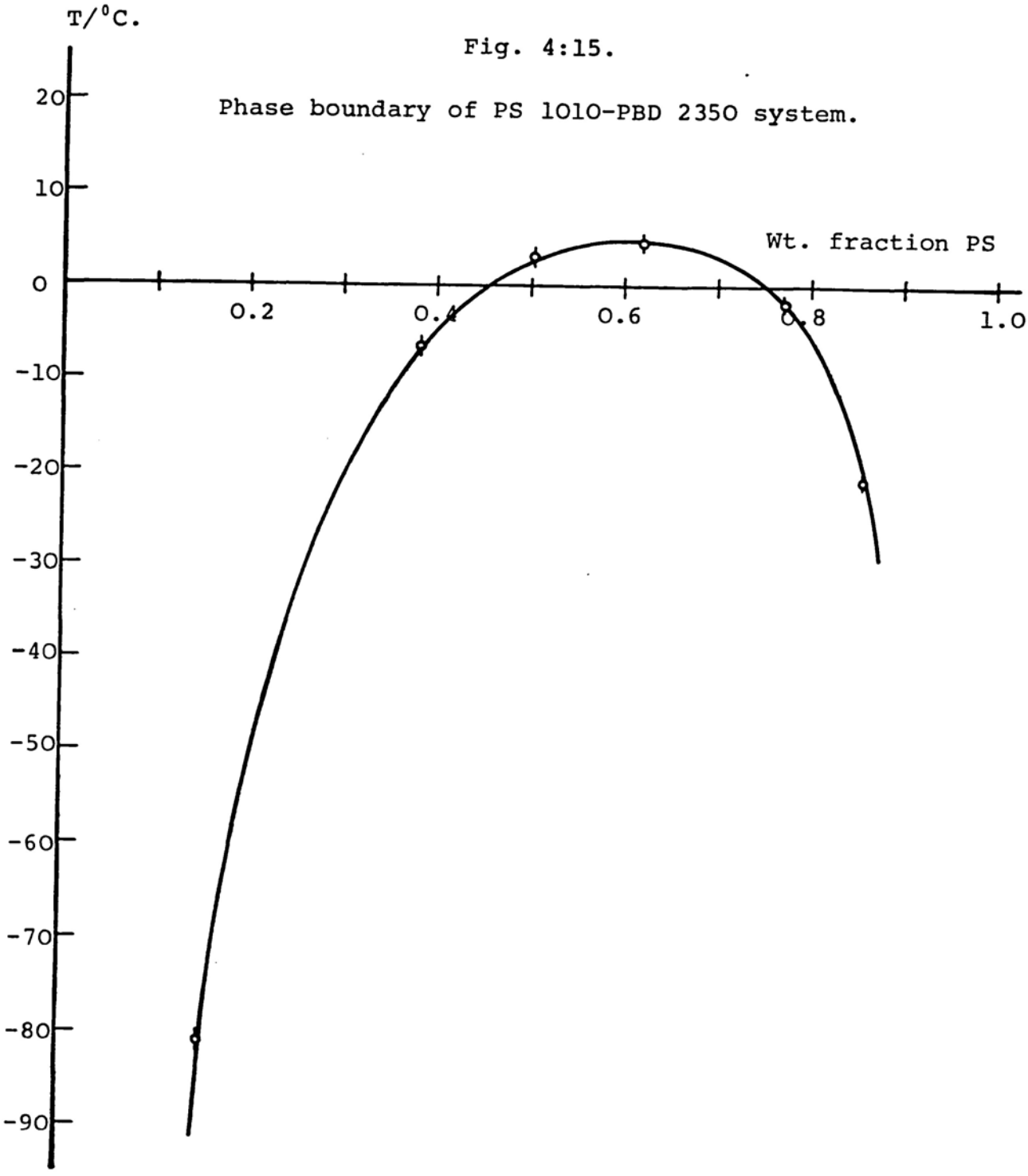
Wt.% PS 1010	50.2	61.8	77.2	38.3	30.0	16.4
Cloud point/ $^{0}C(\pm 1^{0}C)$.	2.9	4.9	-1.5	-6.5	-20.7	-81.0

B). PS 1520-PBD 2350 system.

Figure 4:16 is a typical intensity versus temperature plot obtained at various concentrations for this system. The point A where the scattered intensity begins to increase rapidly is taken to be the cloud point or binodal temperature. Following the method proposed by Scholte[59] and neglecting the angular dependence for the angle of observation used, plots of $1/I_{45^{0}}$ versus temperature were made for the intensity readings between A and the peak of the plot in figure 4:16. Figures

Fig. 4:15.

Phase boundary of PS 1010-PBD 2350 system.



4:17 and 4:18 show the best and worst plots obtained for different runs made at each of the concentration indicated. On extrapolation to infinite intensities, the 'spinodal' temperature should be obtained.

Table 4:26 shows the binodal and 'spinodal' temperatures for the various wt.% PS concentrations indicated. All temperature values are averages of a minimum of three separate cooling runs.

Table 4:26.

Cloud points and 'spinodal' temperatures of PS 1520-PBD 2350 system.

Wt.% PS 1520	Cloud point/ K(±1K)	'spinodal' temperature/K(±2K)
35.92	341.2	339.0
51.93	356.6	354.6
86.36	349.6	341.8
76.91	357.3	356.0
44.73	352.5	350.0
66.00	359.6	357.5
22.55	332.8	329.9
12.57	306.6	299.0
18.96	328.2	321.3
27.35	341.3	336.6

Heating cycles were also carried out. As can be expected, the cloud points were between 6 to 10 degrees higher than those measured on the cooling cycle due to the larger temperature lag between the samples and the block on a heating run. This is further compounded by the fact that the phase transitions

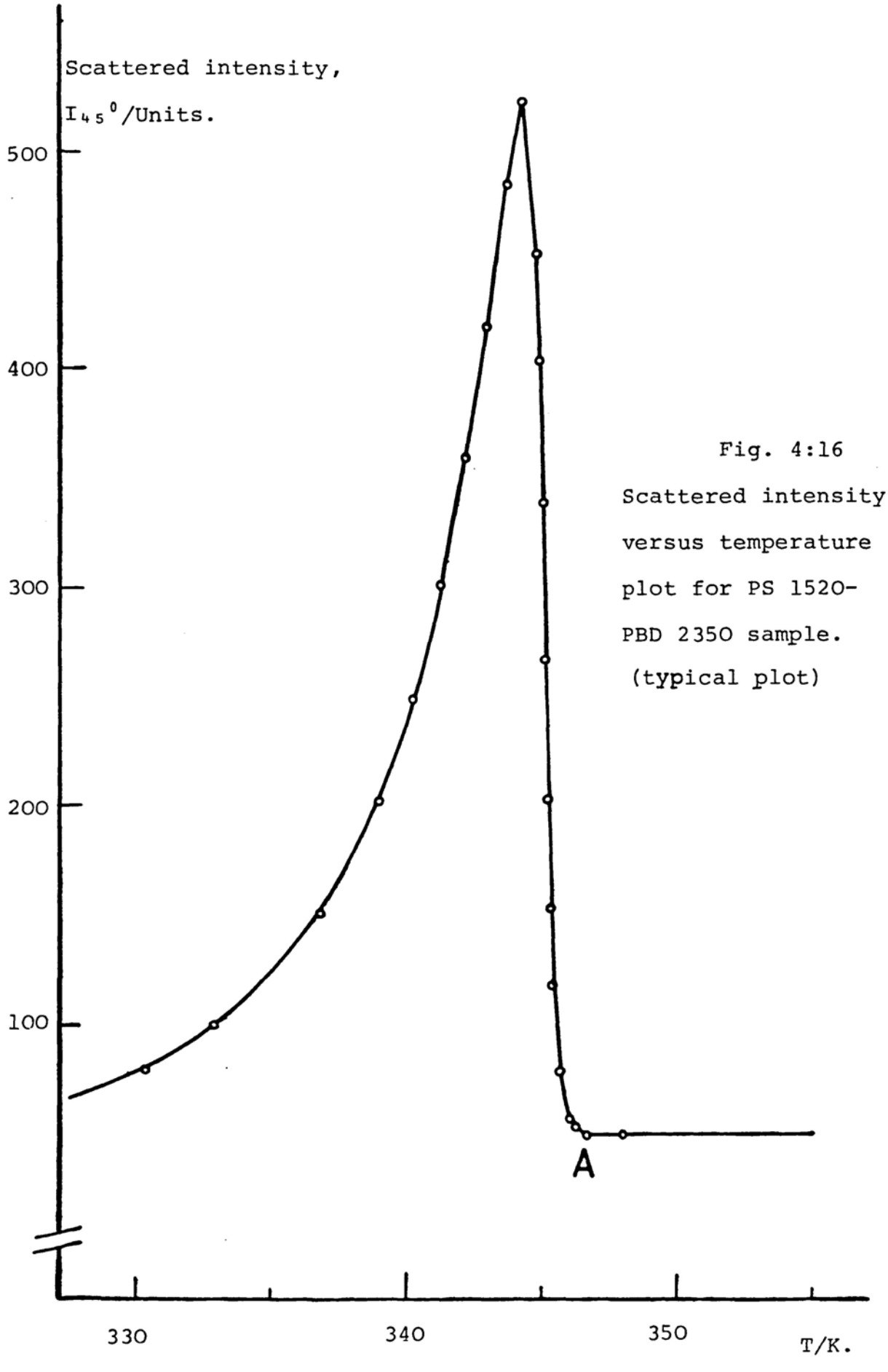


Fig. 4:16
Scattered intensity versus temperature plot for PS 1520-PBD 2350 sample. (typical plot)

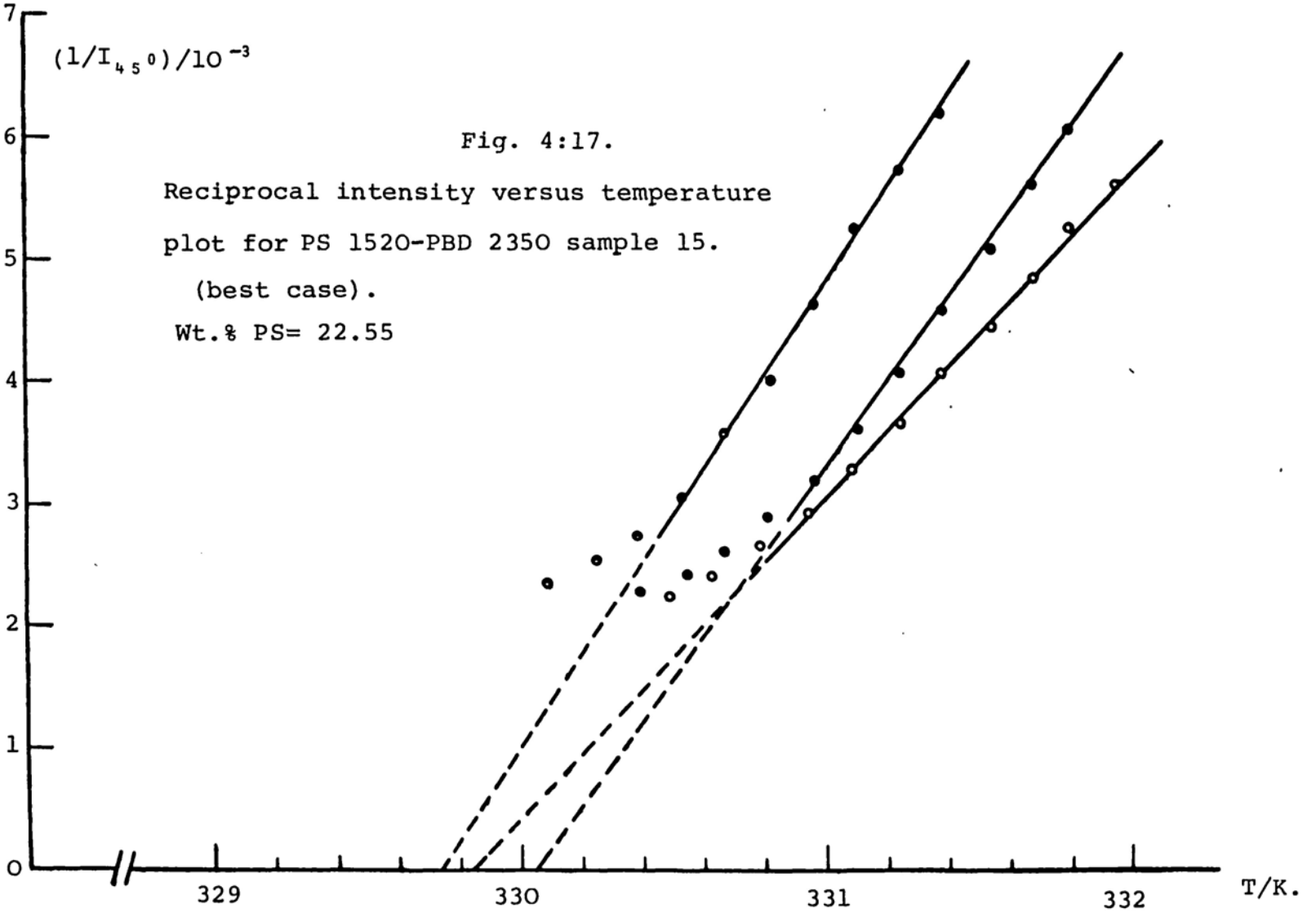


Fig. 4:17.

Reciprocal intensity versus temperature plot for PS 1520-PBD 2350 sample 15. (best case).

Wt.% PS= 22.55

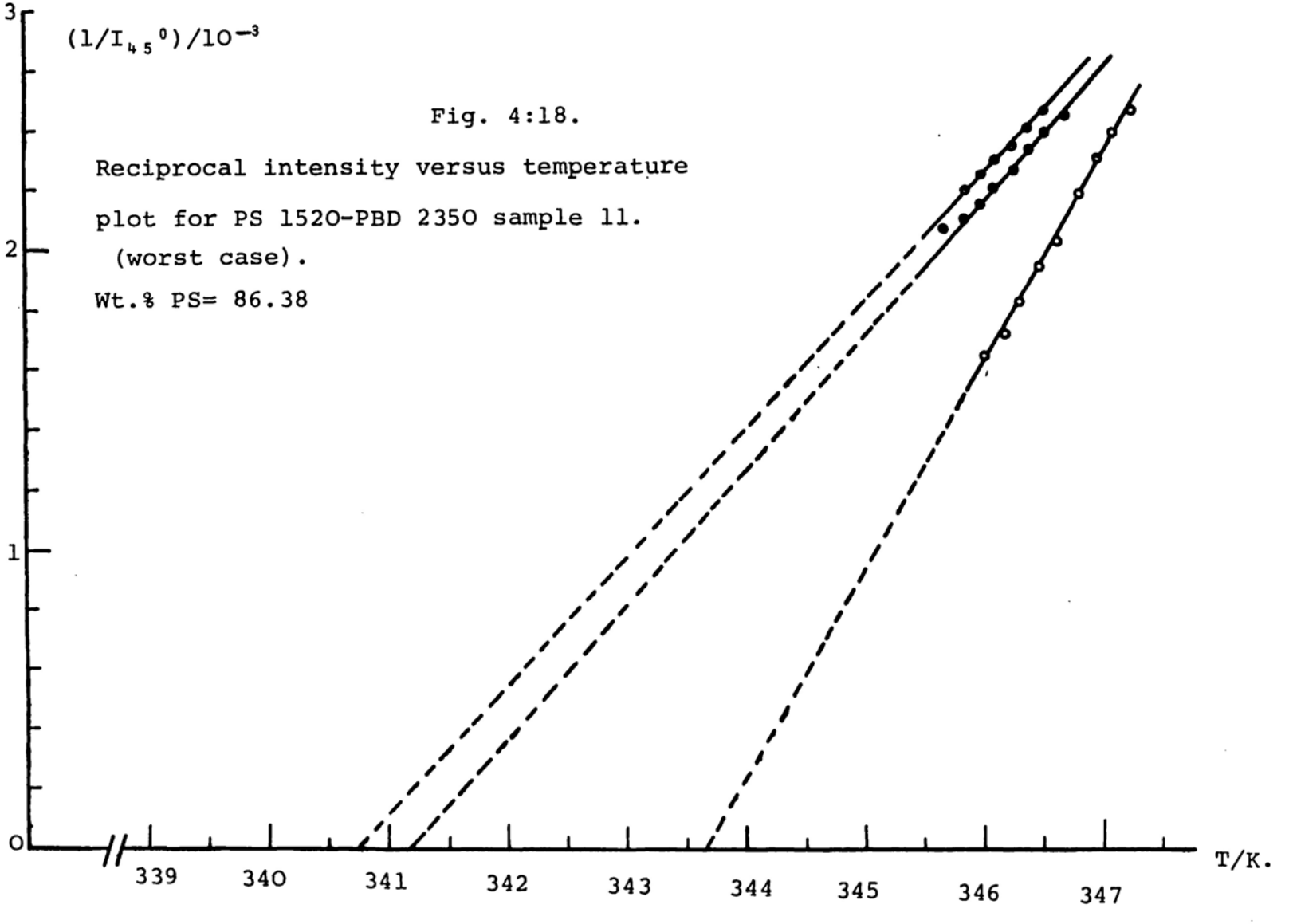


Fig. 4:18.

Reciprocal intensity versus temperature plot for PS 1520-PBD 2350 sample 11. (worst case).

Wt.% PS= 86.38

observed are approached from the inhomogeneous two phase region. Figure 4:19 is a plot of the binodal and 'spinodal' temperatures against weight fractions of PS. The plot shows a shoulder at about 0.3 weight fraction of PS. The half-filled points are pulse induced critical scattering (PICS)[60] measurements on the same system determined at Essex University. The PICS binodal results are in good agreement with the turbidimeter results.

The word 'spinodal' is put within quotation marks because at present, we have no independent experimental proof that the lower curve in figure 4:19 is the spinodal curve. Preliminary efforts to obtain the spinodal temperatures by PICS measurements were unsuccessful due to insufficient pulse time applied. It is hoped that PICS and phase volume measurements will be carried out in the near future.

However, to a first approximation, considering the critical point of the system to be at a weight fraction of 0.37 PS concentration, tie lines could be drawn[61] across as shown. Considering the ends of the tie lines poorer in PS as phase 1 (or ϕ_1') and that richer in PS as phase 2 (or ϕ_1'') with PS as component 1, χ_{12} values can be evaluated empirically via the equations,

$$\ln\{(1-\phi_2')/(1-\phi_2'')\} + \{1-(x_1/x_2)\}\{\phi_2'-\phi_2''\} = x_1\chi_{12}(\phi_2''^2-\phi_2'^2) \qquad 4:16$$

and

$$\ln(\phi_2'/\phi_2'') + \{1-(x_2/x_1)\}\{\phi_2''-\phi_2'\} = x_2\chi_{21}\{(1-\phi_2'')^2-(1-\phi_2')^2\} \qquad 4:17$$

(all notations having the same meanings as in chapter 2)

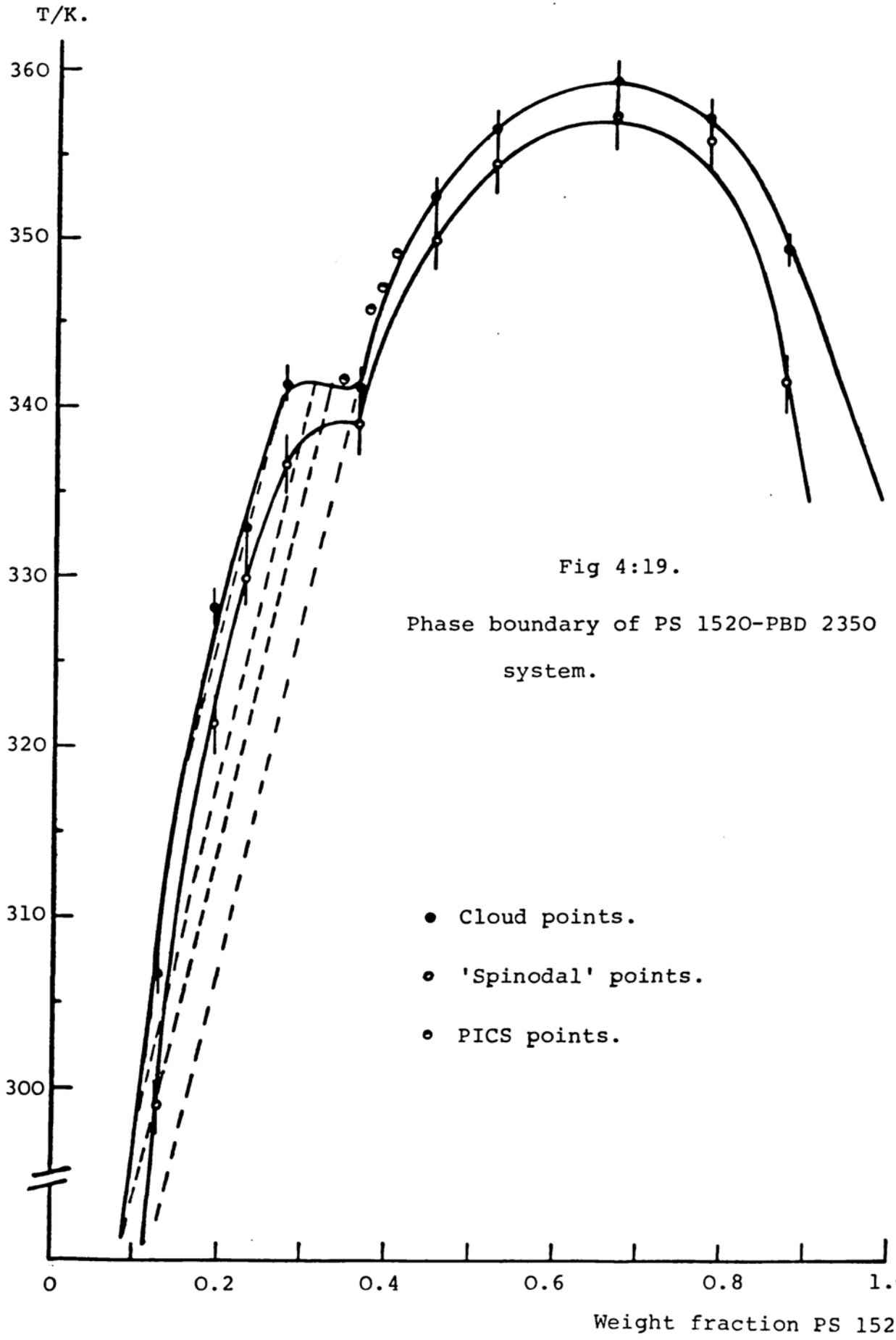


Fig 4:19.

Phase boundary of PS 1520-PBD 2350 system.

Equations 4:16 and 4:17 are obtained by applying the conditions

$$\Delta\mu_1' = \Delta\mu_1'' \qquad 4:18$$

and

$$\Delta\mu_2' = \Delta\mu_2'' \qquad 4:19$$

respectively to equation 2:26.

Table 2:27 shows the χ_{12} and χ_{21} values obtained. Though the χ_{12} and χ_{21} values are almost equal (to within experimental error), they are however, not sufficient evidence to support the contention that the lower curve in figure 4:19 is the spinodal.

Table 4:27.

Values of χ_{12} and χ_{21} calculated from equations 4:16 and 4:17 for the concentrations of the components indicated.

ϕ_1'	ϕ_2'	ϕ_1''	ϕ_2''	χ_{12}'	χ_{21}''
0.150	0.850	0.265	0.735	0.180_4	0.175_1
0.087	0.913	0.326	0.674	0.204_5	0.176_3
0.106	0.894	0.305	0.695	0.195_2	0.176_9
		Average values		0.193_4	0.176_1

Component 1 = PS 1520, component 2 = PBD 2350.

The χ_{12}' and χ_{21}'' values obtained above agree well with the the values obtained from the heats of mixing measurements although the molecular weights of the components are different.

CHAPTER 5.

DISCUSSION.

5:1. Experimental.

In the initial stages of the modification of the calorimeter, various difficulties were encountered and dealt with. These, together with scope for improvements that could be made also to the cloud point apparatus will be outlined below.

5:1.1. Calorimeter.

The heat sink was originally designed in three sections which slot fitted each other and were held together by four equally spaced straight through bolts and nuts. Springs at one end of the bolts facilitate spring loading of the reaction cell. This was done to enable good thermal contact between the reaction cell and the front copper plate of the heat flow unit. However, it was found that, with spring loading, a shearing torque was introduced to the structure by the rocking motion of the stirring mechanism. This torque manifested itself in the form of regular spikes on both sides of the baseline on the chart recorder when an empty cell was loaded into the heat sink and stirred. The frequency of the spikes depended on the rate of stirring while the height of the spikes depended on the amount of spring loading required due to cell width variations. Since the thermoelectric modules appeared to act as extremely sensitive pressure transducers, the original NBS design of having push-fitted cell in a fixed heat sink structure was adopted.

When an empty cell was loaded into the calorimeter and the calorimeter inverted, a baseline shift was observed in the exothermic direction. This shift was reduced on attaching the aluminium L-shaped piece onto the cell press, and was further substantially reduced when the cell loading guide passageway was completely sealed along its length by a piece of polycarbonate wrapped with insulation. When the experiment was repeated, but this time with the heat sink returned to the starting position after the inversion, an exothermic peak was observed instead of the baseline shift. An endothermal peak was observed in the original NBS micro-calorimeter, for which no obvious cause could be found. The same is true here for the exothermic peak observed, though the reduction of the baseline shift suggests that this could be partly due to frictional air motions caused by the inversion and stirring process and partly by the shifting of the pressure point exerted on the thermoelectric modules during stirring. This could be deduced from the fact that reducing the spaces available for air movements reduces the shift, especially around the area of the cell and the heat detection units. A slightly reduced shift is also observed when the heat sink is unloaded as compared to the shift with a loaded empty cell. Also no baseline shifts at all were observed in the electrical calibration experiments. Since the calorimeter would be operating in later experiments in the inverted and stirring modes, no attempts were made to determine the amount of heat represented by the peak when the heat sink was inverted and then brought back to the starting position. To correct the experimental baseline shift observed, a baseline superimposition

method was adopted as described in section 4:4.1. The correction for the baseline shift in this way also eliminates the need to correct for frictional heat effects generated in the sample by stirring. The main disadvantage is that the experimental time is doubled.

Bearing equation 4:12 in mind, it can be seen from the description of the thermoelectric modules that they are not quite ideal for the purpose for which the calorimeter was built. Having only 9 junctions, they have much larger time constants than 49 or 64 junction cells which are commonly used today. This disadvantage is partly compensated for by the larger thermal conductivity of the cells, as they were originally designed for heat pumping. However, this compensation is at the expense of the sensitivity of the calorimeter. This reduction in sensitivity is a major drawback for the measurement of heats of mixing of oligomers. This is because the heats of mixing of oligomers would either produce a smaller or comparable amount of heat over a longer time period than more fluid mixtures. For example, the aqueous acid-base reaction takes less than ten minutes for a complete run while at the other end the PS-PBD run takes an hour. Hence for further work, the sensitivity of the calorimeter should be improved. This could be achieved by replacing the present thermoelectric modules with modules containing more junctions per module and smaller cross-sectional area per junction. Apart from increasing the sensitivity, these new, advanced modules can also extend the operational temperature range of the calorimeter as they can be operated up to $200^{0}C$.

An attempt was made to improve the sensitivity of the

calorimeter by placing the thermoelectric cells in two layers to increase the path length ℓ. However, it was found that in this configuration, the time constant τ was unacceptably long. Copper cells were originally designed to be used in the calorimeter, but the high thermal capacity precluded use of this material, despite its excellent thermal conduction properties. Instead aluminium cells were used.

The baseline shift can be avoided if the PTFE sample holder is replaced by one made of metal. This would enable the heat sink to be returned to the starting position after initiation of the mixing, so that the fore and after period baseline would be the same. This could not be done on the PTFE sample holder because of its poor heat conducting properties. This was verified by the fact that the heat measured in this way is about 5% less than the heat measured in the inverted position. The same overall design of the cell could be used, except that a PTFE washer must be added on top of the metal lip of the sample holder to act as a liquid seal and a PTFE piece be inserted between the base of the sample holder and the cell press to act as a thermal insulator.

The observed time constants mentioned above were based on the assumption that the reaction cell and contents are at a uniform temperature. This is true for materials with a high thermal diffusivity and is not true for oligomers. This implies that the path length from the center of the cell to the side walls of the cell adjacent to the heat detection units should be as small as possible. The size of the cells used was ultimately governed by the small amounts of heat expected to be liberated by the oligomeric mixtures and the available sizes of the aluminium rectangular tubings.

5:1.2. Light scattering turbidimeter.

In general, the overall design was found to be adequate for the designed purpose, although improvements could be made. Laser light could be substituted for the tungsten light source. The intense, monochromatic beam could be split to serve the 4 samples. This would eliminate the need for the focussing lenses and enable sample sizes to be reduced. To improve resolution, photomultipliers could be used.

To facilitate temperature scans below room temperature, copper cooling pipes could be embedded either in the block or in the inner surfaces of the insulation , through which evaporated liquid nitrogen gas could be circulated. As can be seen from figure 4:16 the cloud point determination is good. The reproducibility is of the order of $1^{0}C$ in blends which contain at least one fluid component, except at the two extremes of the phase boundary where the cloud points are not far above room temperature. Here the reproducibility is about $2^{0}C$. Blends of high molecular weights have been investigated on the turbidimeter in the form of thin films by other members of the group. The cloud point determinations and their reproducibilities were found to be good.

The major drawback in the design is that the scattering effect is observed only at a fixed angle. This could occasionally lead to multiple scattering peaks being observed. This could be due to several possible causes such as large variations in particle sizes crossing the beam, dust particles and refractive indices changes with temperature of the blend components among others.

5:2. Results.

5:2.1. Chain length compatibility (PPG-PPG and PPGM-PPGM systems) at 30°C.

The heats of mixing of PPG of different molecular weights with PPG 400 were observed to be small and endothermic while those for the PPGM 400-PPGM 1500 were exothermic and very small. The values for equivolume mixtures of PPG 400-PPG 2000 and PPG 400-PPG 1500 agree in sign with those reported by Booth[55] et al, but the agreement in magnitudes was far from satisfactory, discrepancies of more than 10% being observed. The heat of mixing curves showed cusps or dips which became more pronounced as the molecular weight of one of the component was increased. Although the PPG 400-PPG 1025 curve could be smoothed out within experimental error, as could all the other curves, nevertheless there appeared to be the possibility of 2 dips occuring in that curve. Considering the overall forms of the heat of mixing curves, it is tempting on general grounds to smooth out the experimental curves, but the reproducibility and sharpness of the dip readings argues against this. On the other hand admitting the existence of the dips lead to the question of their causes, for which no suitable explanations can be envisaged.

The calculated free energy curves for these systems showed complete thermodynamic chain length miscibility, despite the positive heats of mixing. This is due to the comparatively larger entropic effect of the systems. Increasing the chain length of the variable component

decreases the compatibility as evidenced by the decrease in entropy and the increase in enthalpy. Since the entropic component will continue to decrease as the molecular weight increases, possible chain length incompatibility could occur, provided the enthalpy change continues to increase slowly with increases in molecular weight. If the free energy curve for the PPG 400-PPG 2000 system is examined closely, there appears to be a minute ripple in the curve at about 0.45 $\phi_{PPG\ 400}$, although experimental error could account for this. The presence of such a ripple would imply chain length incompatibility within certain concentration ranges. There is no evidence of chain length incompatibility in polydispersed polyethylene and polystyrene[2], although the methods and conditions used are different.

The interaction parameters for these mixtures, as calculated from the Flory-Huggins expression (equation 2:24) are found to be linear in $\phi_{PPG\ 400}$. Where the chain length difference is the smallest, this parameter is independent of PPG 400 concentrations, within experimental error. As this difference increases, sloping linear plots were obtained, showing increasing concentration dependences.

5:2.2. PEGM-PPGM system in the temperature range 30°C to 70°C.

(A). Experimental runs at 30°C.

The heats of mixing obtained for the PPGM 400 and PPGM 1000 samples with PEGM 600 agree well (within expeimental error) with the results reported by Booth et al, as shown in table 5:1, for the same temperature.

Table 5:1.

Heats of mixing of equivolume mixtures.

system	results of Booth et al[55]	this work
PEGM 600-PPGM 400	2.65 J/cm^3.	2.59 J/cm^3.
PEGM 600-PPGM 1000	2.69 J/cm^3.	2.64 J/cm^3.

Apart from the reproducibility in absolute magnitudes, the nature of the two curves were also very well reproduced, with a slight but noticeable difference between their heats of mixing along one branch of the curve. These two curves serve as a further test of the calorimeter, in addition to the chemical test since Booth et al's work used an LKB commercial microcalorimeter.

At this experimental temperature, Booth et al showed the heats of mixing of PEGM 600 with PPGM of molecular weights up to 1000 to be independent of the molecular weight of the PPGM component. This was found in the present experiments. However, on increasing the molecular weight of the PPGM component to 1500 and 2000, the magnitudes of the endothermic heats of mixing were found to become smaller. This observation conforms with the Flory-Huggins theory, which predicts extremely small or zero heats of mixing for mixtures of high molecular weights. The heat of mixing curve for the PEGM 600-PPGM 2000 system showed a cusp at about equivolume concentration, although the curve could be smoothed out just beyond the limits of experimental error.

Inspection of the calculated free energy curves reveals some interesting features. The PEGM 600-PPGM 400 curve is concave upwards over all PEGM 600 concentrations, implying

complete thermodynamic compatibility. The free energy curves for the other three systems showed a negative upward concavity for part of the concentration range and also a positive upward convex region, with no obvious trends in terms of molecular weights. The general shape of these curves implies thermodynamic compatibility over the concentration range where the curve is negative and concaved upwards and thermodynamic incompatibility over the concentration range where the curve is convexed upwards.

These curves should be contrasted with cloud point data available for these systems from the works of Booth et al[38] and Tripathi[13]. The PPGM 400-PEGM 600 calculated free energy curve is in agreement with the cloud point data for this system, which showed a maximum UCST of about 27°C. The free energy curves calculated for the PPGM 1000 and PPGM 1500 with PEGM 600 systems, however, do not agree with the cloud point data which showed maximum UCSTs of 27.5°C and 29.5°C at 0.6 and 0.5 $\phi_{PEGM\ 600}$ respectively. Whereas cloud point data indicated complete miscibility over all PEGM 600 concentrations at 30°C, the free energy curves showed compatibility up to a blend composition of about 0.2 $\phi_{PEGM\ 600}$ only. These two observations are difficult to reconcile. The PEGM 600-PPGM 2000 free energy curve predicts compatibility up to a blend composition of about 0.3 $\phi_{PEGM\ 600}$. This is in agreement with cloud point data up to that concentration. Cloud point data for this system further indicates that compatibility should occur from a concentration of 0.8 $\phi_{PEGM\ 600}$ onwards. The calculated free energy curve however does not show this. The cloud point data also implied that resultant of the heat of

mixing and subsequent phase separation was being measured between the concentrations of 0.3 and 0.8 $\phi_{PEGM\ 600}$. This would account for the cusp in the enthalpy of mixing curve since the maximum UCST of the system occurs at about that concentration.

A closer look at the calculated $-T\Delta S_m$ curve for the PEGM-PPGM system as a whole indicates a rapid decrease in magnitude in this quantity on increasing the molecular weight of the PPGM component from 400 to 1000, followed by a gradual decrease on increasing the molecular weight further from 1000 to 2000. The free energy curves calculated for this system showed that above a certain PPGM molecular weight there is a sensitive balance between the heat of mixing and entropy of mixing values, both in terms of magnitudes and sign. Below this molecular weight, the entropic component dominates and largely determines the thermodynamic compatibility of the system.

The χ_{12} values obtained from the heats of mixing at this temperature are approximately linear in $\phi_{PEGM\ 600}$ and constant from about 0.4 $\phi_{PEGM\ 600}$ up to 0.9 $\phi_{PEGM\ 600}$. From 0.4 $\phi_{PEGM\ 600}$ up to pure PPGM, the χ_{12} values were seen to increase. These χ_{12} values are slightly larger than the χ_{12} values reported by Tripathi from cloud point measurements where the critical χ_{12} values were in the region of 0.11 to 0.14. They are also much larger than the values of about 0.1 for the PEGM 600-PPGM 1500 and PEGM 600-PPGM 2000 systems reported by Booth et al[38] where they assumed the χ-parameter to be a function of concentration and temperature. Both these results are much more dependent on the Flory-Huggins theory with its inherent assumptions while the χ_{12} values obtained

in this work are from directly measured values analysed with a minimum of theoretical assumptions.

(B). Experimental runs at 50°C.

The results obtained for the system at 50°C showed dips in all the molecular weight components used, although the curves could be smoothed out just beyond the limits of experimental error. The magnitudes of the heat of mixing were smaller than those at 30°C, as expected for systems exhibiting endothermal heats of mixing. This does not agree with the work of Allen, Gee and Nicholson[8] which showed heats of mixing that were independent of temperature.

Combining the heat of mixing results with the calculated entropy of mixing results to give the free energy of mixing curves yielded some curiously shaped curves. The PEGM 600-PPGM 1000 free energy curve, though completely negative, showed two distinct concave parts while the PEGM 600-PPGM 1500 and PEGM 600-PPGM 2000 curves both showed two negative concave and one positive convex sections each, with the PPGM 2000 curve more negative than the PPGM 1500 curve. Reconciliation of these results with cloud point data is difficult since the temperature of measurement was well above the highest of the maximum UCSTs of the systems examined. Complete miscibility should have been observed and the calculated free energy curves should be concave over all PEGM 600 concentrations for the three systems.

The χ_{12} versus $\phi_{PEGM\ 600}$ plots also showed some peculiar dependence on $\phi_{PEGM\ 600}$ at this temperature.

(C). Experimental runs at 70°C.

The dips in the heat of mixing curves are less pronounced and smoothing of the experimental curves are possible within experimental error. Although comparision in terms of magnitudes between the runs made with the new batch of PEGM 600 with runs made with the previous batch of PEGM 600 at the previous two temperatures are not possible, nevertheless the general pattern of behavior is still valid for comparision, as judged by the single PEGM 600-PPGM 2000 curve made with the previous batch of PEGM 600.

The free energy curves are most interesting. As expected at this temperature, they are all negative. However, instead of being completely concave upwards over all PEGM 600 concentrations as is expected for complete thermodynamic compatibility, they showed a flat or slightly convex central section, implying incompatibility in the composition range where the convexity occurs.

The general feature of these free energy curves appears to correspond in some way with the shape of the χ_{12} versus $\phi_{PEGM\ 600}$ curves. The χ_{12} values decrease from pure PPGM with increasing PEGM 600 concentration to a minimum at some PEGM 600 concentration which depends on the molecular weight of the PPGM used, reach a maximum and then decrease again with increasing PEGM 600 concentration. The concentration at which the minimum occurs in the χ_{12} curves corresponds to the first minimum in the calculated free energy curves as the PEGM 600 concentration increases from zero. Obviously, this coincides with the concentrations at which the dips occur in the heat of mixing curves.

In general, although the calculated free energy of mixing curves for the PEGM-PPGM mixtures over the temperature range examined may show odd shapes that sometimes defy interpretation when viewed in conjunction with other data, nevertheless the direction in which these free energy of mixing curves shift with increasing temperature is correct. Since the free energy of mixing parameter is an interplay between the heat of mixing and the entropy of mixing, either of these quantities could be in error to a certain extent. As the heat of mixing values are obtained from careful experiments, the calculated entropy of mixing values must be suspect.

5:2.3. Polystyrene-polybutadiene system.

(A). Calorimetry data at 70°C.

The values for the heat of mixing of the two systems PS 1010-PBD 960 and PS 1010-PBD 2350 were much larger than expected since calculations using tabulated solubility parameter values[62] predicted a heat of mixing of approximately 0.03 J/g at this temperature. The trend observed in the PEGM-PPGM system is also observed in the limited data here i.e. the larger the molecular weight of the variable component, the smaller is the heat of mixing, although the difference here is very much smaller than those in the PEGM-PPGM case.

The calculated free energy of mixing curves (sometimes referred to as the calculated free energy curves) are both negative, but of a strange shape. The PS 1010-PBD 2350 curve showed two distinct regions, one of which is concave upwards

while the other is flat. Although this implies thermodynamic compatibility over all concentrations of PS 1010, nevertheless one would have expected a curve which would show concavity over all concentrations, judging from the cloud point data of the system which shows a maximum UCST of 5°C at a concentration of 62 wt.% PS 1010.

The PS 1010-PBD 960 free energy of mixing curve could be smoothed out either into a single curve which shows concavity over all concentrations or into a curve with a flat central section, both implying thermodynamic compatibility over all concentrations. HOwever, the experimental curve showed two distinct sections which are both concave upwards, implying thermodynamic incompatibility in certain concentration ranges. This appears to be in contradiction with cloud point data available for the PS-PBD system of other molecular weights. Since the PS 1010-PBD 2350 system has a maximum UCST of 5°C, one can safely assume that the maximum UCST of this system is well below 5°C. Hence this system should exhibit complete thermodynamic compatibility at all concentrations at 70°C.

The χ_{12} values obtained for the PS 1010-PBD 2350 system give a constant value of approximately 0.16 g^{-1} while the χ_{12} values for the PS 1010-PBD 960 system falls in the range of 0.12 to 0.2 g^{-1} with the maximum value occuring at a concentration of about 0.3 $\phi_{PS\ 1010}$.

(B). Cloud point measurements of PS 1520-PBD 2350 system.

As can be seen from figure 4:16, the intensity change when phase separation occurs is of the order of hundreds of units. Hence no correction for photodiode dark current is

necessary, except where the turbidity changes very slowly with temperature changes. Correction of dark current in these situations are extremely useful in defining a sharper cloud point. As mentioned earlier, multiple peaks could be observed occasionally as a result of having a fixed angle of observation.

Assuming the 'spinodal' obtained to be the true spinodal of the system, χ_{12} values could be evaluated by applying tie lines parallel to the tangent at the 'critical point'. The χ_{12} values so obtained, shown in table 4:27, are much larger than the values obtained by Yip[12] and Tripathi[13], but in agreement with the values calculated from heats of mixing, although the molecular weights used in the heats of mixing are different. However, one must bear in mind that the tie lines used by Yip and Tripathi were parallel to the volume fraction axis of their cloud point curves.

Generally, the overall results of this work raise two questions. They are:

(a). Are the measurements of the heats of mixing accurate enough to warrant the existence of the dips or flat tops in the heat of mixing curves or are they just figments of experimental errors? Although the accuracy of the calorimeter is good judging from the chemical test, the reproducibilities could be improved.

(b). If the results are accurate enough to define the true shapes of the heat of mixing curves including the dips or cusps, then the shapes and magnitudes of the free energy of mixing curves are questionable when compared with cloud

point data. Since the free energy of mixing (Δg_m) curve is compiled from an observed value of the heat of mixing (Δh_m) and a calculated value of the entropy of mixing ($-T\Delta S_m$) then, in this case, the value calculated for the combinatorial entropy change (ΔS_m) does not reflect the true behavior of the system.

To prevent any premature conclusions being drawn with regards to question (b), it would be more prudent to consider (b) only when question (a) has been confirmed more certainly by further work. As the calorimeter constructed for this work could be easily rendered more sensitive, and hence the experimental error reduced, this should be the first aim of any future work.

CHAPTER 6.

CONCLUSIONS.

The aim of this work was to measure the heats of mixing of oligomeric systems as functions of molecular weight and temperature. The combination of measured heat of mixing values with calculated combinatorial entropy of mixing values yielded the free energy of mixing curves. Comparision with cloud point curves was then used as a test for the usefulness of the Flory-Huggins theory for calculating the combinatorial entropy for binary mixtures.

The heats of mixing for PPG 400 with PPG of higher molecular weights at 30^{0}C were shown to be small and endothermic, despite the hydrogen bonding known to be present in the system. The heats of mixing were shown to increase with an increase in molecular weight of one of the components. The heats of mixing as a function of PPG 400 concentration were shown to exhibit dips which became more pronounced as the molecular weights increased.The calculated free energy of mixing curves were found to be negative and concave over all PPG 400 concentrations, indicating chain length compatibility despite the endothermal heats of mixing. This compatibility was shown to be due to entropic rather than enthalpic effects, i.e. the enthalpic contribution is very small.

The χ_{12} values calculated from the heat of mixing measurements using the Flory-Huggins theory were found to be approximately independent of concentration or showed only a slight concentration dependence, depending on the molecular

weights of the components used.

The heats of mixing of PPGM 400 with PPGM 1500 were found to be very small and exothermic. This, combined with the relatively large entropy of mixing, showed thermodynamic compatibility over all concentrations of PPGM 400 at 30°C, indicating chain length compatibility without specific interactions present. This is in agreement with literature evidence for the chain length compatibility of polydispersed polyethylene and polydispersed polystyrene.

The heats of mixing of PEGM 600 with PPGM of various molecular weights were found to be relatively large and endothermic in the temperature range 30°C to 70°C studied. Under isothermal conditions, the endothermic heats of mixing decrease with an increase in the molecular weights of the PPGM components. On increasing the temperature from 30°C to 50°C, the endothermic heats of mixing for any one molecular weight system were seen to decrease. On increasing the temperature further to 70°C, the heats of mixing appeared to remain constant within experimental error, judging from the single PEGM 600-PPGM 2000 curve available for comparision between 50°C and 70°C. This is in partial agreement and partial disagreement with the work of Allen, Gee and Nicholson which showed the heats of mixing of oligomeric polyisobutylene with polydimethylsiloxane to be independent of temperature.

At 30°C, the heats of mixing of PEGM 600 with PPGM of molecular weights 1500 and below were found to be smooth as a function of PEGM 600 concentrations but the PEGM 600-PPGM 2000 system was shown to exhibit a dip which might be attributed to phase separation occuring at this concentration

for the system. The heat of mixing curves at 50°C and 70°C showed dips (cusps) or flat tops. The magnitudes of these dips or flattenings are small, compared to the overall magnitudes of the quantities measured, but just outside experimental error.

The calculated entropy of mixing ($-T\Delta S_m$) values were seen to have the same order of magnitudes as the measured heat of mixing values, though of opposite sign. Since the calculated free energy of mixing (Δg_m) curves are a fine balance between these two quantities, fluctuations in either of these quantities would manifest themselves in the free energy of mixing curves. The free energy of mixing curves calculated for the PEGM-PPGM systems at the various temperatures were found to reflect this sensitivity. However, the shapes of the calculated Δg_m curves were found to be incompatible with known cloud point data for the systems which showed normal, smooth UCST behavior with critical temperatures near to or below 30°C. The χ_{12} values obtained, as calculated from the measured heat of mixing values using the Flory-Huggins theory, were concentration dependent.

The PS-PBD system was shown to exhibit large endothermic heats of mixing at 70°C. Keeping the molecular weight of the PS component constant and varying the molecular weight of the PBD component, the heats of mixing for the two molecular weights studied were found to be almost constant, within experimental error.

The χ_{12} values obtained were found to be concentration independent in the PS 1010-PBD 2350 system within experimental

error and concentration dependent in the PS 1010-PBD 960 system. The values for both systems studied fall within the range observed for polymer-polymer mixtures, between 0.1 and 0.2 g^{-1}. In addition, a shoulder was shown to exist in the PS 1520-PBD 2350 system phase boundary from light scattering experiments. Spinodal temperatures can, in principle, be obtained from the turbidimetric phase boundary measurements. The χ_{12} values obtained by applying tie lines to the phase boundary obtained agree well with the values calculated from heat of mixing measurements.

The calculated free energy of mixing curves, though negative over all PS concentrations, were found to predict partial compatibility, again in contradiction with measured cloud point data which showed normal, smooth UCST behavior for the systems involved in the heats of mixing, with critical temperatures below room temperature.

Since the calculated entropy of mixing values are of the same order of magnitude as the measured heat of mixing values, in the absence of independent measurements of the entropy of mixing ($-T\Delta S_m$) or free energy of mixing (Δg_m), minor perturbations in the heat of mixing values are important, as judged by the effects of these perturbations on the free energy of mixing curves. The present work shows that a more accurate calculation of the combinatorial entropy (ΔS_m) is needed, if a correct representation of Δg_m as a function of composition is to be obtained. Since the calculated free energy of mixing curves predicted partial miscibility for some of the systems at the molecular weights and temperature ranges studied, a fact which is not born

out by cloud point data, the conclusion that can be drawn is that the theory is not refined enough to give reliable values of the calculated entropies of mixing. In fact, the positive excursions in the calculated values of the free energy of mixing for pairs known to be compatible sets one limit to the inadequacy of the calculated values of the entropy of mixing, $-T\Delta S_m$.

Appendix A:-

Table of chart recorder full scale deflection for amplifier gain control setting.

Amplifier gain setting	Chart recorder f.s.d.
A	100 mV
B	30 mV
C	10 mV
D	3 mV
E	1 mV
F	300 μV
G	100 μV
H	30 μV
J,K,L	10 μV

Appendix B:-

Table of temperature control setting and temperature of calorimeter obtained.

Temperature control setting.	Calorimeter temperature/^{0}C.
0.880	30.1
3.625	50.1
5.325	70.1
7.000	75.0
8.100	85.0

```
0001:
0002:  *
0003:  R                                                                    Experimental
0004:   009201000800012001200110034000900560013007800040008008 0AABB      identification
0005:  *                                                                    data.
0006:  D
0007:  T 00 01 42  00288 39575 00290 39601 00187 39589 00151 39625
0008:  T 00 03 23  00288 39571 00298 39597 00187 39585 00155 39621
0009:  T 00 05 03  00287 39553 00299 39579 00187 39567 00156 39603
0010:  T 00 06 43  00287 39537 00299 39565 00187 39553 00156 39587
0011:  T 00 08 23  00287 39525 00299 39551 00187 39539 00156 39575
0012:  T 00 10 03  00288 39511 00299 39537 00187 39525 00156 39559
0013:  T 00 11 43  00290 39497 00299 39523 00188 39513 00156 39545
0014:  T 00 13 23  00291 39481 00297 39507 00188 39499 00153 39531
0015:  T 00 15 03  00291 39469 00298 39495 00188 39485 00156 39517
0016:  T 00 16 43  00292 39453 00299 39481 00188 39471 00156 39501
0017:  T 00 18 23  00293 39441 00299 39465 00188 39457 00156 39487
0018:  T 00 20 03  00293 39431 00299 39455 00188 39447 00156 39477
0019:  T 00 21 43  00293 39413 00299 39439 00188 39431 00156 39461
0020:  T 00 23 23  00293 39399 00299 39423 00188 39417 00156 39445
0021:  T 00 25 03  00293 39385 00299 39411 00188 39403 00156 39431
0022:  T 00 26 43  00293 39371 00299 39395 00188 39389 00156 39417
0023:  T 00 28 23  00293 39357 00299 39383 00188 39375 00156 39403
0024:  T 00 30 03  00294 39341 00299 39367 00188 39361 00156 39387
```

Elapse time C_1 C_2 C_3 C_4 C_5 C_6 C_7 C_8 Channel number

APPENDIX C:- Listing format of turbidimeter results showing elapsed time of experiment, intensities (odd number channels) and temperatures(even number channels) in Kelvin corresponding to previous channel number.

REFERENCES

1. Olabisi, O., Robeson, L.M. and Shaw, M.T.; "Polymer-Polymer Miscibility", Chapter 3, Academic Press,(1979).
2. Konningsveld, R., Kleintjens, L.A., and Schoffeleens, H.M.; Pure Appl. Chemistry, 39, 1 (1974).
3. Dobry, A. and Boyer-Kawenoki, F.; J. Polym. Sci., 2, 90 (1947).
4. Kern, R.J. and Slocombe, R.J.; J. Polym. Sci.,15,183 (1955).
5. Zeman, L. and Patterson, D.; Macromolecules,5,513 (1972).
6. Robards, A.,Patterson, D. and Delmas, G.; Macromolecules,10,706 (1977).
7. Yu, H.;Adv. Chem. Series; Ser. 99,1, (1971).
8. Allen, G., Gee, G. and Nicholson, J.P.; Part 1, Polymer,1,56 (1960), Part 2, Polymer,2,8 (1961).
9. Konningsveld, R. and Kleintjens, L.A.;J. Polym. Sci., Polym. Symp.; 61,221 (1977).
10. McIntyre, D., Rounds, N. and Campos-Lopez, E.; A.C.S. Polymer preprints;10,531 (1969).
11. McIntyre, D., Wims, A. and O'Mara, J.; A.C.S. Polymer Preprints, Sept., p.1037 (1965).
12. Yip, C.W. and Allen, G.;Personal communications.
13. Tripathi, J.B.P.;"Effect of Pressure on Polymer-Polymer Compatibility", Ph.D. thesis, Imp. Coll.(1979).
14. Flory, P.J.; J. Amer. Chem. Soc.;87,1833 (1965).
15. McMaster, L.P.;Macromolecules,6,760 (1973).
16. Fowler, R.H. and Rushbrooke, G.S.;Trans. Faraday Soc.; 33,1272 (1937).

17. Chang, T.S.; Proc. Cambridge Phil. Soc.;35,265 (1939).

18. Chang, T.S.; Proc. Royal Soc.;169,512 (1939).

19. Miller, A.R.; Proc. Cambridge Phil. Soc.;38,109 (1942).

20. Flory, P.J.; J. Chem. Phys.;9,660 (1941).

21. Flory, P.J., J. Chem. Phys.;10,51 (1942).

22. Huggins, M.L.; J. Chem. Phys.,9,440 (1941).

23. Huggins, M.L.; Ann. N.Y. Acad. Sci.;43,1 (1942),
J. Phys. Chem.;46,151 (1942),
J. Amer. Chem. Soc.;64,1712 (1942).

24. Scatchard, G.; Chem. Rev.;8,321 (1931).

25. Flory P.J.;J. Chem. Phys.,12,425 (1944

26. Tompa, H.; "Polymer Solutions", Butterworths, London, (1956).

27. Scott, R.L. and Magat, M.; J. Chem. Phys.,13,172 (1945).

28. Miller, A.R.; Proc. Cambridge Phil. Soc.;39,54 (1943).

29. Orr, W.J.C.; Trans. Faraday Soc.;40, 320 (1944).

30. Guggenheim, E.A.; Proc. Roy. Soc.(London) A,183,203(1944).

31. Flory, P.J. and Krigbaum, W.R.; Annual Rev. Phys. Chem.; 2,383 (1951).

32. Nishi, T., Wang, T.T. and Kwei, T.K.; Macromolecules, 8,227 (1975).

33. Bernstein, R.E., Cruz, C.A., Paul, D.R. and Barlow, J.W.; Macromolecules,10,681 (1977).

34. McMaster, L.P.; "Copolymers, Polyblends and Composites", Adv. Chem. Ser.,142,43 (1975).

35. Gee, G. and Treloar, L.R.G.; Trans. Faraday Soc., 38,147 (1942).

36. Ewing, M.J.; Trans. Faraday Soc.;46,613 (1950).

37. Booth, C., Gee, G., Jones, M.N. and Taylor, W.D.; Polymer,5,353 (1964).

38. Friday, A., Cooper, D.R. and Booth, C.; Polymer, 18,171 (1977).

39. Flory, P.J. and Schultz, A.R.; J. Amer. Chem. Soc.; 74,760 (1952).

40. Flory, P.J., Orwoll, R.A. and Vrij, A.; J. Amer. Chem. Soc.;86,3507 (1964).

41. Flory, P.J., Orwoll, R.A. and Vrij, A.; J. Amer. Chem. Soc.;86, 3515, (1964).

42. Flory, P.J. and Eichinger, B.E.; Trans. Faraday Soc.; 64,2035 (1968).

43. Prigogine, I., Trappenier, N. and Mathot, V.; J. Chem. Phys.,21,559 (1953).

44. Prigogine, I., Trappenier, N. and Mathot, V.; Disc. Faraday Soc.;15,93 (1953).

45. Tonks, L.; Phys. Rev.;50,955 (1936).

46. Sanchez, I.C.; "Polymer Blends", Vol. 1, p.115, Academic Press, Inc.,(1978).

47. Chai, Z.K.; DIC thesis, Imp. Coll., (1981).

48. Konningsveld, R. and Stepto, R.F.T.; Macromolecules, 10,1166 (1977).

49. Huggins, M.L.; J. Phys. Chem.;74,371 (1970).

50. Huggins, M.L.; J. Phys. Chem.,75,1255 (1971).

51. Huggins, M.L.; J. Phys. Chem.,80,1317 (1976).

52. Olabisi, O.; Macromolecules,8,316 (1975).

53. Prosen, E.J.; NBS report on the design and construction of microcalorimeter, NBS report no. 73-179 (1973).

54. Prosen, E.J., Goldberg, R.N., Staples, B.R., Boyd, R.N. and Armstrong, G.T.; "Microcalorimetry Applied to Biological Processes",-Thermal Analysis:Comparative studies on materials, Edited by H. Kamba and P.D. Garn, p.253, Kodansha Ltd, J. Wiley & Sons, (1974).

55. Cooper, D.R. and Booth C.; Polymer,18,164 (1977).

56. Parker, V.B.; "Thermal Properties of Aqueous Uni-Univalent Electrolytes", NSRDS-NBS-2(U.S. Govt. Printing Office), Washington, D.C. (1965).

57. Pitzer, K.S.; J. Amer. Chem., Soc.;59,2356 (1937).

58. Richardson, M.J. and Savill, N.G.;Polymer,18,3 (1977).

59. Scholte, Th. G.; J. Polym. Sci.,Part A-2,9,1953 (1971).

60. Derham, K.W., Goldsboro, J. and Gordon, M.; IUPAC Macromolecular Microsymposia X11 & X111, Prague, p.97, (1973).

61. Schreinemakers, F.A.H. in Bakhuis Roozeboom, H.W.: Die heterogenen Gleichgewichte vom Standpunkte der Phasenlehre, Braunschweig, Vieweg, Vol 111,part2 (1913). Later volumes edited by Schreinemakers.*

62. Krause, S.; "Polymer Blends" Vol. 1, Chapter 2, p.15, Academic Press Inc., (1978), Edited by Paul, D.R.

* as quoted by Konningsveld et al [2].